Developement of high-performance concrete with lower ecological footprint

Porikam Poil, Kiran Ram

Doctoral thesis / Disertacija

2023

Degree Grantor / Ustanova koja je dodijelila akademski / stručni stupanj: **University of Zagreb, Faculty of Civil Engineering / Sveučilište u Zagrebu, Građevinski fakultet**

Permanent link / Trajna poveznica: https://urn.nsk.hr/urn:nbn:hr:237:978941

Rights / Prava: In copyright/Zaštićeno autorskim pravom.

Download date / Datum preuzimanja: **2025-03-29**

Repository / Repozitorij:

Repository of the Faculty of Civil Engineering, University of Zagreb

University of Zagreb

Faculty of Civil Engineering

Kiran Ram Porikam Poil

DEVELOPEMENT OF HIGH-PERFORMANCE CONCRETE WITH LOWER ECOLOGICAL FOOTPRINT

DOCTORAL THESIS

Zagreb, 2023.

University of Zagreb

Faculty of Civil Engineering

Kiran Ram Porikam Poil

DEVELOPEMENT OF HIGH-PERFORMANCE CONCRETE WITH LOWER ECOLOGICAL FOOTPRINT

DOCTORAL THESIS

Supervisors: Assoc. Prof Marijana Serdar, Ph.D, Prof. Karen L Scrivener, Ph.D

Zagreb, 2023.

GRAĐEVINSKI FAKULTET

Kiran Ram Porikam Poil

RAZVOJ BETONA VISOKIH UPORABNIH SVOJSTAVA SMANJENOG EKOLOŠKOG OTISKA

DOKTORSKI RAD

Supervisors: Assoc. Prof Marijana Serdar, Ph.D, Prof. Karen L Scrivener, Ph.D

Zagreb, 2023.

"I dedicate this PhD thesis to my beloved wife, cherished friends, and doting parents, whose love, faith, and encouragement have been the bedrock of my success, and to whom I owe an eternal debt of gratitude".

Acknowledgement

I am grateful to all those who have helped me throughout my PhD journey. Without their support, I would not have been able to achieve this milestone in my academic career. Firstly, I would like to express my gratitude to all those who have been instrumental in guiding me through this journey. I am thankful to my guide Marijana, who has been extremely helpful since the day I arrived in Zagreb till today. Her knowledge and expertise in the field have been invaluable to me. She has always given me full freedom to work and has been approachable at any time. She helped me during the initial phase, when everything was new to me, including the place, the language, and the administrative process. Overall, without her guidance and support, I would not have been able to complete my PhD.

I would also like to thank my co-supervisor Karen, who has provided me with her immense knowledge and expertise throughout my PhD journey. She was also very helpful during my stay at EPFL, Switzerland. Additionally, my colleague Diana has provided her support remotely, which has been essential for the completion of my PhD.

I am also grateful to Matea and all members of the LATOM group, including Olivera, Alma, Josipa, and Antonio, who have been supportive throughout my PhD. Their encouragement and assistance have been instrumental in my success. I would also like to thank the Sveti Duh family for their support. Furthermore, I am grateful to all the faculty members, laboratory staff, and office personnel at the faculty, who have cooperated with me throughout the duration of my PhD. Their assistance and support have been invaluable to me.

Lastly, I would like to express my gratitude to my wife and family. They were a constant source of support throughout this journey, especially my wife, who has been my pillar of strength. I could not have completed my PhD without their encouragement and support.

Kiran

Extended Summary

The project ACT began with a quest to explore the possibilities of using calcined clay as an alternative binder for cement. Due to the scarcity and high cost of traditional supplementary cementitious materials, the study focused on collecting and characterizing various materials, including low-kaolin clays from Croatia and neighboring countries. After extensive testing and preparation, six different high-performance mortar mixtures were created, incorporating the low-grade calcined kaolin clay, fly ash, and limestone powder. The results showed that all mixes, even those with extremely low kaolin content, were suitable for use in high-performance cement systems.

Building on this success, the study moved to the next phase, focused on formulating high-performance concrete with minimal environmental impact. The mix design used in the Pelješac Bridge was modified to significantly reduce the cement content and substitute it with fly ash and limestone or calcined clay and limestone. Fifteen different mixes were tested for workability, mechanical stability, and resistance to chloride penetration. The results indicated that reducing cement content had a significant effect on durability and service life, and the modified mixes achieved similar or higher sustainability indexes with lower cement amounts.

In the third and fourth phases, the study focused on the impact of kaolinite content on the durability of Limestone Calcined Clay Cement (LC3), particularly when the kaolinite content was less than 40%. Two clays with different kaolinite concentrations were used, and the medium-kaolinitic clay showed better durability performance in terms of chloride penetration resistance. The low-kaolinitic clay was found to be suitable for limestone calcined clay cement concrete in moderate

exposure conditions. The study highlights the importance of clay purity in LC3 systems and suggests that lower-quality clays can be used in areas where high-purity clays are scarce.

In addition, the fourth phase aimed to analyze the effective diffusion coefficient of low-grade clays and their impact on pore structure, chloride binding, and bulk/pore solution conductivity. The results showed that low-grade clays have lower conductivity than Portland cement, resulting in greater chloride penetration resistance. Furthermore, pore structure and chloride binding capacities had a similar influence in LC3 with lower grade clays and Portland cement. Finally, the number of smaller capillary pores (< 5 nm) was closely related to the diffusion coefficient in all mixes, indicating the importance of pore structure in determining the effectiveness of clays in cementitious systems.

Overall, the thesis shows that low-grade clays can be utilized in cementitious systems to reduce the environmental footprint and achieve similar or better mechanical and durability properties. By understanding the impact of different parameters such as kaolinite content, pore structure, and chloride binding capacity, the use of low-grade clays in LC3 systems can be optimized for different exposure conditions. Furthermore, reducing cement content and using alternative binders such as fly ash and calcined clay can significantly reduce the carbon footprint of concrete mix designs without compromising the durability and service life of concrete structures. These findings contribute to the development of more sustainable and eco-friendly construction practices.

Keywords: Carbon footprint, performance-based concrete, limestone calcined clay cement, low kaolinitic clay, chloride diffusion, pore structure, chloride binding, conductivity

Produženi sažetak

Projekt ACT je započeo potragom za mogućnostima primjene kalcinirane gline kao alternativnog mineralnog dodatka u cementu. Zbog nedostatka i visoke cijene tradicionalnih mineralnih dodataka cementu, istraživanje je usmjereno na prikupljanje i karakterizaciju različitih materijala, uključujući gline s niskim udjelom kaolina, s područja Hrvatske i okolne regije. Nakon opsežnih ispitivanja i pripreme, projektirano je šest različitih mješavina mortova visokih uporabnih svojstava, koji sadrže kalciniranu glinu s manjim udjelom kaolina, leteći pepeo i vapnenac. Rezultati su pokazali da su sve mješavine, čak i one s izrazito niskim udjelom kaolina, prikladne za primjenu u cementnim kompozitima visokih uporabnih svojstava.

Na temeljima ovih uspješnih rezultata, započeta je sljedeća faza istraživanja, usmjerena na projektiranje betonskih mješavina visokih uporabnih svojstava s minimalnim utjecajem na okoliš. Sastav betonskih mješavina korištenih u izgradnji Pelješkog mosta je modificiran kako bi se značajno smanjio sadržaj cementa, zamjenom letećim pepelom i vapnencem ili kalciniranom glinom i vapnencem. Za petnaest različitih mješavina ispitana je obradljivost, mehanička stabilnost i otpornost na prodor klorida. Rezultati su pokazali da je smanjenje udjela cementa imalo značajan utjecaj na trajnost i uporabni vijek, a modificirane mješavine dostigle su sličan ili viši indeks održivosti, s nižim količinama cementa.

U trećoj i četvrtoj fazi, istraživanje je usmjereno na utjecaj udjela kaolina na trajnost veziva na bazi kalcinirane gline i vapnenca (engl. Limestone Calcined Clay Cement - LC3), osobito kada je sadržaj kaolina manji od 40%. Korištene su dvije gline s različitim udjelom kaolina, a glina sa srednjim udjelom kaolina pokazala je bolja trajnosna svojstva, u pogledu otpornosti na prodor klorida. Utvrđeno je da je glina s niskim udjelom kaolina pogodna za pripremu LC3 veziva u

umjerenim uvjetima izloženosti. Istraživanjem je istaknuta važnost udjela kaolina u sastava gline i predložena je uporaba glina niske kvalitete u područjima gdje visoko kvalitetna glina nije dostupna.

Pored navedenog, četvrta faza imala je za cilj analizu efektivnog koeficijenta difuzije glina niske kvalitete i njegovog utjecaja na strukturu pora, vezivanje klorida, provodljivost materijala/provodljivost otopine u porama. Rezultati su pokazali da niskokvalitetne gline imaju manju provodljivost od Portland cementa, što rezultira većom otpornosti na prodor klorida. Osim toga, struktura pora i sposobnost vezivanja klorida imali su sličan utjecaj u LC3 vezivima s glinama niže kvalitete i u Portland cementu. Na kraju, količina manjih kapilarnih pora (< 5 nm) bila je usko povezana s koeficijentima difuzije u svim mješavinama, što ukazuje na važnost strukture pora pri određivanju učinkovitosti glina u cementnim kompozitima.

Disertacija pokazuje da se gline niske kvalitete mogu primjenjivati u cementnim kompozitima kako bi se smanjio negativni utjecaj na okoliš i postigla slična ili bolja mehanička i trajnosna svojstva. Razumijevanjem utjecaja različitih parametara, kao što su sadržaj kaolina, struktura pora i sposobnost vezivanja klorida, primjena niskokvalitetnih glina u LC3 sustavima može biti optimizirana za različite uvjete izloženosti. Smanjenjem udjela cementa i korištenjem alternativnih mineralnih dodataka, kao što su leteći pepeo i kalcinirana glina, moguće je značajno smanjiti uglični otisak sastava betonske mješavine, bez ugrožavanja trajnosnih svojstava i uporabnog vijeka betonskih konstrukcija. Ovi rezultati istraživanja pridonose razvoju održivih i ekološki prihvatljivih građevinskih praksi.

Ključne riječi: uglični otisak, projektiranje na bazi svojstava, veziva na bazi kalcinirane gline i vapnenca, gline s niskim udjelom kaolina, difuzija klorida, mikrostruktura pora, vezivanje klorida, provodljivost

Glossary

MIP	Mercury Intrusion Porosimetry
d_c	Critical pore entry radius
$d_{0.5}$	Mean pore entry diameter
TGA	Thermogravimetric analysis
XRD	X-Ray diffraction
σ	Conductivity
D_E or D_{eff}	Effective diffusion coefficient
D_{nssm}	Non-steady state chloride migration coefficient
α	Pore entrapment fraction
GWP	Global warming potential
SCM	Supplementary cementitious materials
FA	Fly ash
LS	Limestone
CC	Calcined Clay
F_{ck}	28-day characteristic compressive strength
SP	Superplasticizer
NaCl	Sodium chloride
NaOH	Sodium hydroxide
HNO_3	Nitric acid
F_s	Friedel's salt
F_{ss}	Friedel's salt solid solution
H_c	Hemi carboaluminate
M_c	Mono carboaluminate
E	Ettringite
CH	Portlandite
T	Temperature in Kelvin
F	Faraday constant
R	Universal gas constant

J_{down}	Chloride flux through sample
EIS	Electrical Impedance Spectroscopy
RH	Relative humidity
R_B	Bulk resistance
ICP-MS	Inductively Coupled Plasma Spectroscopy
z	Valence of ion
C_b	Bound chloride
C_f	Free chloride

DECLARATION OF ORIGINALITY

I declare that my thesis is the original result of my work and that I have used no sources other than those indicated in the thesis.

Kiran Ram Porikam Poil

Signature

Table of contents

Chapter 1 Introduction

Concrete is a highly desired building material worldwide, but the cement industry has a significant carbon footprint of around 8%, making concrete production harmful to the environment. Studies predict that by 2050, construction will require 18 billion tons of concrete, which will increase carbon dioxide emissions from cement production. To produce environmentally friendly concrete, researchers have attempted to increase clinker efficiency by optimizing mix design with the support of the industry. Performance-based concrete design is a simple and efficient strategy to achieve this. However, there are obstacles to lowering the cement content in concrete, such as minimum cement content and maximum water content requirements in standards. To overcome these limitations, engineers can use high-performance concrete with a low ecological footprint, which optimizes cost, service life, and performance characteristics using given materials exposed to given conditions. In the binder side of high-performance concrete, alternative binders such as fly ash, slag, and calcined clays are being used, but their availability in some regions is declining. For instance, slag and fly ash are together available in amounts close to 15% of the total cement production. Therefore, the local availability of each material must be considered. Additionally, the optimization of concrete mixture according to the need is essential to eliminate over-design. The local availability of materials and performance-based design are essential factors in producing environmentally friendly high-performance concrete.

In this thesis, the main materials were collected from various region of South-East Europe. Figure 1.1 is showing the location map of all industries from which waste materials were used. Fly ash, clays, and limestone are the main materials used throughout the work.
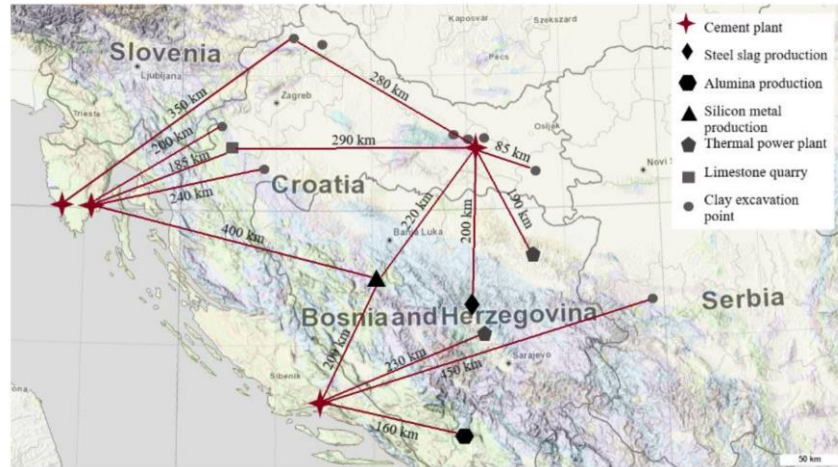
Figure 1.1 *The map showing various location where materials have been collected.*

The main part of the current work was to enable the design of high-performance concrete using locally available materials. Prior to making HPC, there are two factors to keep in mind: 1) optimization of binder and 2) clinker factor. The idea behind these factors is given briefly in the following sections.

1.1 Optimisation of binder

Optimizing the total binder content before considering the use of alternative binders is highly recommended. This approach can help reduce the CO_2 footprint by improving the efficiency of cement use [1]. The efficiency of the binder used in the system depends solely on how the design is carried out for the structures. Figure 1.2a and 1.2b displays the amount of binder and corresponding compressive strength achieved by the concrete from various studies [2], [3]. As it is evident, the amount of binder used to produce concrete of given compressive strength varies significantly. The dispersion of the data points from these graphs itself shows that there is a substantial potential of CO_2 mitigation by simply improving the binder efficiency.
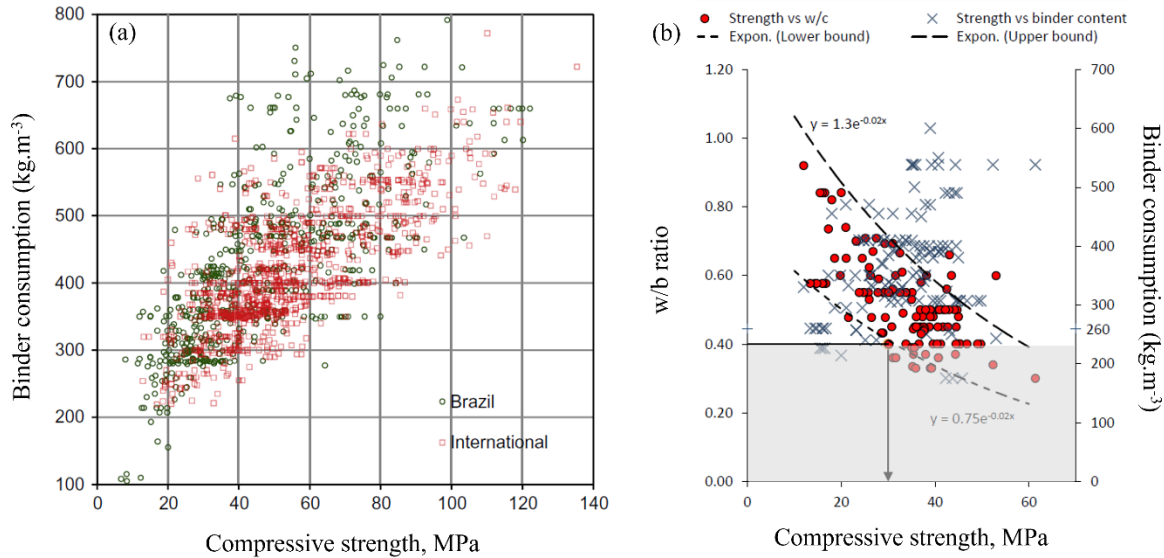
Figure 1.2 *a-b the binder consumption versus compressive strength [2], [3]*

In addition, the majority of the data points are above 300 kg/m³ due to the minimum amount of concrete specified by various standards. Depending on the exposure class, the minimum cement content in concrete per EN 206 must be greater than 260 kg/m³ (for unexposed environment) to up to 340 kg/m³ (for marine environment) in order to ensure a sufficient durability performance. However, the effect of lowering the binder content on the long-term serviceability of concrete structures is still a matter of debate. In addition, achieving the minimum number of fines necessary to ensure acceptable rheology and bonding between the concrete and steel may also contribute to the greater binder content in concrete [4][5]. However, the rheological performance of concrete may be significantly improved by the use of very efficient superplasticizers [6]–[8]. According to Figure 1.3, water can be reduced by up to 40 percent without compromising slump reduction, allowing for maximum binder content optimization. Apart the fresh property, the binder optimization may or may not affect the long-term interaction of concrete with the environment. However, some of the studies revealed that, to consistently attain a sufficient durability performance, it may thus not be essential to enforce a minimum cement content in addition to the

strength class and water/binder ratio, but rather a specific performance of concrete in that environment [9]–[11].
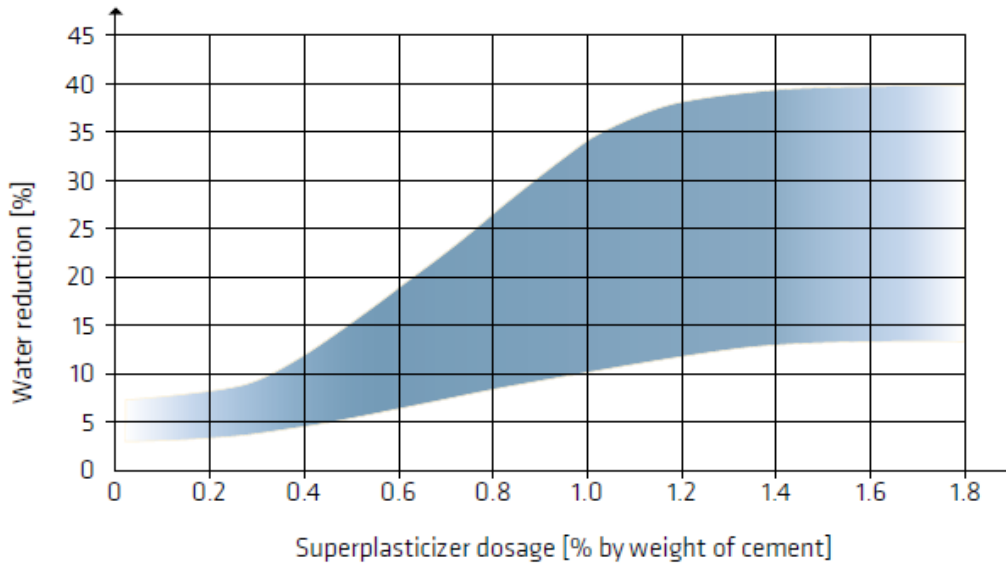
Figure 1.3 Water reduction with different dosage of superplasticizer [12]

The optimization of the binder can be done without compromising strength only by reducing the void volume that must be filled by cement paste. This can be done by proper choice of the aggregate amount in fractions to optimize packing. By utilizing various models and optimization curves, it is possible to pack aggregate skeleton. According to the packing theory, the addition of smaller particles to the concrete matrix is advantageous for filling the voids and decreasing the space for water. Utilizing an optimization curve is the most popular and straightforward method for maximizing concrete packing. In this method, a group of particles with varying particle size distributions are blended so that the total particle size distribution corresponds to an optimization curve [13]–[19]. After the packing of granular materials, the concrete mixture requires only minimum amount of paste, which brings the minimum amount of binder.

1.2 Optimization of clinker factor in the concrete

Suitable supplementally cementitious materials can optimize the amount of clinker in the system after optimizing binder content. In general, supplementary cementitious materials (SCMs) can be used in concrete to reduce the clinker factor, which can significantly improve the mechanical and durability properties of the concrete. The current global clinker factor is approximately 0.78, which means that 78% of the fraction in the clinker is made up of Portland cement. Various countries and energy consortiums are aiming for an average clinker factor of 0.60 by 2050 [20]. SCMs such as fly ash, slags, silica fume, natural pozzolanas, and ternary blends with limestone and alumina rich SCMs are available to replace cement in concrete. However, the availability of classical SCMs is limited. According to the International Energy Association, limestone, fly ash, and slag are the main clinker replacement materials in cement production. Figure 1.4a and 1.4b depict the used amount of classical SCMs in cement. Natural materials such as clay and limestone are abundantly available but are currently used in smaller quantities. Blended cements based on calcined clay and ground limestone are considered promising, enabling a 50% reduction in clinker factor and 40% reduction in carbon footprint [21]–[23].

a)
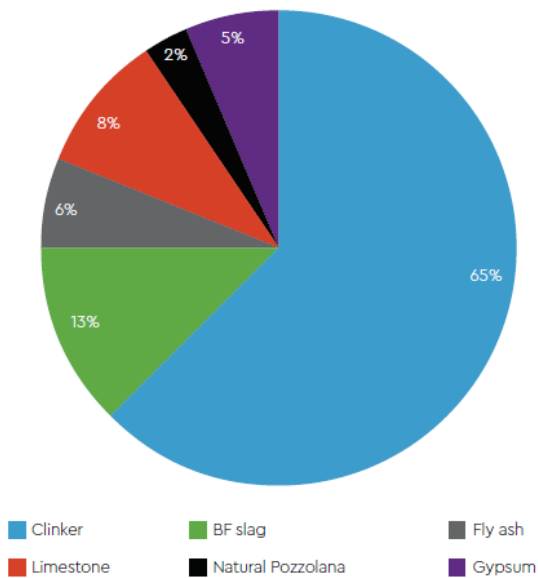
b)
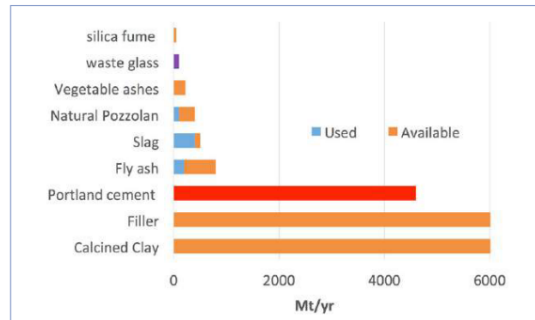
Figure 1.4 *a) Global cement composition (Source IEA-CSI, 2018) and b) Used and estimated availability of possible SCM and fillers [1]*

1.3 Significance of calcined clays

Clay is a widely available material worldwide. Clays that have a significant proportion of kaolinite have been found to be highly pozzolanic if calcined at temperatures between approximately 700-850 degrees Celsius. To replace part of the clinker in blended cement, a combined addition of calcined clay and limestone is used. The cement industry refers to such materials as LC3 - limestone calcined clay cements. Studies have shown that a kaolinite content of around 40% in an LC3 mixture is sufficient to give mechanical properties comparable to plain Portland cement from approximately 7 days as illustrated in Figure 1.5.
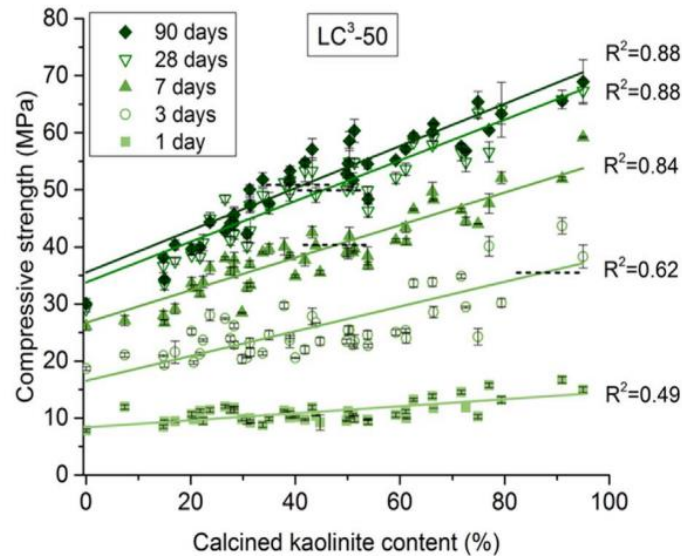
Figure 1.5 *Compressive strength achieved from 46 different clays with varying kaolinite content*
[24]

Clay belongs to a family of minerals referred to as phyllosilicates. These minerals are composed of tetrahedral silicate sheets and octahedral metal oxide (or hydroxide) sheets. The arrangement of these sheets can be either 1:1 or 2:1, and kaolinitic clay falls under the former category. In cementitious system, the kaolinitic clays are mostly used and it is made up of Si-O tetrahedral and Al-O(OH) octahedral sheets. The advantages of kaolinite clay mineral over others such as ilite and montmorillonite, is that kaolinite exhibits better pozzolanic reactivity and can become reactive at lower calcination temperatures [25], [26][21], [27], [28].

After the calcination of kaolinitic clays, metakaolin is formed which is essentially an amorphous alumina silicate ($Al_2Si_2O_7$), which can react with portlandite as a conventional pozzolan reaction to give calcium alumina silicate (C-A-S-H) and aluminate hydrate. In addition, the alumina can react with the limestone to produce carbo-aluminate hydrates. All these products fill space and contribute to the development of mechanical properties of LC3 [21], [24], [27]. Figure 1.6a-c shows different mechanical properties achieved by LC3 based concrete/mortar/paste from various

researchers and all these authors reported that LC3 systems are comparable to 100% Portland systems in terms of the compressive strength, resistance to chloride ingress, while ensuring better service life [29], [30].

a)

b)

c)
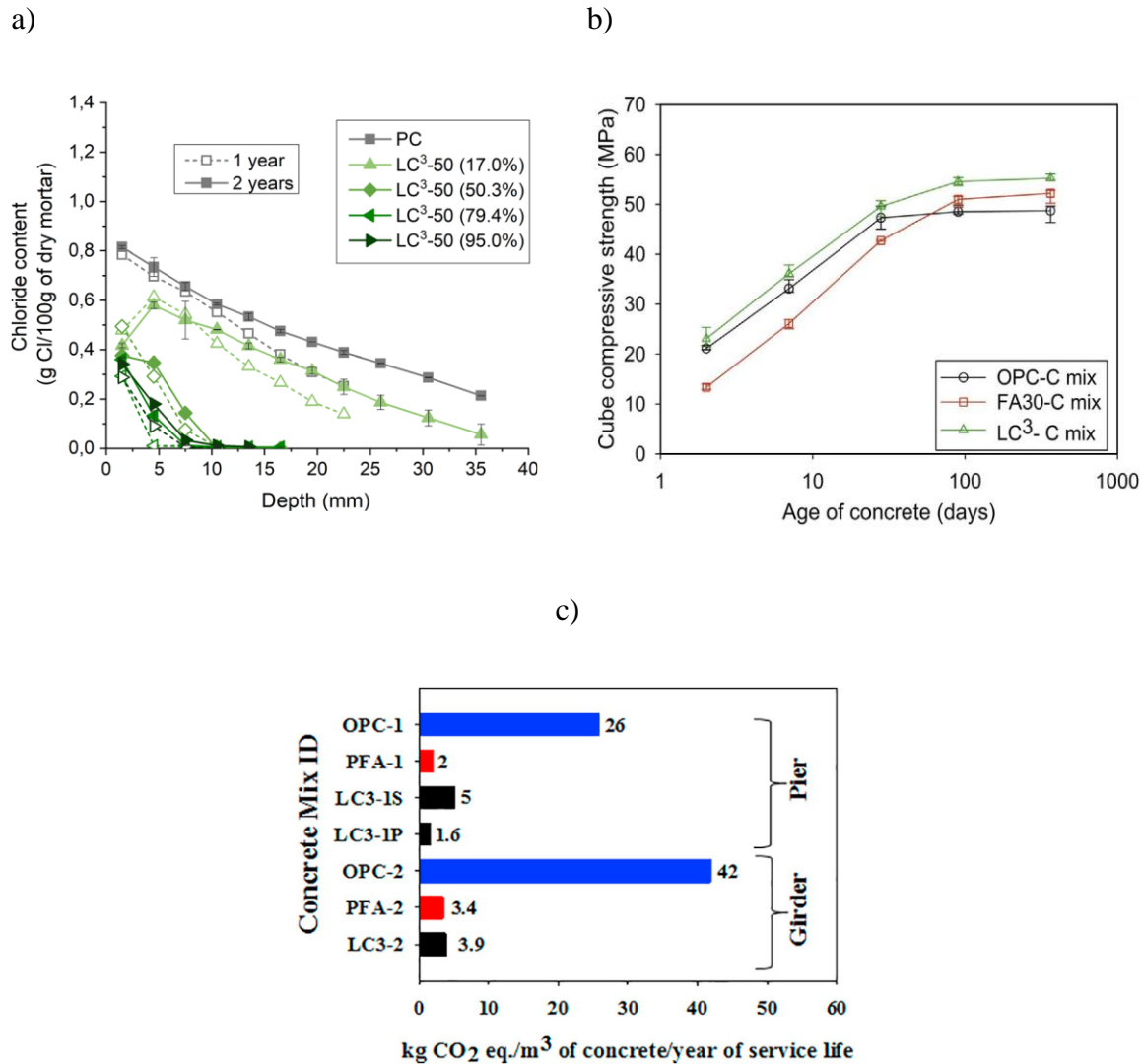
Figure 1.6 *a) Chloride penetration of LC3 system with various kaolinite content [31] , b) Evolution compressive strength of LC3 compared to Portland and Fly ash systems [29] , and c) Service life of LC3 system [30]*

From above figures, it is clearly evident that LC3 systems are recognized for their ability to resist chloride ingress. Furthermore, it is widely acknowledged within the construction industry that the

corrosion of reinforcement caused by chloride penetration, is a major financial burden for existing structures [32], [33]. As a result, the ability to resist chloride penetration is one of the most critical durability issues. Microstructural factors such as rapid hydration, pore structure, bulk and pore solution conductivity, chloride binding, etc. are largely responsible for better chloride penetration resistance in LC3 system. Each parameter's influence was reported in recent studies and major findings are given in the Table 1.1.

Table 1.1 *The influence of different parameters on chloride transport according to recent studies*

Parameter	Major observation	Ref
Pore structure	• The apparent chloride diffusion coefficient decreases with a decrease in critical pore entry radius. • There was no distinct relationship between pore structure parameter and apparent chloride diffusion, but in general the higher diffusion coefficients were found with higher critical pore diameter. • Greater reduction in critical pore diameter and threshold diameter which makes pore structure finer and hence enhanced the resistance against ionic/fluid transport. • The overall pore structure complexity (pore connectivity parameters, formation factor, and electrical tortuosity) was shown to be greater in the LC3 system, resulting in a decrease in chloride permeability. • High-grade clay refined pores in 7 days, however supersaturation was needed to hydrate further. Traditional hydration product growth is limited by small microstructure pores. Due to restricted space, hydration occurs later in the greater capillary region, increasing pore structure complexity and chloride ingress resistance. • Once the limiting critical pore entry radius is reached, metakaolin's reaction no longer makes monosulphate (AFm) phases.	[31][34] [29][30] [37][38] [39] [40][41] [42]– [44]
Bulk and pore solution conductivity	• LC3 system has less pore solution conductivity and the conductivity of the pore solution influencing the diffusion. • The apparent chloride diffusion coefficient was found to be increasing with total alkali contents	
Chloride binding	• Quantification of LC3 phase assemblage before and after NaCl exposure showed more carboaluminate AFm phases in LC3 systems, resulting in increased Friedel's salt. Chloride binding also involves physical binding to C–A–S–H, hence LC3 and PC systems have similar chloride ion binding. • In PC, most of the bound chloride goes to C–A–S–H, whereas in LC3 systems, most of it is chemically fixed in Friedel's salt.	

As stated previously, most of these investigations are conducted with high-quality clay containing greater than 40 percent kaolinite, and a few of them have utilized clay containing over 60 percent kaolinite. In this thesis, these clays are classified as high-grade clays. In general, the amount of portlandite was identified as limiting factor for the further hydration in LC3 [45]. However, there are some literatures nullify the effect of portlandite and they suggest the limited space to grow the hydration product after achieving the critical pore size [24][39]. Based on this, the low kaolinitic clays are expected to be a good choice for LC3 – at least better than Portland system. This is especially interesting for some regions, where the availability of this high-quality clay is very much limited. Consequently, the potential of clays with low kaolinite content in high performance concrete based on LC3 is identified as crucial field.

1.4 Research motivation, objectives, and layout of thesis

The basic motivation of this work identified as to address the availability of potential alternative binders in the South-East region of Europe (specifically Croatia and its surroundings) and the possibility to convert these materials into high-performance concrete with high chloride resistance and low ecological footprint. In the initial stage itself, the potential alternative binders were identified as clays. In total 15 different clays were collected for the entire study but only few of them performed comparably with Portland systems. Other than clays, fly ash was also used to compare the properties with lower-grade clays. Other than the introduction chapter, each chapter presents results and discussion of each objective of current research.

Chapter 2

Objective 1: *Identification and characterisation of the different alternative materials, mainly clays, fly ash, limestone, which can be used to prepare high-performance concrete.*

The major portion of the output and discussion are published as scientific article in *Case studies in Construction Materials.* After the identification of the materials, the next objective was to prepare high-performance concrete which consists of materials selected in the previous phase. Prior to make HPC, the design of concrete was targeting specific performance in terms of strength and chloride ingress. Targeted performance criteria were fixed as per a real-built structure in Croatia, Pelješac Bridge. This chapter investigates the mechanical and durability properties of high-performance mortars containing low-grade kaolin clay, fly ash, and limestone powder along with CEM I and CEM III mixtures. Six different mixes were prepared using binary and ternary binders. Compressive strength, chloride transport coefficients, and bulk conductivity were analyzed using mortar samples. The results demonstrate that all mixes, even those with low kaolinite content, can be used in high-performance cement systems.

Chapter 3

Objective 2: *Analysis of the influence of lower kaolinite content on the durability performance of concrete.*

The results and discussion are published in journal *Materials.* The importance of the kaolinite content was identified. This chapter investigates the impact of kaolinite content on the durability performance of Limestone Calcined Clay Cement (LC3). Two separate clays from East South-East Europe were used, one with 18% kaolinite and the other with around 41% kaolinite. The study measured compressive strength, chloride intrusion, electrical

conductivity, surface resistivity, and sorptivity index on concrete after 28 days, and investigated pore structure development in relation to kaolinite content. The results showed that kaolinite content had a moderate effect on compressive strength, but a considerable effect on durability indices.

Chapter 4

Objective 3: *To investigate the influence of different parameters on chloride ingress such as pore structure, chloride binding, bulk, and pore solution conductivity in LC3 cementitious system with lower kaolinite contents*.

This chapter focuses on the potential of using low-grade clays with less than 40% kaolinite content collected in Croatia. The objective is to analyse the effective diffusion coefficient of these clays and its dependence on various factors. The study concludes that low-grade clays have lower resistivity and greater chloride penetration resistance than traditional OPC. Pore structure and chloride binding capacities were found to be similar in LC3 and OPC systems. The number of smaller capillary pores was found to correlate well with the diffusion coefficient in all mixes.

Chapter 5

Objective 4: *Analysis and quantification of the effect of optimization of concrete mixture design on ecological footprint and service life of the structure using a performance indicator*. The findings and detailed discussion are published in a journal *Materials and Structures*. The aim of this chapter is to evaluate how much the changes in the concrete mix design, which enable carbon footprint reduction, are impacting mechanical properties and predicted service life of concrete structure. The efficient concrete mixture was analysed and benchmarked based on the proposed sustainability framework which considered the mechanical and

durability properties, service life and cost of each mixture. Alternative mixes achieved similar or higher sustainability indexes with lower amounts of cement, indicating that the bridge mix design was "over designed".

Chapter 6

Summarizes the main findings and concluding remarks based on the various objectives. In addition, this chapter includes a brief explanation for the future research about the same topic.

Hypothesis of the current work

The entire thesis work is formulated based on following hypothesis,

1. By using packing density models and synergy between locally available clay and limestone, it is possible to design high-performance concrete with lower CO_2 emission.

2. Substituting part of the cement with a combination of locally available clay and limestone can lead to better performing high-performance concrete in marine (chloride-rich) environment.

Chapter 2 Possibility of using local available materials for high-performance concrete

The objective of this study is to analyse the mechanical and durability properties of a high-performance mortars based on low grade kaolin clay and the effect of electrical conductivity and pore microstructure on the chloride penetration resistance. A total of six mixes were prepared with binary and ternary binders in which a high volume of cement was replaced by low-grade calcined kaolin clay, fly ash and limestone powder. The percentage of kaolinite in the clay used from the Southeast European region was less than 20%. The variations in compressive strength and chloride transport coefficient were analysed experimentally and related to the pore structure and electrical conductivity. Compressive strength, chloride migration and diffusion coefficients, and bulk conductivity were determined using mortar samples, while the pore size distribution was determined by mercury intrusion porosimetry (MIP) on hardened cement paste after 7,28, and 90 days of curing. To understand the capillary absorption of these mixtures, sorptivity indices were measured after 28 and 90 days. The experimental characteristics of the pore size distribution, such as mean pore entry radius ($d_{0.5}$), permeable porosity (P), capillary porosity (ϕ), and critical pore diameter (d_c), were

calculated using the cumulative data of the intruded volume as a function of pressure

obtained by MIP. In addition, the extrusion-intrusion curve was used to calculate the pore

entrapment fraction (α) and the degree of inter-connectivity of the pore structure. The

evolution of pore structure parameters was monitored for up to 90 days and their effects on

strength and chloride penetration were studied in detail. The results showed that all mixes

(even those with low kaolinite content) can be used in high performance cement systems and

the pore structure has a limited effect on chloride penetration.

2.1 Introduction

In recent decades, cement industry researchers have concentrated on developing suitable

cement additives (SCMs) to mitigate CO_2 emissions associated with cement manufacture.

The industry's aim is to manufacture blended cements with the lowest possible CO_2

emissions without sacrificing critical concrete characteristics like as strength and durability.

Recent studies have demonstrated that the cement industry cannot continue to rely on

conventional SCMs such as siliceous fly ash and blast furnace slag in the long run due to

their source depletion [20]. Therefore, there is a need for alternatives that meet both

quantitative and qualitative requirements for construction materials. Calcined clays,

especially in combination with limestone, could be a promising alternative combination to

reduce the environmental footprint of cement [21]. Due to better synergetic action between

clays, limestone and clinker, the higher level of replacement can be achieved in the so-called

LC3 systems (limestone-calcined clay cement) [46]. The primary raw material for LC3

production, in addition to clinker, is clay, which is abundantly available all over the world.

The presence of kaolinite in clays has been found all over the world, but the amount of

kaolinite present varies from one region to another, and this is a critical factor in their overall

performance. Clays containing a significant proportion of kaolinite have been shown to be highly pozzolanic when calcined between 700℃ and 850℃ [47]. The hydration kinetics of limestone-calcined clay cement were indeed significantly influenced by the kaolinite content, which affects the mechanical and chloride transport properties of the concrete [24][31]. However, high grade kaolin clays are not easily available everywhere or they have a more favorable application. One of the possibilities to consider is using low grade kaolin clays, more easily available in sufficient quantities for cement industry. Notwithstanding, recent developments in LC3-based concrete have shown that an intermediate level of kaolin clay may be an appealing option, particularly given its widespread availability [45]- [41].

According to previous research, concrete containing SCMs has a higher resistance to chloride penetration, which is primarily due to the improved pore structure[41]-[48]. Halamickova et al., reported that the chloride diffusion coefficient varies linearly with critical pore entry radius as determined by the Mercury Intrusion Porosimetry (MIP) technique [49]. Although the MIP approach has several drawbacks, it is still a useful tool. One of the major drawbacks of commercial porosimeters is that mercury does not penetrate the very fine pores, which range in size from 1 nanometer to 3 nanometers [50]. In addition, the "ink-bottle" impact and the gel's segmentation of capillary pores can result in an overestimation of fine pores and an underestimation of larger capillary pores [50][51]. Nevertheless, the porosity obtained by MIP is a permeable porosity that covers most of the interconnected pores that have a direct impact on the durability of concrete [52]. The intrusion-extrusion cycle in MIP can also indicate the presence of entrapped pores, which is expressed as a network of discontinuous pores [53], which is expressed as network of discontinued pores. Understanding the porosity and pore size distribution of cement-based materials with various SCMs can be used to

endorse chloride penetration. However, Shiyu et al. found that the electroneutrality of the pore solution and the surface properties of the hydration product influence the chloride transport in ternary blended cementitious systems more than their pore structure [54]. Additionally, electrical resistivity had an impact on chloride transport in cementitious systems, particularly when it came to the movement of chloride by electrical potential [55]–[59]. The approach fully excludes the impacts of other negatively charged species in the pore solution, making it the most disadvantageous of the electrically accelerated processes[60].

The primary goal of this study is to determine the endurance of a cementitious system composed primarily of low-grade kaolin clay in harsh coastal conditions. A low-grade kaolin clay (containing 20% kaolinite) and limestone were combined to produce a mortar with a high cement substitution level. The chloride penetration resistance and compressive strength of this mortar were compared to those of mortars with a similar degree of cement substitution by fly ash and limestone, as well as to those of reference mortars based on pure clinker cement (CEM I) and blended cement with slag (CEM III/B). Furthermore, this study attempted to demonstrate how pore structure parameters affect compressive strength and chloride penetration. Also, the influence of conductivity on chloride penetration and movement in blended mixes is discussed. The mechanical properties and durability of each mix were found to be related to the pore structure, while the chloride transport coefficients were found to be related to the bulk conductivity and surface resistivity. The findings of this study contribute to a better understanding of the effect of pore structure on chloride transport, particularly in low-grade limestone-calcined clay cements.

2.2 Materials and methods

2.2.1 Binder composition

Six mixes were prepared for this study, where Portland cement (CEM I 42,5R) was used as the primary binder. Binary binder systems were prepared with 70% CEM I and 30% SCM, with mixes labelled FA30 (mix with 30% fly ash) and CC30 (mix with 30% calcined clay). Ternary binder systems were prepared with 70% CEM I, 30% SCM and 15% limestone, with mixes labelled FA30LS15 (mix with 30% fly ash and 15% limestone) and CC30LS15 (mix with 30% calcined clay and 15% limestone). Additional to these mixes, CEM III/B (36-65% replaced with slag) was also used to compare the properties of blended binder systems with commercially available binders. Table 2.1 and Table 2.2 show the chemical composition of each constituent and mineralogical components of SCMs respectively. More information about these materials, such as reactivity obtained using isothermal calorimetry and bound water test can be found in previous paper [61]. Figure 1.1 illustrates Scanning Electron Microscopy (SEM) images of fly ash and clay to understand the surface morphology of the materials and Figure 2.2 shows the particle size distribution of used materials. The kaolinite content of calcined clay was 17% by thermogravimetric analysis [62]. All SCMs were previously dried at 60 °C for 24 h and ground in disc mill for 30 seconds. In the case of calcined clay, the dried ground raw clay was calcined in a furnace at 800 ± 20 °C for one hour and preparation of clay followed by the protocol [27]. All mortar mixtures were prepared using crushed sand (0-4 mm) and water-binder ratio of 0.5.
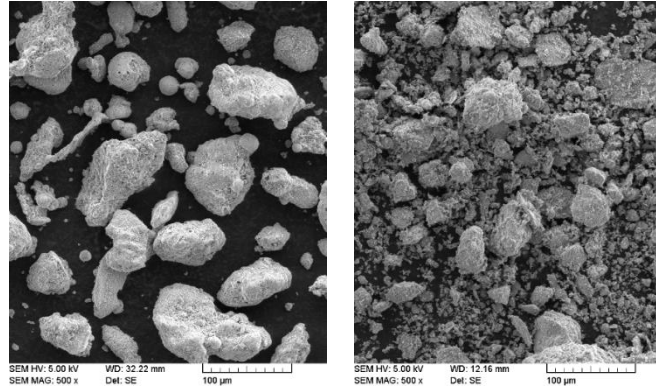
Figure 2.1 *SEM images of fly ash (left) and calcined clay (right)*

Table 2.1 *Chemical composition and particle size distribution of materials used in the study.*

Component	CEM I	CEM III	Fly ash (FA)	Calcined clay (CC)	Limestone (LS)
CaO	63.19	31.28	11.52	1.74	71.59
SiO_2	19.51	38.83	53.28	49.80	20.21
Al_2O_3	4.21	10.34	19.11	17.04	4.32
Fe_2O_3	2.85	1.32	9.05	5.80	1.43
MgO	0.85	9.73	2.78	1.42	1.69
Na_2O	0.20	0.87	0.26	0.84	0
K_2O	0.48	1.82	1.51	2.00	0.15
TiO_2	0.12	0.31	0.52	0.75	0.52
P_2O_5	0.45	1.55	0.36	0.29	0.42
SO_3	2.3	0.01	1.48	0.06	1.48
D_{10}, μm	0.32	0.45	1.55	4.03	3.43
D_{50}, μm	9.95	12.71	15.24	10.72	18
D_{90}, μm	50	58.85	72.68	24.79	63.82

Table 2.2 *Mineralogical data of clay and fly ash used in this study.*

Component	Fly ash (FA)	Calcined clay (CC)
Quartz	5.4	21.7
Muscovite	-	27.3
Mullite	2.2	-
Vermiculite	-	2.4
Illite	-	1.3
Hematite	0.3	-
Amorphous content	89.3	14.3
Loss of Ignition (%)	8.22	7.60
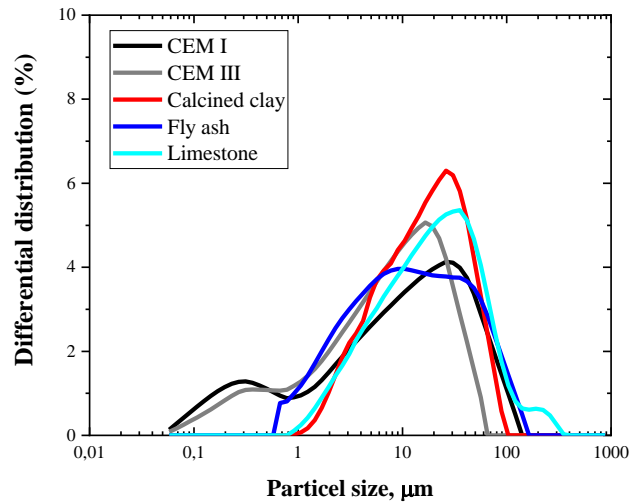
Figure 2.2 *Particle-size distribution of various materials used in the study.*

The mortar mix was prepared and fresh state properties (flow, temperature, density and air content) tested in accordance with EN 196-1 [63]. The mortar specimens were cast in a prismatic mould (40 × 40 × 160 mm) for tensile and compressive strength testing, and a cylindrical specimen with a diameter of 100 mm and a height of 200 mm was prepared for chloride migration and diffusion test. Cylindrical specimen with a diameter of 70 mm and height of 100 mm were prepared for sorptivity indices and water-filled porosity test. After 2, 7, 28, and 90 days of curing, compressive strength tests were performed, and chloride tests

were performed after 7, 28, and 90 days of curing. Sorptivity test was performed after 28 and 90 days of curing. All specimens were kept in a moisture-controlled room for curing until the specified time of testing. Three specimens were taken for compressive strength, chloride transport coefficients, bulk conductivity, surface resistivity, and sorptivity and pore structure determined on mortar samples.

2.2.2 Chloride transport coefficients

The resistance to chloride penetration was evaluated by both migration and diffusion experiments according to standards NT BUILD 492 [64] and NT BUILD 443 [65], respectively. In both tests, the cylindrical specimens were cut into three specimens with thickness of 50 mm. All the specimens were preconditioned by saturated Ca $(OH)_2$ solution in vacuum for 24 hours. Following the procedure described in standard NT BUILD 492, the non-steady state migration coefficients were calculated based on measured chloride penetration depth under forced movement (by external potential) of chloride ions across the mortar specimen. In this method, a quick qualitative assessment regarding chloride ingress resistance can be obtained. In migration test, after exposure to prescribed external potential, specimens were cut diametrically after the test duration and sprayed with the silver nitrate solution to measure the depth of penetrated chlorides. The equation used to calculate the non-steady state chloride migration (D_{nssm}) coefficient is given below:

$$D_{nssm} = RT/zFE.(x_d - \alpha\sqrt{x_d})/t$$

(2.1)

where x_d is the average measured depth of chloride penetration after the test duration, while other parameters were taken from the NT BUILD 492.

In the diffusion test, the specimens were coated with epoxy resin on all sides except the bottom one for chloride exposure. After coating, the specimens were left another 24 hours for epoxy to fully dry, and then fully immersed in 16.5% NaCl solution for 35 days. After 35 days, the profile grinding (depths were taken according to NT BUILD 443) was performed to obtain powder for chemical analysis. The total chloride content in the powder was determined using potentiometric titration method described in standard EN 14629-2007 [66]. Thereafter, the effective chloride diffusion coefficients (D_E) were determined by fitting the total chloride contents in second Fick's law according to NT BUILD 443:

$$C\ (x,t) = C_s - (C_s - C_i\ ).\ \text{erf}\ (x\ |\ \sqrt{(4D_E\ t)}) \tag{2.2}$$

where $C(x,t)$ is the measure chloride content at depth (x) and exposure time (t). The values of effective chloride diffusion coefficients could be extracted after fitting the measured chloride contents. Additionally, the relation between non-steady state chloride migration coefficient and effective diffusion coefficients were determined.

2.2.3 Bulk conductivity and surface resistivity

The initial current values from chloride migration experiment were used to calculate the bulk conductivity of the specimen according to ASTM C 1760 [67] according to the following Equation:

$$Conductivity, \sigma = 1273.2\ .\ I_i/V.\ L/D^2 \tag{2.3}$$

where 'I'$_i$ is measured as initial current by imposing voltage of 'V' to the specimen and other parameters were taken from the standard. The bulk resistivity of the pore solution was calculated as the reciprocal of the conductivity obtained from Eq. 2.3.

Chapter 2

Possibility of using local available materials for high-performance concrete.

The surface resistivity of each mixture was determined by Wenner 4-probe resistivity meter on the sides of cylindrical specimens, which was used to determine the chloride transport coefficients [68]. The measurements were taken in saturated condition at four different locations of each specimen. A total of 12 readings were taken and the average reported as surface resistivity.

2.2.4 Sorptivity

The sorptivity and water-permeable porosity of each sample was determined based on South African Durability Index Manual [69]. After the curing, the specimen was dried at 50℃ for 7 days and then stored for 4 hours in a desiccator. Specimens were placed on the tray, which contains saturated Ca (OH)$_2$ solution. Specimens were supported by wooden rollers and the level of solution was limited to 2 mm from the surface. The weight of specimen was noted down after 3, 5, 9, 12, 16, 20, and 25 minutes. After the weight estimation, the samples were conditioned in saturated calcium hydroxide solution for one day. The calculation of sorptivity index was performed using Eq. 2.4

$$S = (F \times d)/(M_{sv} - M_{S0})\qquad(2.4)$$

where 'F' is the slope of the best fit line between mass gain and square root of time, average thickness 'd', M_{sv} and M_{S0} are the vacuum weight and initial weight of samples.

2.2.5 Pore structure parameters using mercury intrusion porosimeter (MIP)

Mercury intrusion porosimetry (MIP) with up to 400 MPa was used to measure the pore structure parameters for each mix. The pore entry radiuses were calculated by combining the results from Pascal 140 and Pascal 440 instruments, assuming a contact angle of mercury as 140^0. For MIP, cement paste specimen with the same mixture composition was prepared and cured in humidity chamber for the desired curing periods. After curing, the hydration was

stopped using solvent exchange method with isopropanol immersion for 7 days. Subsequently, the samples were dried under vacuum for 48h. During the MIP test, the pressures were transferred to the pore entry diameter using Washburn equation[32]. The hardened properties of cement based systems mostly depend on the volume of capillary pores, *i.e.* pores in the range of diameter between 10 nm to 10 µm [33]. The critical pore entry diameter (d_c) represents the grouping of the largest fraction of interconnected pores in cementitious system. Critical pore entry diameter is corresponding to the peak in the differential pore volume curve indicating the pore size corresponding to the maximum volume intrusion. After the test, total cumulative and differential curves were obtained for each sample. Capillary pore volume (ϕ) of a mixture was evaluated as the total pore volume in the range of 10 nm to 10000 nm pore diameter [35]. The critical pore entry diameter (d_c) was determined as the diameter at the maximum value of differential pore volume in distribution curve. Mean pore entry diameter ($d_{0.5}$) was evaluated based on the following equation [70],

$$\ln d_{0.5} = (\sum_{i=1}^{n} \ln \llbracket v_i\, d_i \rrbracket)/(\sum \llbracket V_i \rrbracket) \tag{2.5}$$

where, for the continuous intrusion curve divided into n discrete radii ranges, v_i is the incremental intrusion of mercury corresponding to i^{th} radius range represented by the mean radius d_i. Pore entrapment can be determined from the intrusion-extrusion curves of MIP. The pore entrapment fraction α is defined as ratio of the pore entrapment volume and the total intrusion volume, Eq.2.6

$$\alpha = (Pore\ entrapement\ volume)/(Total\ intusion\ pore\ volume) \tag{2.6}$$

Pore entrapment fraction explains the complexity of pore structure. Larger pore entrapment indicates the higher complexity in pore structure, and pore distribution with high unevenness [34].

2.3 Results

2.3.1 Evolution of mortar compressive strength

All mixtures were made with a water-to-binder ratio of 0.5. Table 2.3 shows the fresh properties of all mixtures. In their fresh state, mixes have similar consistency, density, and air content. The mixture with limestone-calcined clay has a smaller flow diameter, which is in accordance with the previous studies [35]. In general, fly ash improves cementitious system flow, but in this case, the flow was reduced. Fly ash used in this study has a lower percentage of spherical particles, as can be seen in the SEM images (Figure 2.1). Furthermore, the fly ash has a higher loss value of loss of ignition (8.22%). Fly ash used came directly for the industry, material was not pre-treated or selected, and it consists of a high amount of unburned carbon. The unburned carbon potentially consumed more water from the system and caused the low flowability in this system [36].

Table 2.3 Fresh properties of the mixes used in this study.

Mix	Flow diameter, mm	Temperature, ^{0}C	Density, kg/m^3	Air content, %
CEM I	169.5	17.4	2353.7	2.6
CEM III	175	17.3	2320	2
FA30	156	19.6	2270	2.7
CC30	165	19.5	2325	2.4
FA30LS15	162.5	18.8	2272	2.4
CC30LS15	150	20.7	2320	2.1

Chapter 2

Possibility of using local available materials for high-performance concrete.

After 2, 7, 28, and 90 days of curing, the compressive strength of the mortar mix was evaluated, and the results are shown in Figure 2.3. The initial strength of ternary mixes was lower than CEM I mix, which was expected due to the slow reactivity and dilution effect of limestone powder. In the case of calcined clay, lower initial strength was also anticipated since used clay has a relatively low amount of kaolinite, which directly influences the strength development [24]. After 7 days both fly ash and calcined clay mixes improved their strength. The highest increase for CC30 mix was achieved between 7 and 28 days, while FA30 mix gained comparable strength after prolonged (after 90 days) curing.

The pattern of strength gain in the ternary binder system was comparable to that of the binary system, although the final obtained strength was lower. When compared to fly ash mixtures, calcined clay mixes with and without limestone had higher strength after 28 days, but the tendency reversed with longer curing. Finally, even though FA30LS15 and CC30LS15 contain just 55% cement, they reached a compressive strength of 65-70 % of that of CEM I mortar after 90 days of curing. Despite the lower clinker percentage, the synergistic effect of limestone and alumina in SCMs is clearly responsible for the comparable performance of ternary mixes [37], [38]. CEM III mix showed the lowest strength at all curing ages compared to CEM I and binary mixes, but a comparable compressive strength at all ages of curing to that of ternary mixes. Unlike most fly ash systems, the present one had the same strength as CEM I after 7 days. This was clearly due to the higher lime content of fly ash used [39].
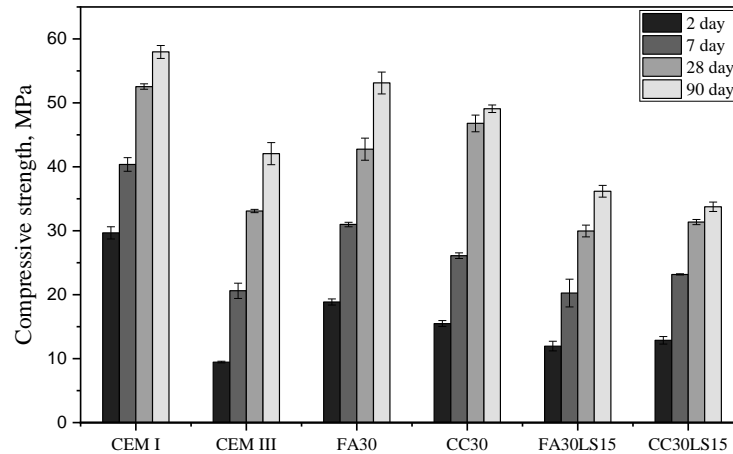
Figure 2.3 *Evolution compressive strength of all mixes*

2.3.2 Evolution of chloride transport coefficients

Chloride diffusion and migration coefficients were determined for better understanding of the chloride transport. The non-steady state chloride migration coefficients of each mix evaluated after 7, 28, and 90 days of curing are presented in Figure 2.4. Compared to the CEM I specimen, the addition of fly ash and calcined clay reduced the chloride migration coefficient by 25-30% after 28 days and approximately 30-35% after 90 days in binary binder systems. After 7 days of curing days, ternary blends showed very high values of migration coefficient, which is correlated to their high electrical conductivity at early ages [40]. However, after 28- and 90-days chloride migration coefficients were significantly lowered for CC30LS15 (lowered 56% after 28 days and 83% after 90 days) and FA30LS15 (lowered 54% after 28 days and 80% lowered after 90 days) mixes. Thus, the chloride penetration resistance significantly improved ternary mixes after 90 days, even with very low kaolin clay. CEM III specimen exhibited the highest chloride penetration resistance among all the mixes despite of lower compressive strength.
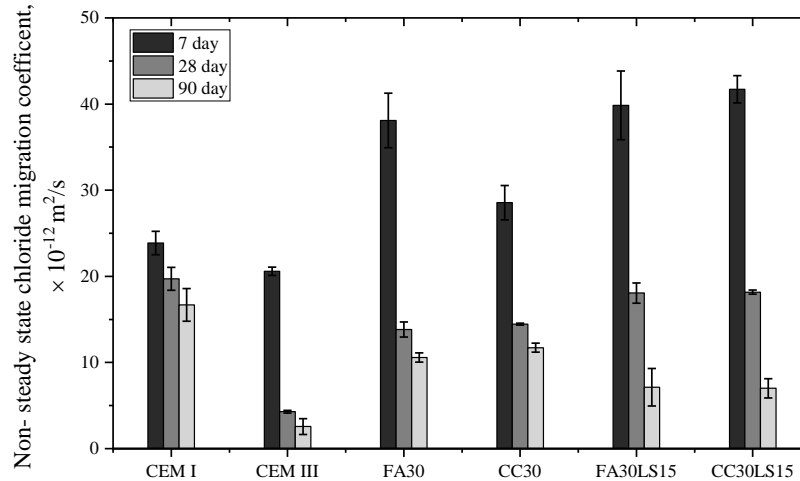
Figure 2.4 *Evolution of non-steady state chloride migration coefficient of all mixes after 7, 28 and 90 days of curing*

The effective chloride diffusion coefficients were also determined based on chloride profile, and the results are shown in Figure 2.5 and 2.6. The chloride content of eight layers (0.5 mm from the exposure surface to 22.5 mm) were measured after the mortar specimen thoroughly immersed in sodium chloride solution for 35 days. A total chloride content of each layer was determined to evaluate the chloride diffusion coefficient at different curing ages.
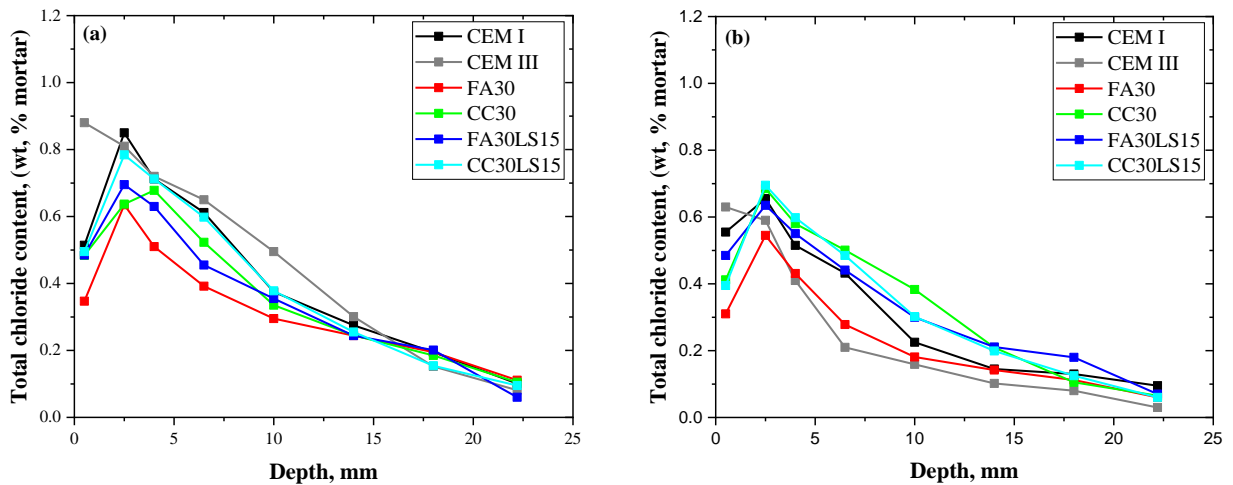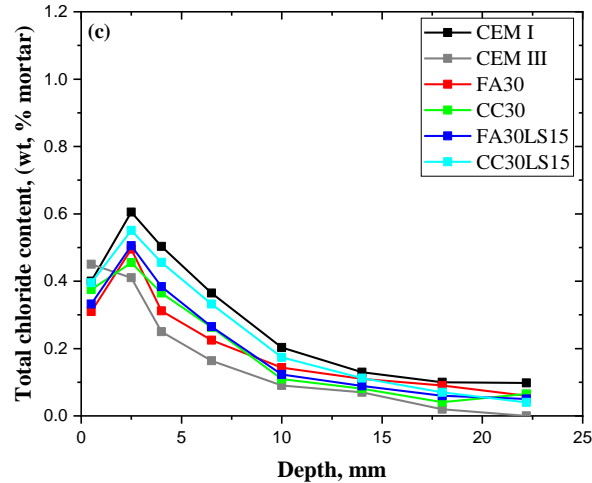
Figure 2.5 *Chloride profile of different mixes after 7 days (a), 28 days (b), and 90 days (c)*
in 16.5 % NaCl solution

Chloride migration coefficients are much higher than diffusion coefficients at all ages. The higher values of migration might be due to the electrical gradient caused by ions, the interaction between ions and cementitious phases, the dissolution of the cementitious matrix, chemical deposition on pore walls and combined effect of all these factors [41].
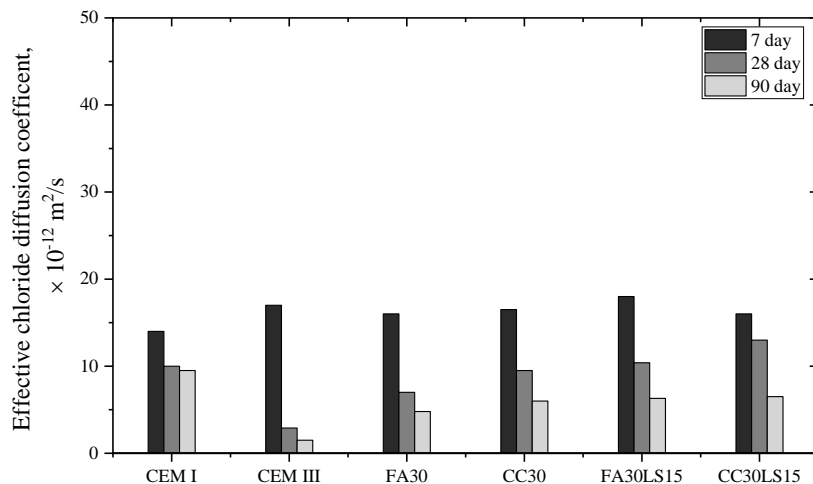
Figure 2.6 *Effective state diffusion coefficients of all mixes after 7, 28 and 90 days of*
curing

Chapter 2

Possibility of using local available materials for high-performance concrete.

The CEM I mix showed higher rates of chloride ingress compared to all composite mixes at 28 days. This can be attributed to lower porosity and higher ionic resistance of binary and ternary blended mixes [42]. Among the ternary and binary systems, the lowest chloride diffusion coefficient was observed for fly ash mix after prolonged curing. In overall, CEM III specimen showed lowest chloride diffusion coefficient similar to chloride migration.

2.3.3 Electrical conductivity and surface resistivity

Figure 2.7 shows the conductivity variation of each binder systems at different ages. The trend is clearly attributed to the chloride migration property of each mix. All of the binder systems had high conductivity at 7 days and then decreased as the curing time increased. After 90 days, CEM III has a significant reduction in conductivity (nearly 85%), which is supported by the results of chloride migration.
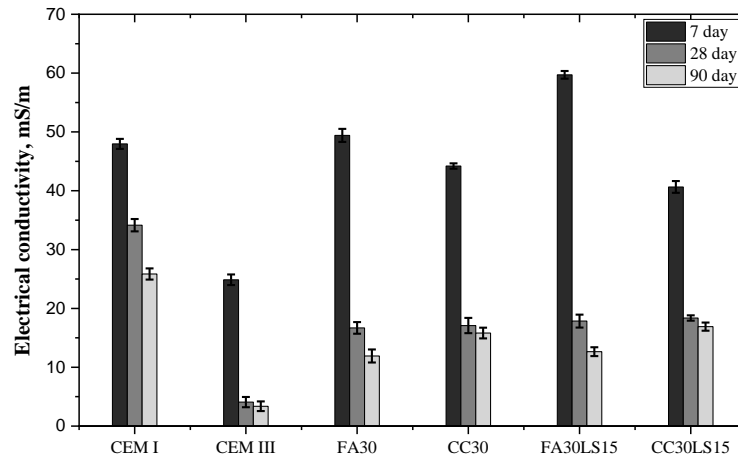
Figure 2.7 *Evolution of electrical conductivity of all mixes after 7, 28 and 90 days of curing*

Figure 2.8 depicts the surface resistivity of each mixture measured using Wenner probe. CEM III showed the highest surface resistivity among all mixtures and all blended mixes showed better resistance than CEM I. The surface resistivity reached similar range of values (30-35 k.ohm.cm) for all blended mixtures at 90 days.
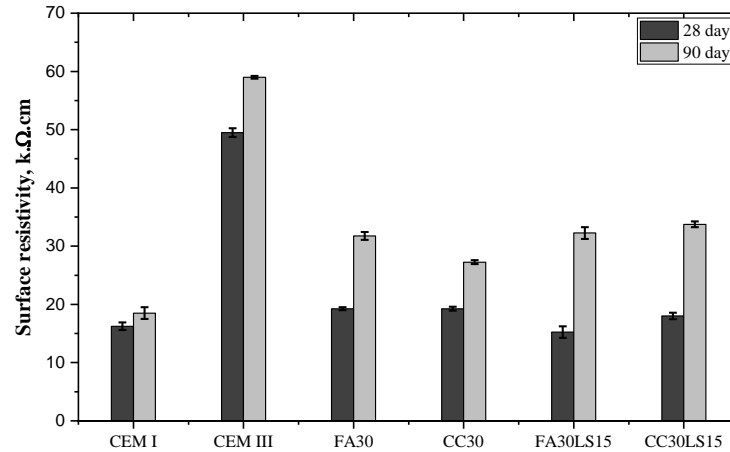
Figure 2.8 *Surface resistivity of all mixture after 28 and 90 days of curing*

2.3.4 Sorptivity

The absorption rate, which is attributed to the sorptivity index, is commonly used to evaluate

the capillary absorption of cementitious systems. The concrete can be classified based on its

soprtivity values according to the limiting values proposed by Alexander et al. [43].
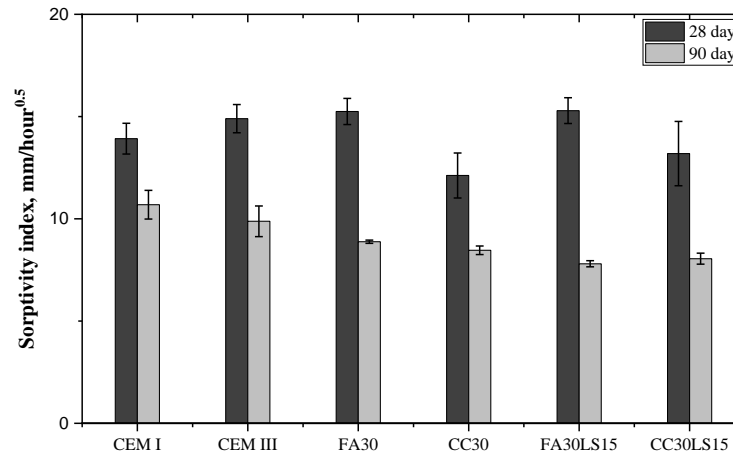
Figure 2.9 *Sorptivity index of all mixes after 28 and 90 days of curing*

Figure 2.9 illustrates the sorptivity indices of all the mixtures. After 28 days of curing, the

mixtures with calcined clay showed better soprtivity index than other mixes, whereas the

ternary blended showed the least absorption tendency after prolonged curing. The addition

of fly ash and calcined clay improved the absorption resistance of moisture, especially with

combination of limestone powder.

2.3.5 Evolution of pore structure

Figure 2.10 shows the pore size distribution of each specimen after 7, 28, and 90 days of

curing, respectively.
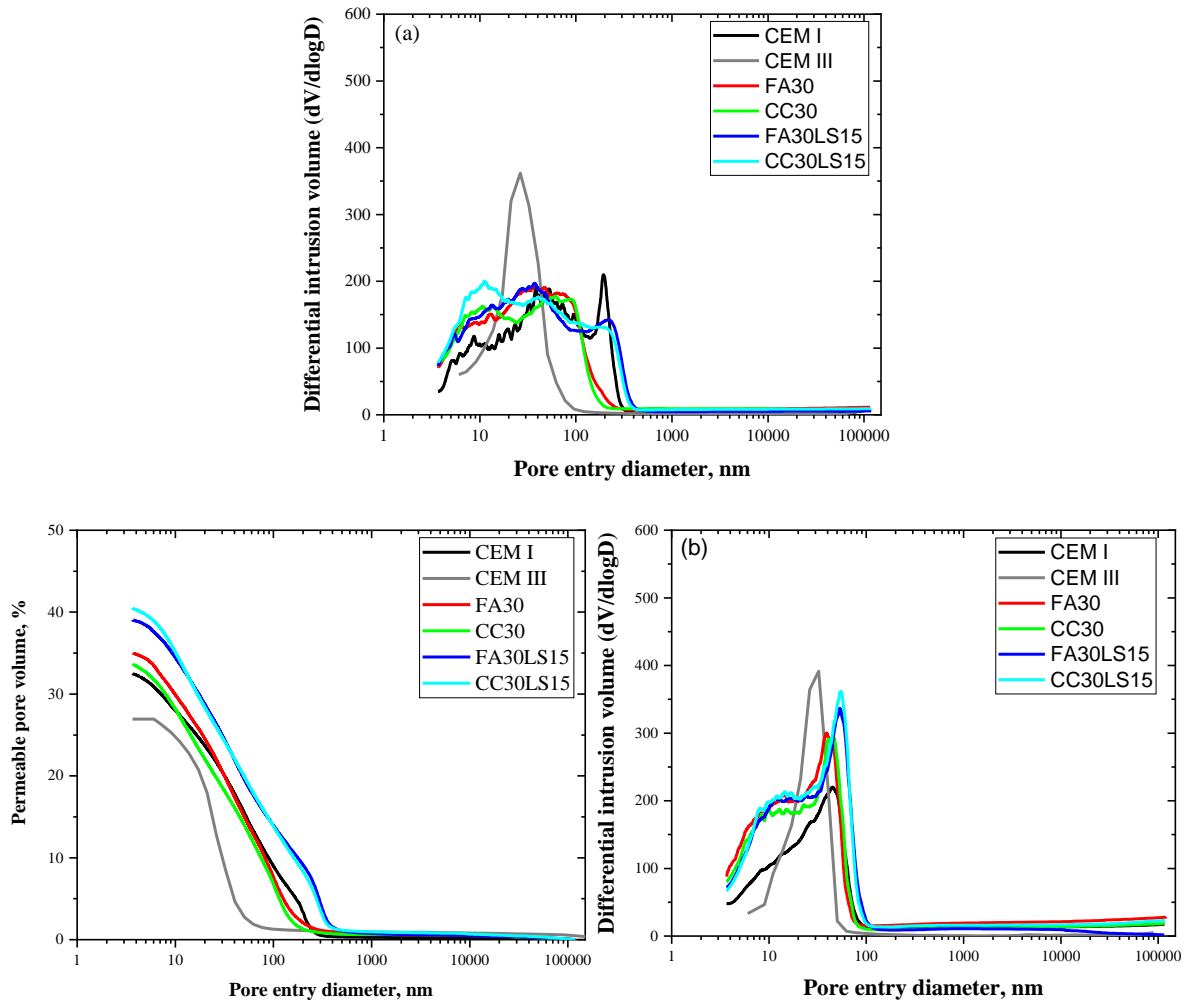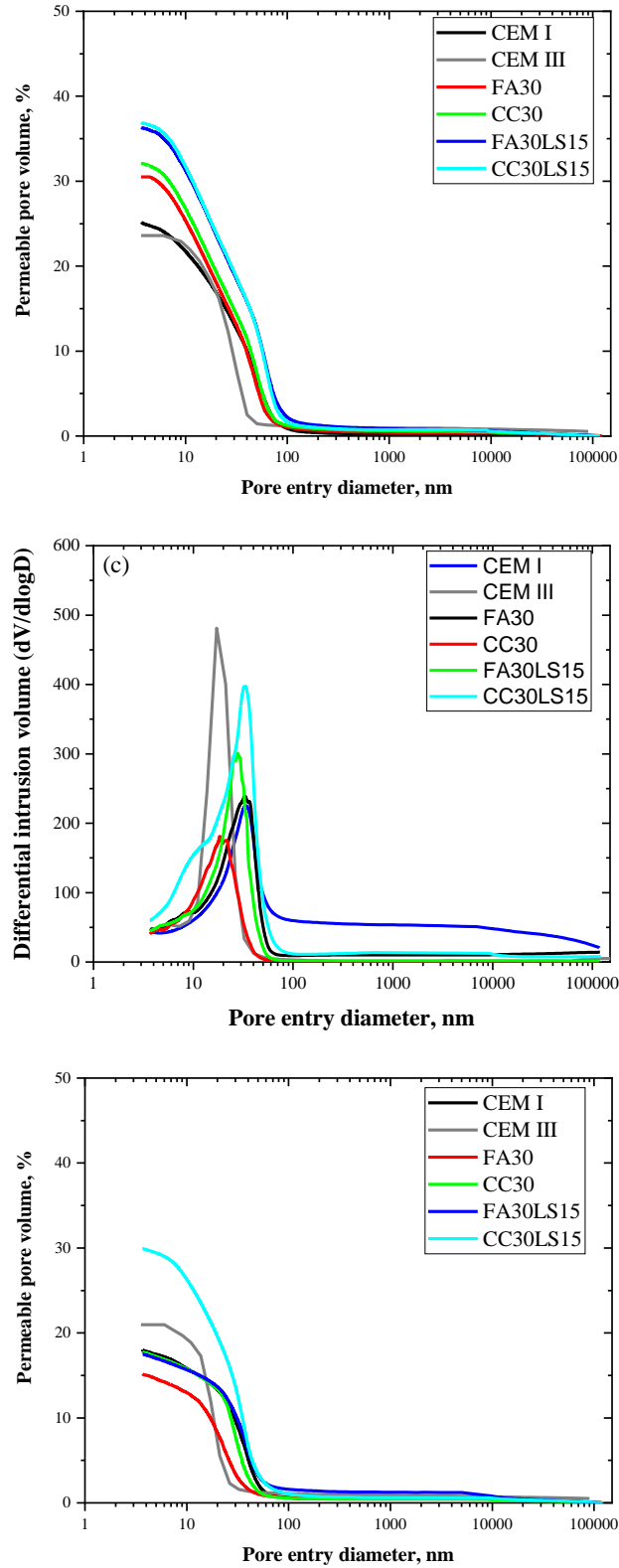
Figure 2.10 *Differential intrusion curve after a) 7-days, b) 28-days, and c) 90 days curing.*

The differential intrusion curves illustrate that critical pore size changed with curing time, and that the total pore size range was steadily reduced with prolonged curing. While considering the differential intrusion curve, binary and ternary mixes showed better refinement of pore structure parameters compared to CEM I. The differential curves are getting more narrowed in calcined mixes and thus a finer critical diameter was measured compared to other mixes. The capillary pore volume, mean pore entry diameter, critical pore entry diameter, and pore entrapment fraction were determined from MIP curves and all the data are given in Table 2.4. It can be observed that the parameters describing pores were significantly reduced from 7 days to 90 days of curing for all mixes. On the other side, parameters which can be used to describe the absence of inter-connectivity of pores (pore entrapment fraction) increased with prolonged curing.

Table 2.4 Pore strucutre paramerters from MIP analysis

Mix	Age, days	Permeable porosity, %	Median pore entry diameter ($d_{0.5}$) nm	Critical pore entry diamter (d_c) nm	Capillary pore volume, %	Pore entrapment fraction (α)
CEM I	7	32.5	23.42	23.22	27.8	0.46
	28	25.14	15.93	19.35	20.93	0.54
	90	18.03	15.73	16.535	15.34	0.62
CEM III	7	26.96	10.71	13.37	23.40	0.41
	28	23.59	11.26	12.68	21.12	0.43
	90	20.1	8.48	8.99	18.13	0.68
FA30	7	35.01	19.93	32.54	29.43	0.53
	28	30.49	12.98	19.62	25.01	0.57
	90	15.17	10.63	9.42	12.55	0.74
CC30	7	33.65	18.56	31.19	27.58	0.49
	28	32.1	13.50	22.91	26.34	0.53
	90	15.8	14.30	13.73	12.42	0.73
FA30LS15	7	39.04	25.41	39.85	33.98	0.50
	28	36.31	16.30	27.78	30.66	0.55
	90	17.56	17.05	14.48	15.13	0.78
CC30LS15	7	40.48	24.65	27.23	34.46	0.46
	28	36.9	16.13	20.8	31.16	0.51
	90	25.99	13.97	15.42	17.69	0.75

2.4 Discussion

In the first part of the discussion, different durability parameters are compared to understand, eliminate, or highlight their impact on chloride diffusion. Among correlations which are analyzed are correlation between chloride migration and diffusion coefficients, and the impact of electrical resistivity and sorptivity on these coefficients. In the second part of the discussion, parameters of pore structure are correlated to mechanical and durability properties of tested mortars, to analyse whether the differences in properties of blended systems can be explained by the pore structure.

2.4.1 Relation between different durability properties

a) Relation between chloride migration and diffusion

The migration coefficients were much higher than the diffusion coefficients across all tested ages and for all mixes, with similar trend reported in previous studies [44]. Figure 2.11 shows the correlation between chloride migration and chloride diffusion for all tested mixes, with a coefficient of determination $R^2 = 0.94$.

$$D\_nssm = 1.86 \times D\_E$$
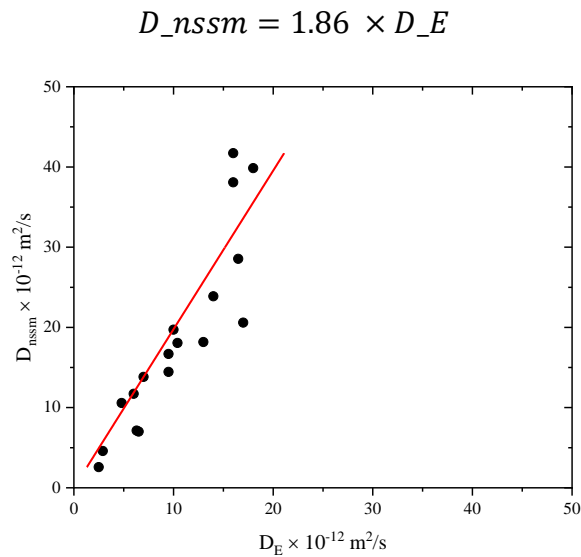
Figure 2.11 Relation between chloride migration and diffusion

The migration coefficients and diffusion coefficients for tested mixes are strongly correlated, but with chloride migration values being 1.86 times higher than the values of chloride diffusion. This is especially evident in early ages of blended mortars, where the values of chloride migration coefficients are significantly higher than those of chloride diffusion. The higher values of migration coefficients than diffusion coefficients could be explained by the single species theory assumption in the calculation, which is not taking into the account the effect of other charged ions in the pore solution on chloride penetration [60]. Therefore, despite the obvious advantage of the rapid method for testing chloride migration, the

migration coefficients obtained will be an over-estimation of chloride ingress compared to

the coefficients obtained by diffusion test. These types of correlation were developed in

various studies, and are especially useful to determine the diffusion coefficients and the

service life [45]. For instance, the relation between design values of the chloride diffusion

coefficient and the laboratory-measured values were used to evaluate the durability

performance during the construction of Hong Kong–Zhuhai–Macau sea link project [46].

   b) Relation between bulk conductivity / surface resistivity and chloride transport

      properties

The chloride migration process in cementitious system is mainly influenced by the potential

drop across the specimen, meaning that the electrical conductivity and resistivity of mortar

play a significant role. Figure 2.12 shows the correlation of chloride transport coefficients

with corresponding bulk conductivity and surface resistivity, taking into account values at

28 and 90 days of curing.
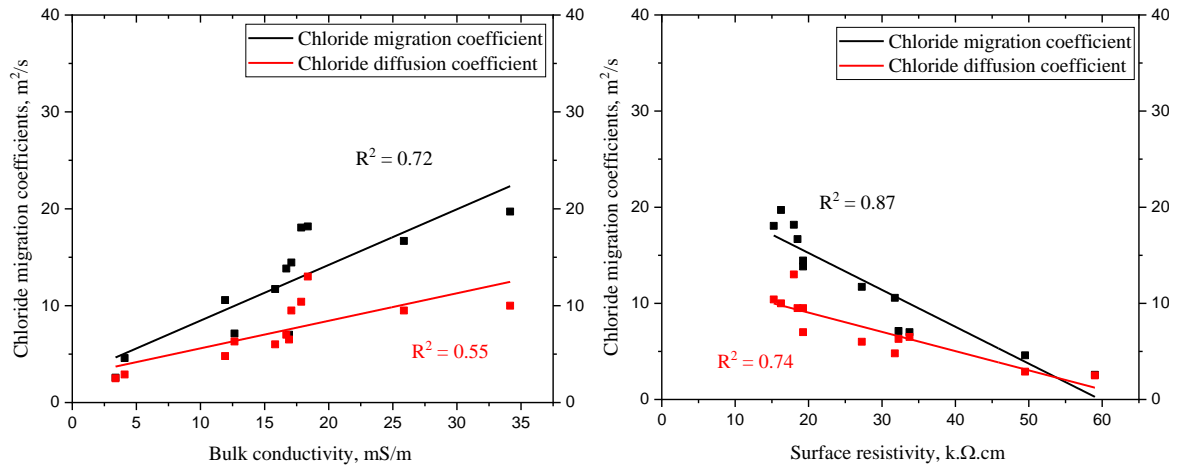
Figure 2.12 *Linear regression analysis of bulk conductivity and surface resistivity against chloride migration and diffusion coefficients*

From the Figure it can be observed that the chloride migration coefficients are strongly influenced by the bulk conductivity and surface electrical resistivity of the mortar [47], [48], which is less of a case with chloride diffusion coefficients. In a cementitious system, the electrical conductivity is mainly determined by the pore solution chemistry. The ion precipitation in the pore solution strongly varies with binder composition [49], and it is very difficult to decouple the effects of pore structure and resistivity of a cementitious system on chloride penetration [60].

  c) *Relation between sorptivity and chloride transport properties*

Capillary absorption plays a significant role in the diffusion process, since one of the mechanisms of chloride transport is convection. Because SCMs are present in binary and ternary mixtures, their sorptivity indices are lower. The addition of SCMs to the system provided an additional pozzolanic and filler effect, resulting in a significant reduction in chloride absorption [50]. Furthermore, mortar with high sorptivity index would allow more chlorides to penetrate, especially in the surface layer of specimen. Figure 2.13 shows the

correlation between sorptivity indices and surface chloride content obtained after exposure

of specimens according to NT BUILD 443 tests.
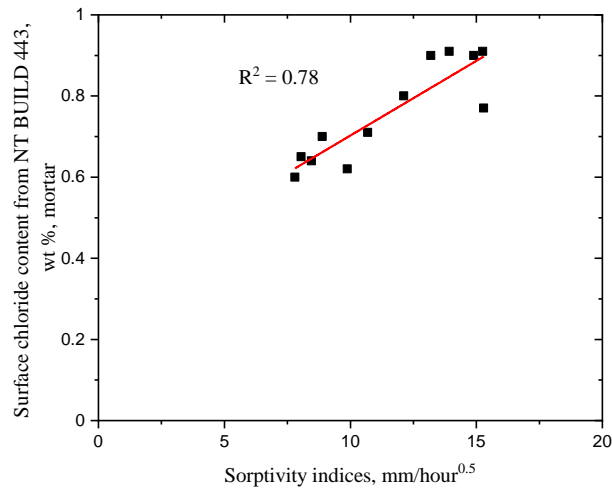
Figure 2.13 Correlation between sorptivity indices and surface chloride content from NT

BUILD 443

The correlation clearly shows that mortars with the higher sorptivity have a higher chloride

intake from solution. Due to the capillary suction, concrete can immediately absorb the

solution (containing chloride ions) from the environment, increasing the surface chloride

concentration and therefore increasing chloride penetration [85]. However, chloride contents

from other depths were not found to be correlated to the sorptivity index in the binary/ternary

systems, rather to the physical and chemical characteristics of the binder.

2.4.2 Implication of pore structure on mortar properties

a) Compressive strength and pore structure

In general, increasing porosity reduces strength of cementitious materials, but the magnitude

of this effect is dependent on pore size, shape, and distribution [52]–[55]. It was previously

established that the strength of cement-based materials is directly proportional (1-permeable

porosity(P)) and inversely proportional to square-root of median pore entry diameter ($d_{0.5}$)

[52][70][56]. Therefore, the relation can be written as:

$$\sigma = KC\ ((1 - P))/\sqrt{r}0.5 \tag{8}$$

where K is the constant of proportionality and C is the cement content of the mix as fraction.

The values of P and $d_{0.5}$ were determined using MIP curve and are given in Table 2.4. To

determine the constant of proportionality, K, the experimental results of compressive strength

were plotted against the corresponding $C(1-P)/$sqrt $(d_{0.5})$. Figure 2.14 presents the

relationship and the K value obtained was 260.15, with a coefficient of determination $R^2 =$

0.98.
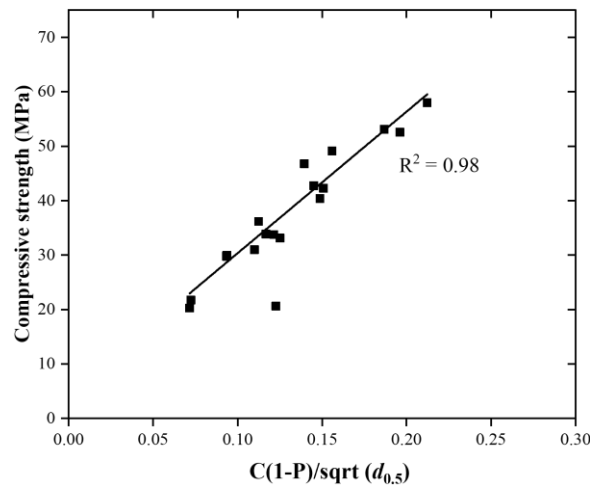
Figure 2.14 *Plot of compressive strength versus pore parameters C(1-P)/sqrt (d0.5)*

   b) *Effect of permeable porosity and capillary porosity on chloride transport*

There are several studies indicating a significant influence of the pore structure on the

chloride transport mechanisms [57][58]. Among different types of pores, the penetration of

chlorides is mainly attributed to the capillary pore size range [60]. The results of the total

porosity accessible to mercury, *i.e.,* permeable pore volume, indicate that the pore volume is

decreased significantly after 90 days of curing. In blended system, the values of permeable

porosity were higher than in CEM I at the early age because of the lower clinker amount, and

consequently slower hydration reaction. CEM III samples also showed higher permeable

porosity than CEM I but less than those observed for blended systems. The results show that after 90 days the porosity values decreased for fly ash and calcined clay mix, indicating that they start to alter the microstructure once the pozzolanic reaction occurs [31][60]. Figure 2.15 shows the correlation between total permeable porosity and capillary pore volume with chloride migration and chloride diffusion coefficients.
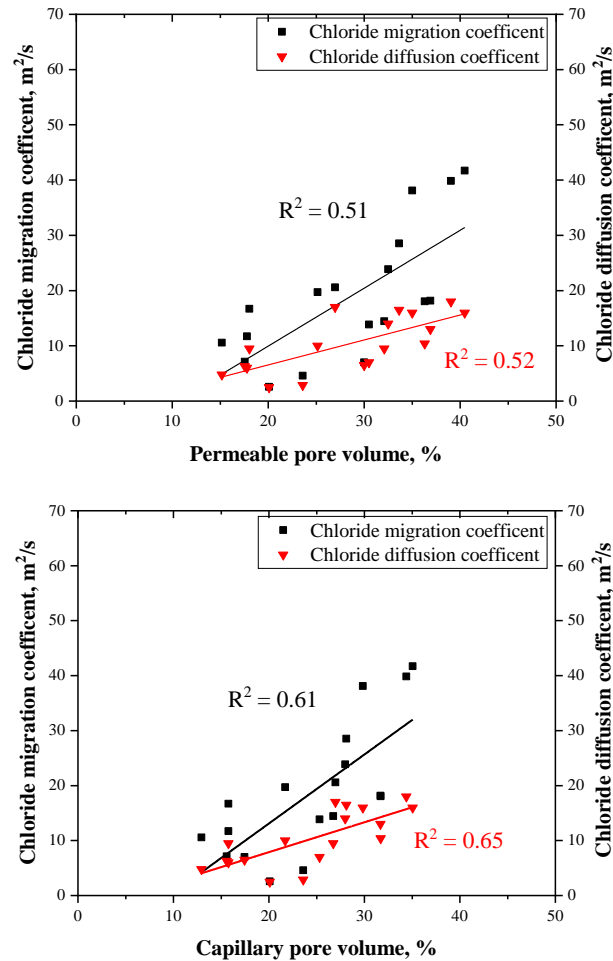
Figure 2.15 *Linear regression analysis of total permeable pore volume and capillary pore volume against chloride migration and diffusion coefficients*

The effective capillary pore volume is statistically more significantly correlated to transport phenomena in the tested systems, than the total permeable porosity. Furthermore, better correlation between pore parameters and transport parameters is obtained for diffusion than

for migration coefficients. The volume of capillary pores decreases from 7 to 90 days due to the progress in hydration in all the mixtures. As expected, the 7-day value of capillary pore volume is very high, which is also reflected in the higher values of chloride transport coefficients. In the beginning of the hydration, the capillary pores are fully percolated and larger than C-S-H gel pores. Therefore, these capillary pores accelerate the chloride movement, thus higher values of chloride transport coefficients are obtained [61]. In the fly ash mix, the capillary pore volume has decreased around 60% from 7 days to 90 days and in the same period the chloride migration and diffusion coefficients decreased by around 70-73%. However, the capillary pore volumes of fly ash mix at both 7 and 28 days were higher than CEM I mix, while the chloride transport properties at 90 days were lower. The same trend was also observed for calcined clay mixture. In the case of CC30, capillary pores do not change significantly from 7 to 28 days, but after 28 days the pore volume was reduced for around 42%. When water-filled pores, obtained from sorptivity test, and capillary pores obtained from MIP, were compared (diagram not shown here), it was evident that the pore refinement due to the addition of SCMs mainly occurs in the capillary pore region, especially in the case of ternary blends [50]. Researchers have reported that in the early stage the calcined clay perform better than other SCMs, but in this study the lower content of kaolinite was responsible for lower clay reactivity [5]. However, the pore structure of calcined clay mix was continuously refined until 90 days, leading to the enhancement in the resistance to chlorides compared to CEM I. In CEM III, the values of the transport coefficients were the lowest, which was however not reflected in their porosity. More recent research [31] has shown that the low amount of kaolinite in clay mixtures influenced the capillary pore refinement, leading to less refinement than would be seen in a pure clay.

c)   Effect of inter-connectivity of capillary pores on chloride transport

Inter connectivity of capillary pores plays significant role in chloride transport in cementitious system [62]. In SCM based binders, due to the pozzolanic reactions, the consumption of portlandite and formation of secondary C-S-H, inter-connectivity of pores is decreased with time which leads to a decrease in the chloride penetration [63]. There are different ways to show the degree of inter-connectivity of the pore structure and the major parameters which can be drawn from MIP are critical pore size and pore entrapment fraction. The values of critical pore entry diameter and pore entrapment fraction are plotted against chloride migration and diffusion coefficients and illustrated in Figure 2.16. Critical pore entry diameter in MIP results implies the largest fraction of interconnected pores in a cementitious system. All the values of critical pore entry diameter are reported in Table 2.4 and values were decreasing with prolonged curing. Similar to capillary pore volume, all the mixes showed high critical pore radius at 7 days, and then progressively lower values with hydration time. After 90 days, the lowest dimeter found was for fly ash mix FA30 and the highest for CEM I. Another parameter describing inter-connectivity is pore entrapment fraction. As seen in Table 2.4, the pore entrapment fraction increased with hydration progress. After 90 days of curing, both binary and ternary mixes showed better structure discontinuity in their pore structure, and that reflected their transport properties. Compared to pore entrapment fraction, critical pore entry diameter would be better explanation of chloride transport in ternary mixes. In any case, ternary mix with fly ash and limestone exhibited the highest value of tortuosity and CEM I the lowest.
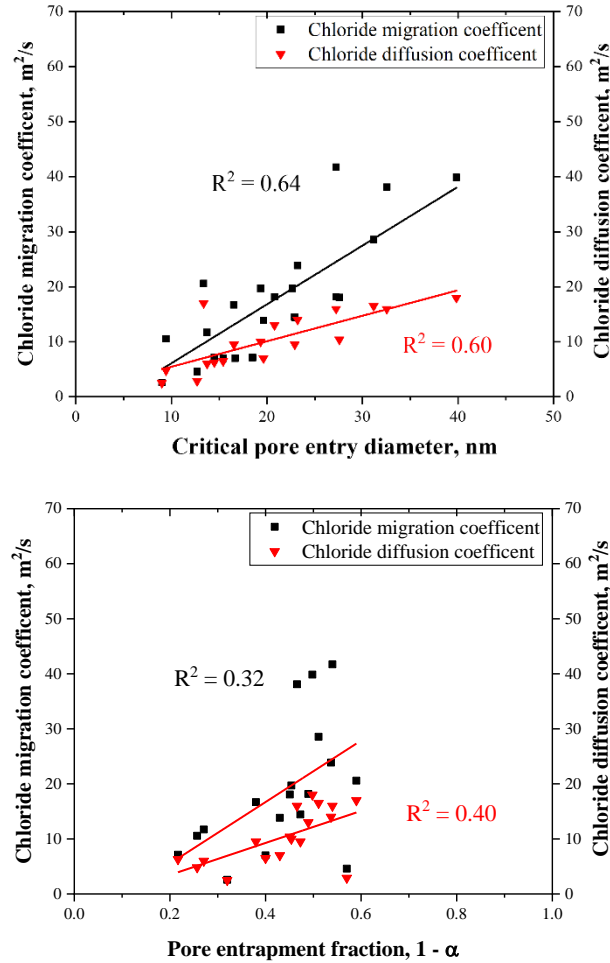
Figure 2.16 *Linear regression analysis of critical pore entry radius and pore entrapment fraction against chloride transport coefficients*

The evolution of migration and diffusion coefficient are increasing with critical entry diameter. Yang C and Halamickova reported that the migration coefficients are directly proportional to the critical entry radius [91][49]. In this study, all samples showed a general tendency that higher critical pore diameter produces higher chloride penetration. In general, the pozzolanic reaction from fly ash and calcined clay can offset the dilution effect by filling the interim space between with C-A-S-H, continuing to progressively contribute and accelerate pore diameter reduction [64]. It is therefore that the values of critical pore entry diameter were found to be lower in fly ash and clay mixes, compared to CEM I after 90 days.

Pore entrapment fraction and chloride transport coefficients were also subjected to regression analysis, with the correlation found to be weaker than for other pore structure parameters. This could be due to the direct determination of pore connectivity values, particularly due to mixture heterogeneity in cementitious system. CEM III samples had the highest resistance to chloride penetration of all tested mixes, but the pore structure could not be improved enough to achieve this trend.

In terms of compressive strength and chloride diffusion coefficient, the low-grade kaolin clay mixtures performed similarly to CEM I and CEM III. The pore structure parameters of the calcined clay mixture were refined after 90 days of curing, and the refinement contributed to the resistance to ion movement, as shown by the chloride migration results. The chloride migration coefficients showed a weaker linear dependence on the pore structure parameters compared to the diffusion coefficient. The reason could be that the migration coefficients are strongly influenced by the conducting ions in the pore solution [83]. Therefore, all pore structure parameters have a limited effect on chloride penetration in blended cementitious systems, indicating that other parameters of blended systems, such as chloride binding capacity could have a prevailing role [49][15][65][66]. The binding of chloride ions in various hydrates, particularly C-A-S-H and AFm phases, retards chloride penetration in cementitious systems. In the systems based on limestone-calcined clay, the amount of carbo-aluminate hydrate increases as kaolinite content rises. Therefore, the effective binding capacity might be advantageous for kaolinite-rich clays [6], [5]. Maraghechi et al. [6] measured the apparent diffusion coefficient of a cementitious system with different amounts of kaolinite, from 17% to 95%. They found that the chloride diffusion was greatly reduced as the amount of kaolinite increased. However, when the kaolinite content went from 50 to

95%, the effect on the chloride ingress resistance was less significant. Due to the high level

of replacement, the amount of portlandite available for clay is limited, preventing formation

of additional hydration products. Therefore, the optimal would be that all of the portlandite

is used up in the reaction with calcined clay and limestone, leaving no unreacted metakaolin

behind [45]. Present study confirms that even clays with a lower amount of kaolin, such as

those in mixes CC30 and CC30LS15, can be used to prepare concrete with good resistance

to chloride ingress.

2.5 Conclusion

This chapter put forward insights on how the mechanical and chloride penetration resistance

change with the substitution of cement with low-kaolin clay. Furthermore, the study analyzed

the impact of different durability parameters, such as sorptivity and surface electrical

resistivity, and pore structure parameters, on chloride transport in blended systems. Pore

structure parameters that were analyzed include capillary porosity, critical pore entry radius,

mean entry radius, and pore entrapment fraction.

The ternary mixes with the addition of limestone prepared and tested in this study had similar

durability to the binary mixes and were better than Portland cement. However, their

mechanical properties were significantly lower compared to the CEM I mortar. The chloride

migration coefficients of blended mixes were strongly influenced by the electrical

conductivity and surface resistivity of the system. This influence was stronger in the case of

chloride migration coefficients than chloride diffusion coefficients. Chloride migration

coefficients were significantly higher (1.86 times) than diffusion coefficients. The over-

estimation in chloride migration coefficients should be taken into account when using values

of rapid chloride migration test in the estimation of service life of blended mixes.

Regardless of the MIP constraint, the results showed an acceptable correlation between certain pore structure parameters, such as permeable and capillary pore volume, critical pore diameter and pore entrapment fraction, and the chloride transport coefficient. The critical pore diameter and capillary pore volume showed a stronger influence on chloride penetration than other parameters. Moreover, the correlation of pore structure parameters was relatively stronger with chloride diffusion than with chloride migration coefficients. Regardless, pore structure parameters cannot be used to fully explain chloride ingress in blended cementitious systems. This study highlights the importance of revealing the chloride interaction due to the binding effect of the C-S-H surface and the effects of the charged C-S-H surface to fully understand chloride ingress in these systems.

All of the alternative cementitious materials used in this study were locally available. Despite the relatively low kaolinite content, the calcined clay used in the study performed better than ordinary Portland cement mortar in terms of chloride penetration and showed comparable results to slag cement. Thus, even low-grade, locally available clays can be a good choice for cementitious materials with good resistance to chloride penetration and low CO_2 content.

Chapter 3 Impact of different kaolinite content on limestone calcined clay cement concrete

The kaolinite content is principally responsible for the durability performance of Limestone Calcined Clay Cement (LC3), which calls into question its global applicability. The clay supply has a significant impact on the LC3 system's reduced carbon footprint advantage. The influence of kaolinite concentration from two separate clays (collected in East South-East Europe) on the durability performance of concrete was investigated in this study. The low-kaolinitic clay had 18% kaolinite, while the medium-kaolinitic clay contained around 41% kaolinite. The compressive strength, chloride intrusion, electrical conductivity, surface resistivity, and sorptivity index were measured on concrete after 28 days. Furthermore, the pore structure development of these mixtures was investigated in relation to the kaolinite content of the mixtures. The reactivity test was performed on clays to measure their reactivity levels within the cementitious system. The results show that kaolinite content has a moderate effect on compressive strength, but it has a considerable effect on other durability indices. When compared to the Portland cement mixture, the chloride migration and diffusion coefficients were reduced by 50% and 36%, respectively, in the combination with a medium

kaolinite content (more than 40%). The low-kaolinitic clay, on the other hand, achieved 60% of the chloride penetration resistance of the medium-kaolinitic clay. Furthermore, low-kaolinitic clay has been demonstrated to be suitable for low-carbon concrete in moderate exposure conditions.

Keywords: Kaolinite calcined clay; chloride penetration; electrical resistivity; chloride binding; capillary pore volume; critical pore entry diameter

3.1 Introduction

The global climate has changed dramatically in recent decades. Since the pre-industrial era, global warming has led to a temperature increase of 1.1°C [1]. It is widely known that industrial carbon emissions contribute significantly to global warming. Similar to other industries, the cement industry has implemented a variety of strategies to reduce its carbon footprint. Over the past several decades, low-carbon cement has received the most attention. The majority of low-carbon cements employ supplementary cementitious materials (SCMs), thereby reducing the clinker factor. The concrete industry aims to achieve a clinker factor of 0.52 by 2050, down from the current value of 0.62 [2]. Typically, fly ash, blast furnace slag, and natural pozzolana are employed in the production of low-carbon cements [3–6]. However, most of these materials are byproducts from industries which are also going through green transition. Fly ash, for example, is a byproduct from coal-fired power plants that are expected to close in the coming years [7]. If adequate replacement for the most common SCMs is not found, the transition to carbon neutrality will be delayed. Due to their widespread availability, kaolinitic clays become an important source of SCMs in this scenario [8]. Particularly, Limestone Calcined Clay Cement (LC3) has proven its capability to be a good replacement as a binder in concrete [5–8]. The LC3 system has better early-age

strength, chloride ingress resistance, and a carbon footprint that is 40 percent lower than Portland cement [9–19].

In general, thermal activation of kaolinitic clays leads to the formation of metakaolin, which gives the clays their reactivity. In the LC3 system, metakaolin reacts with portlandite, water, and sulfate to form C-A-S-H, ettringite, and AFm phases [14], [15]. Other clay minerals, such as illite, also contribute to pozzolanic reactivity; however, various researchers have reported that the benefits are negligible compared to kaolinite [16]. Therefore, the quantity of kaolinite within the clay is the determining factor for properties of LC3. Avet et al. reported that the amounts of reacted metakaolin in the LC3 system were quite similar for calcined clays with more than 50% kaolinite content and concluded that optimum kaolinite content is about 60 percent [17].

Clays with the recommended kaolinite cannot be found everywhere. Flegar et al. found that most of the clays collected in Croatia had no more than 20% kaolinite [20]. Few studies have been conducted on the use of low-grade clay in concrete, and it has been reported that low-grade clays could be used to replace cement [21–24]. In the long run, the phase assemblage of the LC3 system was found to be quite similar regardless of the different kaolinite content, while the kinetics of the evolution of hydration products were distinct [25]. Therefore, clays with lower kaolinite content could also be a viable solution to make LC3 system.

The primary focus of this study was to analyze the performance of concrete with two different clays collected from East South-East Europe: one with a moderate amount of kaolinite and the other with a very low kaolin content. LC3 systems were formulated using these two clays to evaluate their durability in terms of electrical resistivity, chloride penetration, and water

absorption. The aim of the research was to compare their durability and identify critical

properties which are the most impacted by the kaolinite content. In addition, the effect of

kaolinite content on the binding of chlorides and pore structure was systematically evaluated.

3.2 Materials and methods
3.2.1 Materials

Portland cement of type CEM I 42.5R (as per EN 196-1) was used in all mixtures as a primary

binder. Two different clays were used, labeled A and B. The kaolinite of raw clays was

determined using thermogravimetric (TG) analysis, and the mass loss between 400 °C and

600 °C was attributed to the dihydroxylation of kaolinite [16]. Limestone used in the study

was obtained as waste powder from a limestone quarry in Zvečaj. In addition, CEM II/B-S

(blended cement with blast furnace slag) was utilized to make a mix for comparing the

performance of limestone-calcined clay mixes to a classical blended cement available at the

market. As shown in Table 3.1, the raw materials' chemical oxide compositions were

measured using X-ray fluorescence. In addition to oxides, the mineralogical composition of

clinker and two clays was evaluated using X-ray diffraction technique (Table 3.2) and the

XRD pattern illustrated in Figure 3.1. Following the whole process illustrated in Figure 3.2,

clays were made as a binder. Figure 3.3 depicts the results of laser diffraction tests on the

particle size distributions of all materials.

Table 3.1 *Chemical oxides of each material used in this study.*

Chemical oxides	CEM I 42.5R	CEM II/B	Clays		Limestone powder
			A	B	
CaO	63.19	46.94	2.17	2.39	71.59
SiO$_2$	19.51	33.65	62.41	61.77	20.21
Al$_2$O$_3$	4.21	7.55	21.35	28.72	4.32
Fe$_2$O$_3$	2.85	2.94	7.26	3.03	1.43
MgO	0.85	3.39	1.78	0.68	1.69
Na$_2$O	0.20	0.78	1.05	<0.01	0
K$_2$O	0.48	0.74	2.50	2.3	0.15
TiO$_2$	0.12	0.22	0.94	0.87	0.52
P$_2$O$_5$	0.45	<0.01	0.36	<0.01	0.42
SO$_3$	2.3	4.02	0.07	0.22	1.48
Kaolinite content (%)	--		41.6	18	--

Table 3.2 *Mineralogical composition of clinker and clays.*

Component	Clinker	Component	Clay -A	Clay -B
C$_3$S	56.4 (1)	Quartz	23.2 (4)	21.7 (1)
C$_2$S	5.4 (1)	Muscovite	14.6 (1)	27.3 (1)
C$_3$A	5.6 (1)	Rutile	0.9 (2)	-
C$_4$AF	6.2 (1)	Kaolinite	41 (1)	18
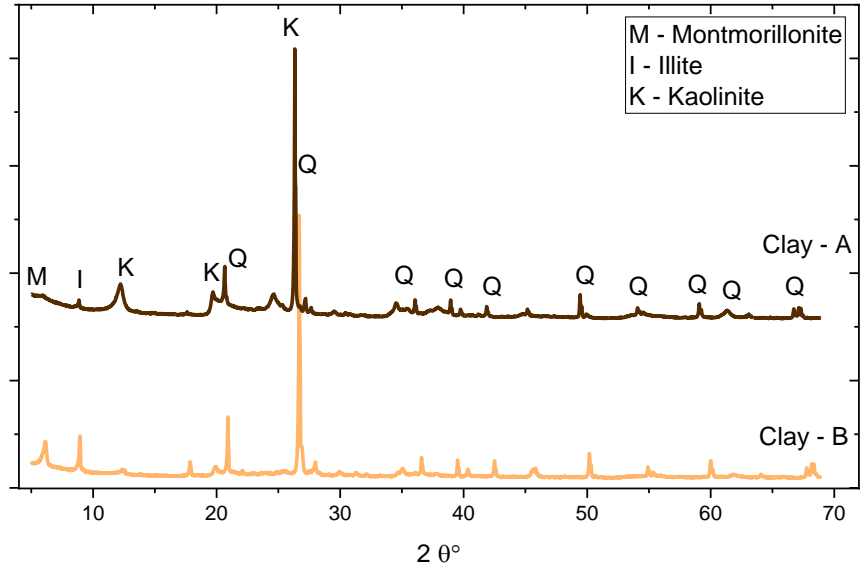
Figure 3.1 *XRD pattern of raw clays.*

Figure 3.2 *Steps involved in the preparation of LC3 in the lab for this study.*
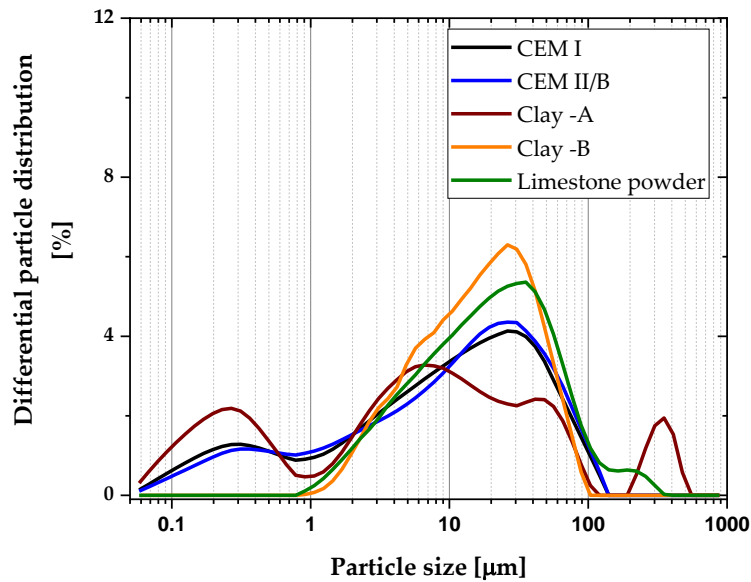
Figure 3.3 *Particle size distribution of all materials used in this study.*

Three aggregate classes were utilized, including two coarse aggregate classes (16/8 and 8/4) and one fine aggregate class (0/4). Table 3.3 contains the physical properties of each aggregate fraction. In this study, the calcined clay to limestone powder ratio was taken at 2:1, according to several previous studies [8]. The mix proportions adopted in this study are listed in Table 3.4. LC3-A and LC3-B are concrete mixtures using calcined clay A and B, respectively. Limestone calcined clay mixtures were prepared with CEM I as the primary binder.

Table 3.3 *Physical properties of aggregates used in this study.*

Property	Fine aggregate (0/4)	Coarse aggregate (4/8)	Coarse aggregate (8/16)
Maximum particle size (mm)	4	8	16
Water absorption (%)	1.3	0.6	0.3
Specific gravity at SSD*	2.79	2.81	2.82

*Surface saturated dry condition

Table 3.4 *Mixture design of all mixtures used in this study.*

Mixture	Binder kg/m³	w/b	Water, kg/m³	Cement, kg/m³	Calcined clay, kg/m³	LS kg/m³	SP* %	Aggregate, kg/m³ 8–16	4–8	0–4
CEM I			136	340	-	-	0.7	510	512	1014
CEM II	340	0.40	132	340	-	-	1.2	518	520	1029
LC3-A			136	187	102	51	1.8	513	514	1018
LC3-B			136	340	102	51	1.1	536	538	1064

* wt. % of binder content

In addition, a commercial superplasticizer (SP) with a solids content of 35% was used to ensure sufficient workability. Similarly, 1% gypsum was added to each mixture (in LC3 systems) of blended cement to prevent false settings produced by the system's under-sulphation [26]. All mixes were made and verified for fresh properties according to EN 12350 specifications. Specimens were demolded twenty-four hours after casting and placed in the humidity chamber (relative humidity maintained at greater than 95% and temperature maintained at 20 °C) until the day of testing.

3.2.2 Test methods

The entire experimental program was divided into three categories: reactivity and durability properties. All the techniques are explained in the following section.

a) Reactivity test

A reactivity test was conducted using TAM Air isothermal calorimeter with 8 channels (TA Instruments, New Castle, USA) as per ASTM C1897-20 [27]to determine the reactivity levels of clays with different kaolinite content. This test would give the pozzolanic reactivity of clays to isolate the clinker effect. Paste samples were prepared, which contained clay (i.e., SCM), sulfate, and alkali, and placed into an isothermal calorimeter at a temperature of 40 °C for seven days. During these seven days, the total heat generated was monitored, indicating the reactivity of clay. The bound water content of these two clays were also measured as an indicator of reactivity.

b) Concrete preparation and compressive strength

Clinker, calcined clay, limestone, and gypsum were manually mixed to obtain a homogenous mixture prior to concrete mixing. The highest capacity of the pan mixer used to mix the concrete was 70 L. The order of mixing was similar for each batch including the control mixture. The initial mixing of the dry components for two minutes was followed by the addition of 90% of the water and further mixing for two minutes. In the final phase, the superplasticizer was mixed with the remaining water for a further three minutes. In total, the mixing time met the requirement mentioned by the superplasticizer manufacturer to achieve the maximum dispersion of admixture. After mixing, the slump, wet density, temperature, and air content were measured immediately. Three concrete specimens of 15 cm × 15 cm × 15 cm were prepared to measure the compressive strength after 7 and 28 days of curing, and the test parameters and procedures followed the EN 12390-3 standard.

c) Chloride ingress resistance

Cylindrical specimens of 20 cm height and 10 cm diameter were prepared to test the chloride

penetration resistance of the mixtures. After 28 days of curing, the cylindrical specimens

were split diametrically into three slices with a thickness of 5 cm. Chloride penetration

resistance was measured after 28 days of curing using Rapid Chloride Permeability Test -

PROOVE´it (Germann Instruments, Copenhagen, Denmark), as per NT BUILD 492 [28].

Using this method, a non-steady-state migration coefficient (Dnssm) is obtained, calculated

by the Nernst-Plank equation expressed in Equation 3.1.

$$D_{nssm} = RT/zFE . (x_d - \alpha\sqrt{x_d})/t \qquad\qquad (3.1)$$

where xd is the average measured depth of chloride penetration after the test duration, while

other parameters were taken from the NT BUILD 492.

Chloride diffusion coefficients of each were evaluated based on NT BUILD 443 [29], and

the specimens were coated with epoxy resin on all sides except the bottom one for chloride

exposure. After coating, the specimens were left another 24 h for the epoxy to fully dry and

then fully immersed in 16.5% NaCl solution for 35 days. After 35 days, the profile grinding

(depths were taken according to NT BUILD 443) was performed to obtain powder for

chemical analysis. The total chloride content in the powder was determined using the

potentiometric titration method described in standard EN 14629-2007 [30]. Thereafter, the

effective chloride diffusion coefficients (De)P were determined by fitting the total chloride

contents in second Fick's law according to NT BUILD 443,

$$C (x, t) = C_s - (C_s - C_i) . \operatorname{erf} (x | \sqrt{(4D_e\ t)}) \qquad\qquad (3.2)$$

where $C(x,t)$ is the measure of chloride content at depth (x) and exposure time (t). The values

of apparent chloride diffusion coefficients could be extracted after fitting the measured

chloride contents. The free chloride content of each depth was also determined as water-

soluble chloride, according to ASTM C1218. After the determination of free chloride and

total chloride content, the bound chloride was determined as a difference between the total

and free chloride.

d) *Electrical conductivity/surface resistivity*

The electrical conductivity of each mixture was determined after 28 days of curing according

to ASTM C1760 [31]. The initial current values from the chloride migration test were used

to calculate Equation 3.4.

$$Conductivity, \sigma = 1273.2 \, . \, I_i/V.L/D^2 \qquad\qquad (3.4)$$

where current (I) is measured as the initial current by imposing voltage (V) to the specimen,

and other parameters were taken from the standard.

The surface resistivity of each mixture was determined by Wenner's four-probe resistivity

meter on the sides of cylindrical specimens, which was used to determine the chloride

transport coefficients [32]. The measurements were taken in saturated condition and at four

different locations of each specimen. A total of 12 readings were taken, and the average was

reported as surface resistivity.

e) Sorptivity

Sorptivity, the rate of absorption in concrete, is commonly used to evaluate the resistance of concrete to moisture penetration via capillary absorption. This factor was identified as a major contributor to the initial penetration of chloride into the specimen [13], and this initial penetration has a significant impact on the subsequent movement of chloride and, consequently, the de-passivation of steel. In this study, the sorptivity of each sample was determined based on the South African Durability Index Manual [33]. After curing, the specimen was dried at 50°C for seven days and then placed in a desiccator for four hours. After drying, specimens were placed on a tray which contained saturated Ca (OH)$_2$ solution. The specimens were supported by wooden rollers, and the solution level was restricted to within 2 mm of the surface. The specimen's weight was measured after 3, 5, 9, 12, 16, 20, and 25 min. After weighing the samples, they were conditioned for one day in a saturated calcium hydroxide solution. The sorptivity index was calculated using Equation 3.5,

$$S = (F \times d)/(M_{sv} - M_{S0}) \qquad\qquad (3.5)$$

where 'F' is the slope of the best fit line between mass gain and the square root of time, average thickness 'd', M_{SV}, and M_{S0} are the vacuum weight and initial weight of samples.

3.3 Results
3.3.1 Reactivity

Figure 3.4 illustrates the normalized total heat per gram of clay produced by clay A and B from the reactivity test, respectively. Clay A liberated 388.43 Joule per gram of clay, while clay B was only 215.97 Joule per gram. Therefore, the pozzolanic reactivity of the calcined clay A was 1.79 times more than B in terms of the total heat.
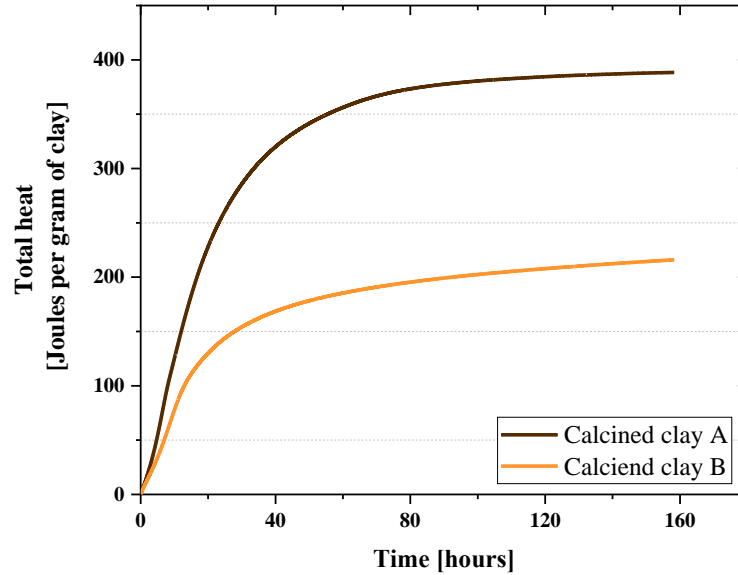
Figure 3.4 *Total heat produced by each clay from R3 test.*

Furthermore, the bound water of these two clays were determined as 10.9% for clay A and 9.4% for clay B.

3.3.2 Fresh properties and compressive strength

All the concrete mixtures were targeted for the slump between 90-120 mm. The values of fresh properties are given in Table 3.5.

Table 3.5 *Fresh properties of each mixture*

Mixture	Paste volume, l/m^3	Slump, mm	Temperature, °C	Wet density, kg/m^3	Air content, %
CEM I	246.03	90	24.3	2512.1	3.5
CEM II/B	242.4	105	24.1	2539.9	3.1
LC3-A	261.01	100	23.5	2491.12	3.9
LC3-B	243.65	95	22.3	2395.3	2.8

Figure 3.5 depicts the compressive strength of each mixture. As anticipated, CEM I produced greater strength than the other combinations. The LC3-A mixture achieved 82% of compressive strength compared to the CEM I mixture after 28 days of curing and 75% of compressive strength compared to the CEM I mixture after seven days. The strength of LC3-B was found to be 69% of the compressive strength of CEM I mix after 28 days of curing.

Chapter 3
Impact of different kaolinite content on limestone
calcined clay cement concrete
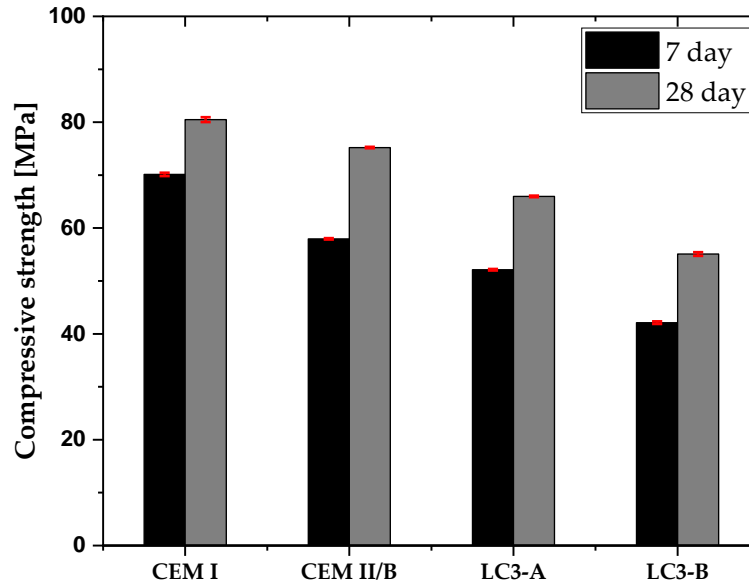
Figure 3.5 *Compressive strength of each mixture*

3.3.3 Water sorptivity index

Figure 3.6 depicts the sorptivity index of the concrete samples. The results indicate that CEM I and CEM II/B have a greater sorptivity index than both LC3 mixes. Compared to the Portland cement system, LC3-A was 2.2 times less susceptible to water absorption and 1.25 less than LC3-B. Among clay mixtures, kaolinite content plays an important role. Higher kaolinite content improved the water absorption in LC3 systems.
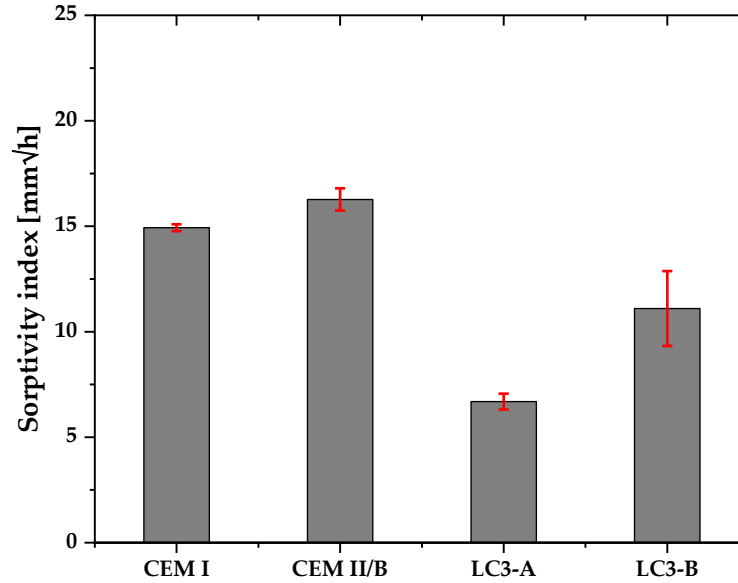
Figure 3.6 *Water sorptivity of each mixture*

3.3.4 Bulk conductivity and surface resistivity

The electrical conductivity and surface resistivity of each mixture are displayed in Figure
3.7a-b. Compared to all other mixtures, CEM I exhibited the highest conductivity, whereas
LC3-A exhibited the lowest conductivity. As expected, the trend of surface resistivity was
just opposite to the conductivity. According to ACI classifications on corrosion rate [36], if
the surface resistivity of a combination is greater than 20 k.ohm.cm, it has a negligible risk
of corrosion. Thus, both LC3 mixes met this requirement, despite their high replacement
levels. Furthermore, the calcined clay's kaolinite content significantly enhanced the electrical
resistance.
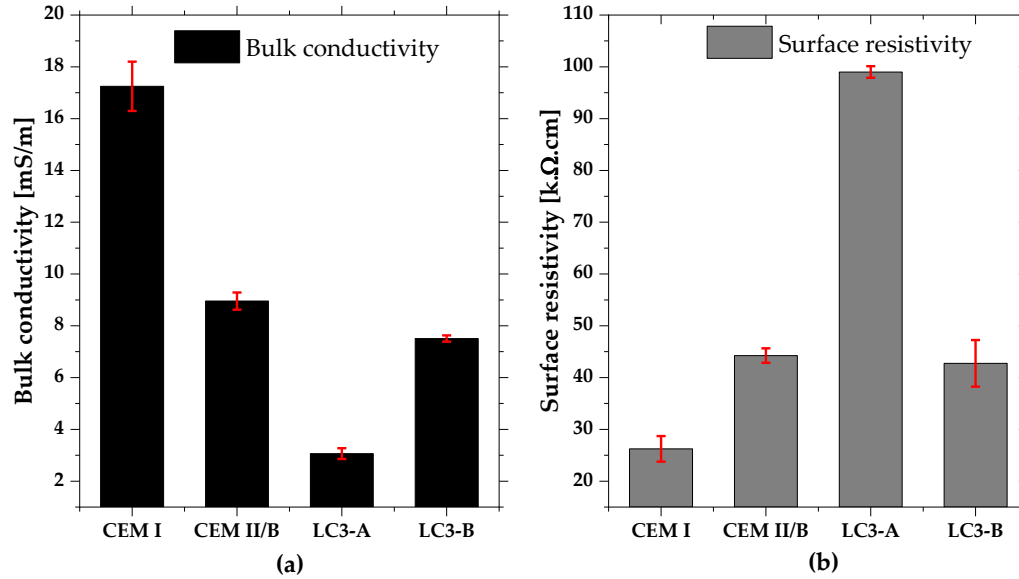
Figure 3.7 a) Bulk conductivity, and b) Surface resistivity of each mixture.

3.3.5 Chloride migration and chloride diffusion

The chloride transport coefficients for each mixture are shown in Figure 3.8a-b. Both tests

showed that the LC3 mixes were resistant to chloride penetration. Even though there was

less clinker in LC3-A than in CEM I, the chloride transport coefficients were found to be

two-times lower compared to that of CEM I. Additionally, LC3-A outperformed the

composite cement CEM II/B. Furthermore, even the LC3-B mix, regardless of a low kaolinite

content, performed slightly better than the CEM I mix.
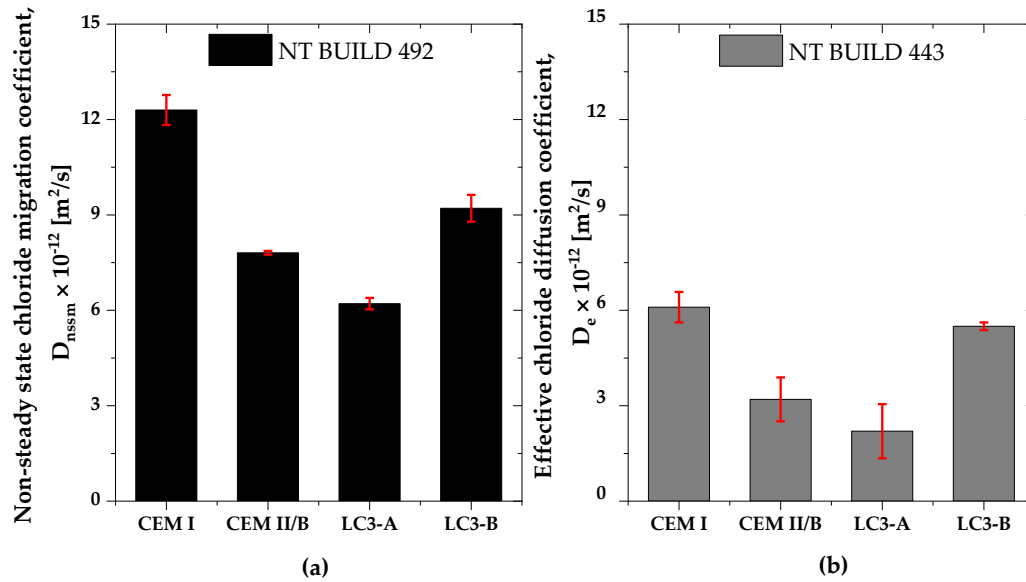
Figure 3.8 *Chloride transport coefficient based on a) NT BUILD 492, and b) NT BUILD 443.*

After evaluating the chloride profile of each mixture, the total chloride content was separated into bound and free chloride contents based on Equation 3.5. Figure 3.9 depicts the chloride distribution of each mixture subjected to salt solution. The chloride concentration at each depth reveals that chloride penetration into LC3-A concrete is significantly lower. In addition, the amount of free chloride in the LC3-A mixture was exceedingly low, and most of the chloride was bound. Even the LC3-B mix, which displayed comparable chloride penetration to the mix with CEM I, had a significantly lower content of free chlorides.

Figure 3.9 *Total chloride content of each mixture categorized into bound and free chloride content.*

Figure 3.10 illustrates the quantity of bound and free chloride of all mixtures at a depth of 10 mm from the exposed surface.

Figure 3.10 *Bound and free chloride content at the depth of 10 mm from exposed surface towards salt solution*
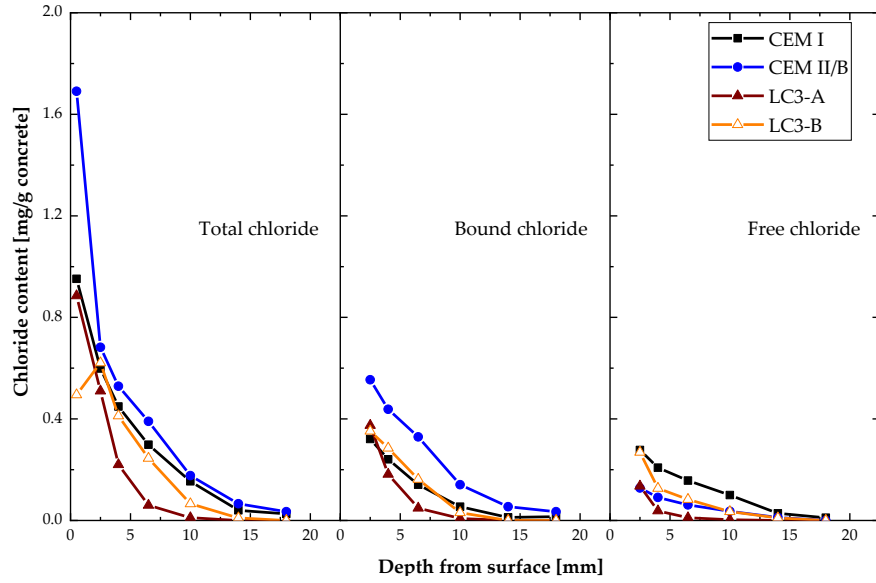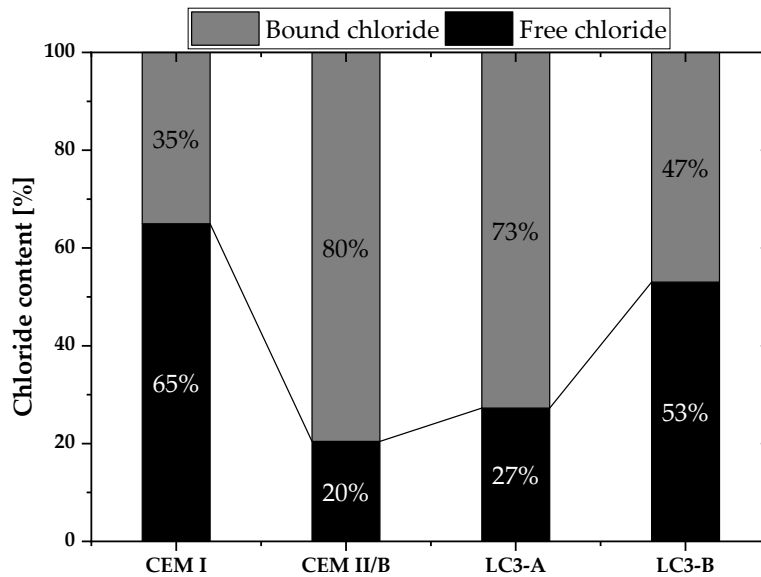
As shown in Figure 3.10, LC3-A contained 73% of bound chlorides, but LC3-B contained only 47%. The calcined clay's kaolinite content considerably increased the chloride binding capacity of the system. When compared to all other mixes, CEM II/B demonstrated the highest binding capacity, even though the chloride transport coefficient was found to be slightly higher than LC3-A mix.

3.4 Discussion

The higher reactivity of calcined clay can be directly attributed to the presence of kaolinite [17]; clay with the higher amount of kaolinite shows higher reactivity. This was confirmed by reactivity tests, clearly demonstrating the dependence of reactivity on kaolinite content. In addition, the bound water content of two clays implied that clay A has more reactivity than clay B.

The mix with calcined clay A and calcined clay B achieved 84% and 65% of compressive strength compared to concrete mix with CEM I, respectively. In a blended system, the degree of hydration of the clinker plays a crucial role on the pozzolanic reaction. For example, if the clinker replacement with metakaolin is excessively high, there will not be enough portlandite for the pozzolanic reaction from metakaolin to occur [38][39]. Therefore, even with a higher kaolinite content, there is minimal improvement in compressive strength between clay B and clay A (less than 10 MPa). In comparison to other results reported for the LC3 system [9][10][12], the compressive strength of clay A is somewhat lower. As stated in the section on materials, the clinker itself has a higher alkali content, which might affect the hydration of the LC3 system. The optimal amount of alkali is 0.48 Na2Oeq, but the clinker's higher alkali content exceeded this limit, which has a slight impact on compressive strength [40].

LC3 mix with clay A had greater resistance to capillary absorption than LC3 mix with clay B. In general, the addition of SCMs, along with the combined pozzolanic and filler effects, results in a more complex pore network and a decrease in the water absorption from external environment [9] [41]. Figure 3.6 demonstrates that the LC3 system enhances the resistance against capillary absorption. In addition, the higher kaolinite content enhances the pozzolanic reaction, which might be the cause of less sorptivity index of clay A than clay B. In addition, the bimodal particle size distribution of clay A provides more finer particles than clay B, hence reducing the water absorption through capillary suction [42]. However, LC3-B demonstrated greater resistance to capillary absorption than CEM I and CEM II/B, demonstrating the potential of low-grade clay as an alternative binder in concrete in environments where sorptivity of water is the prevailing durability indicator.

Compared to other pozzolanic materials used in concrete, the LC3 system is renowned for its higher electrical resistivity and chloride ingress, especially with high kaolinite content. In the case of LC3-A, the surface resistivity was significantly higher than other mixes, which is in accordance with previous research. LC3-B mixes showed comparable resistivity to CEM I mix. The higher surface resistivity of the LC3 system can be attributed to the differences in the kinetics of microstructural development in the binder systems, as well as to the presence of denser microstructure in the LC3 systems [12] [43]. The lower reactivity of clay B resulted in the reduction of surface resistivity of the LC3-B mixture. However, the resistivity of LC3-B was still comparable to CEM I.

In both chloride penetration resistance tests, concrete LC3-A demonstrated superior performance compared to concrete mixes CEM I, CEM II and LC3-B. There are several reasons for this improved behavior, all confirmed in this study and in the literature, which

include pore structure refinement, bulk conductivity, chloride binding, and pore solution

chemistry [44–51]. The chloride transport coefficients are directly correlated to the surface

resistivity, as observed. In addition, the higher kaolinite content contributed to a significant

improvement in the development of resistivity, and thus their chloride penetration resistance.

Higher discontinuity in the pore network of the LC3 system is attributable to the hydration

product and the LC3 system's reactivity, both of which are evidently related to the kaolinite

content [43][12].

After the resistivity, the binding capacity of the LC3 system is considered to be one of the

important parameters to influence the chloride penetration [48]. As shown in Figure 3.10,

approximately 73% of the total chloride in LC3-A was bound, whereas LC3-B possessed

only 47% of bound chlorides. Maraghechi et al. reported that the amount of Friedel's salt in

the LC3 system is greater than in the Portland cement system containing more than 40 percent

kaolinite [43]. This is due to the greater number of carbo-aluminates phases in the LC3

system. The quantity of kaolinite in the clay can therefore contribute to a higher number of

carbo-aluminate phases, which can improve chloride binding [9]. However, while comparing

the diffusion coefficients of CEM II/B and LC3-A, it was discovered that the impact of

chloride binding on chloride transport was minimal. In the case of CEM II/B, there is a

greater amount of bound chloride, but the resistance to chloride penetration is not as high as

it is for LC-A. The extent of the impact of chloride binding on chloride transport is still

debatable, especially in the LC3 systems.

3.5 Conclusion

The main aim of the current study was to analyze the durability of LC3 concrete prepared with low- to medium-kaolinitic calcined clay found in East South-East Europe. In the LC3 system, the impact of the alkali content on the development of compressive strength was discovered. The high alkali content weakens compressive strength, especially at an early age. Following conclusions are drawn from the study:

- The compressive strength was found to be satisfactory even with low kaolin clay, even though higher kaolinitic clay was needed to attain comparable strength to that of CEM I and blended cement. Concrete with the higher kaolinitic clay was able to achieve around 85% of compressive strength compared to CEM I after 28 days.

- Chloride penetration, electrical activity, and sorptivity of the concrete improved significantly with higher kaolinite content. Chloride diffusion and migration resistance improved by at least 50% compared to Portland cement system with higher kaolinitic clay. Among clays, the chloride penetration resistance differs by 30% and the sorptivity indices value differs by 41%. The kaolinite content was found to be very important in durability performances of LC3 concrete.

- Electric resistivity of the LC3-based concrete dominantly influenced the chloride penetration over the chloride binding and pore structure.

- Low-kaolinite clay (18% in this study) could be a potential material to make concrete for mild exposure conditions, while higher grade kaolin clay (42% in this study) would be needed for aggressive exposure conditions.

Chapter 4 Understanding the governing parameters of chloride transport in limestone calcined clay cements based on low-grade kaolin clay

Abstract:

Limestone calcined clay cement (LC3) is regarded as one of the most promising cementitious systems for lower ecological footprint of cement. The purity of clays or the kaolinite content is the most important factor in determining the effectiveness of these clays in cementitious systems. In places where high-purity clays are scarce, the only solution is to investigate the potential of using lower-quality clays. In this chapter, focus was on three clays collected in the South-East Europe with kaolinite content of less than 40 percent. Analysis of the effective diffusion coefficient of various low-grade clays and its dependence on pore structure, chloride binding, and bulk/pore solution conductivity was the primary objective of the study. Study reveals that cement pastes based on limestone and low-grade clays have higher bulk and pore solution resistivities than OPC paste, resulting in their higher chloride penetration resistance. The pore structure and chloride binding capacity were in similar range of influence in LC3 with lower grade clays and the Portland cement system. In addition, the number of smaller capillary pores (< 5 nm) correlated well with the diffusion coefficient in all mixes.

Keywords: kaolinite, effective chloride diffusion coefficient, critical pore entry radius, chloride binding, formation factor, pore solution conductivity

4.1 Introduction

The production of cement and concrete is a major contributor to CO_2 emissions, and the utilization of supplementary cementitious materials (SCMs) has been recognized as an effective strategy to reduce these emissions. However, the current availability of traditional SCMs, such as fly ash and slag, is limited and expected to decline in the future. As a potential solution, kaolinitic clays calcined at high temperatures (ideally 750-800°C) could be used as a source of SCMs. Kaolinitic clays have been shown to reduce clinker production and lower the carbon footprint of cement and concrete. In particular, the synergies between calcined clay and limestone in limestone calcined clay cement systems allow for clinker reductions of up to 50 percent. Previous research has shown that a kaolinite content of over 40% in the calcined clay is ideal for producing high-strength LC3 (limestone calcined clay cement) compared to reference Portland cement[24], [99]. However, the vast majority of deposits of kaolinitic clays available worldwide are impure, containing impurities such as quartz, iron, and other types of clays, which reduce the pozzolanic reactivity of these clays. Therefore, the usage of intermediate to lower grade kaolinitic clay is more feasible due to its broad availability at a reasonable cost, in comparison to high-quality kaolinite clays used to produce pure metakaolin, which are extremely expensive, scarce and have niche application in other industries.

One of the main advantages of LC3-based concrete is its resistance to chloride ingress [100][29], [35], [36]. The transport of chloride in cementitious materials is influenced by multiple factors, including pore structure, phase assemblage, and bulk/pore solution conductivities. The main pore structure parameters that influence chloride transport include total capillary porosity, bulk porosity, critical pore size, tortuosity, and formation factor.

Among these parameters, critical pore size is considered the main pore structure parameter that controls chloride transport [36], [38], [109]–[117], [101]–[108]. Hydration product binding capacities were also found to be a significant parameter in controlling chloride transport [43], [98], [126]–[131], [118]–[125]. Chemical binding occurs when chlorides interact with C_3A or monosulphate phases to create Friedel's salt or with C_4AF to form a Friedel's salt analogue. Conductivity of the system, both as a bulk and in its liquid phase (i.e., the pore solution), is another factor affecting chloride transport. Portland cement systems typically have high alkali content, resulting in high conductivity compared to blended systems [100][35], [74], [132]–[135]. The LC3 system was found to have lower pore solution conductivity compared to the Portland cement system [35][100].

Most of the aforementioned parameters in LC3, e.g., pore structure, phase assemblage, and bulk/pore solution conductivities, depend on the purity of the clays used. To understand the impact of these parameters, this paper focuses on three different clays obtained from South-East Europe with varying kaolinite content of 43%, 25%, and 18%. The aim of the experiments was to analyse the pore structure, chloride binding capacities, bulk, and pore solution conductivity, and to understand how these parameters were affected by the kaolinite content.

4.2 Materials and methods:
4.2.1 Materials

This study used ordinary Portland cement (CEM I 52.5R), limestone powder, and three kaolinitic clays sourced from the Southeastern Europe (Croatia and Serbia). The clay's chemical and physical properties are listed in Table 5.1, and the particle size distribution of all materials is displayed in Figure 4.1. The clays were calcined at 800°C for an hour in a

high temperature furnace, and their kaolinite content was determined by Thermogravimetric Analysis (TGA), the results of which are shown in Figure 4.2. The mean particle size of all materials was measured with a laser diffractometer.

Table 4.1 *Chemical and physical properties of all materials*

| Component	CEM I 52.5R	Clay_A	Clay_B	Clay_C	Limestone (L)
CaO	51.97	2.39	2.06	2.17	71.59
SiO_2	30.78	61.77	62.22	62.41	20.21
Al_2O_3	6.96	28.72	26.81	21.35	4.32
Fe_2O_3	3.15	3.03	2.08	7.26	1.43
MgO	1.31	0.68	1.39	1.78	1.69
Na_2O	0.55	0.01	0.67	1.05	0
K_2O	0.72	2.30	3.97	2.50	0.15
TiO_2	0.15	0.87	0.81	0.94	0.52
P_2O_5	0.01	0.01	0.01	0.36	0.42
SO_3	4.43	0.22	0.10	0.07	1.48
Kaolinite content, %	-	43.1	25.3	17.6	-
D_{10}, µm	0.32	0.18	2.96	4.03	3.43
D_{50}, µm	9.95	6.37	9.31	10.72	18
D_{90}, µm	50	69.65	57.83	24.79	63.82
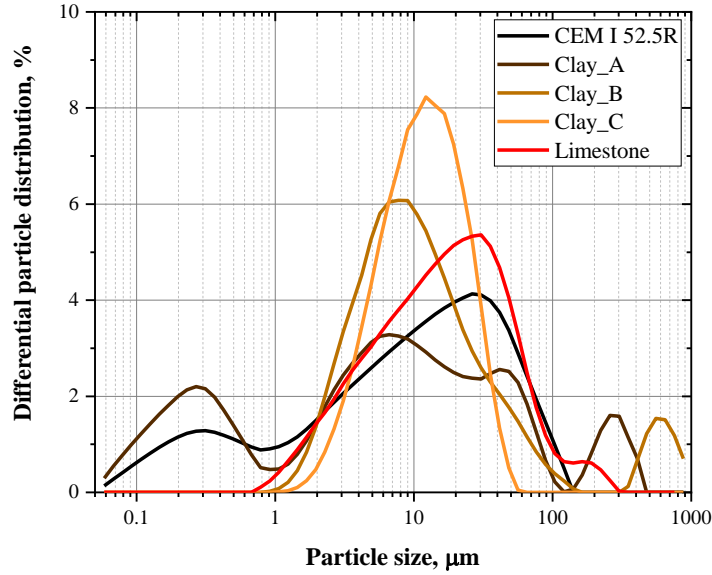
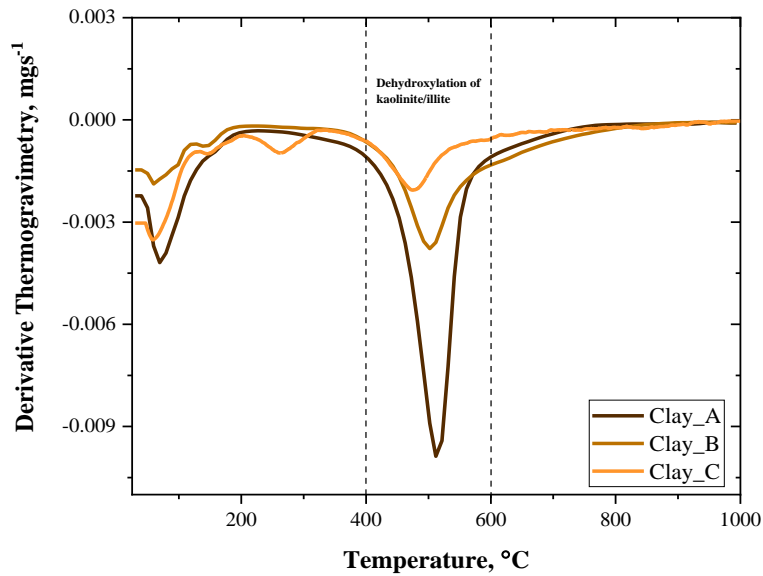*Figure 4.1 Particle size distribution of all materials*

Figure 4.2 Derivative curve of thermogravimetric analysis of all clays

A ternary blend of OPC, limestone and calcined clay with a 50% clinker content (referred to as LC3) was made with a calcined clay to limestone ratio of 2:1, which has been shown to perform well in prior chapters ([136], [137]). The different mixtures were labelled as CEM

I, LC3_A, LC3_B, and LC3_C, depending on the type of clay used. To ensure a properly sulfated system, 1% gypsum was added to the blend due to the presence of calcined clay with a significant amount of aluminates [31].

4.2.2 Sample preparation and curing

Samples for the tests were made in the form of paste. The paste was prepared by blending the powder with distilled water at a 0.5 water to binder ratio. A high-shear blender was utilized for the paste preparation, and it was mixed for 2 minutes at a speed of 1600 rotations per minute. The specimens were prepared in small plastic containers of 50 mm in height and 33 mm in diameter, except for bulk resistivity (explained in respective section). After mixing, the containers were kept sealed for 24 hours before demoulding, and then cured in water for 28 days in larger containers to reduce the volume of water used. To protect the sample from leaching and mimic curing the specimens in their own pore solution, a sacrificial specimen of the same batch was also added to each container (as depicted in Figure 5.3).

Figure 4.3 *Samples curing in their own pore solution.*

4.2.3 Determination of chloride ingress resistance – mini migration setup for paste

The resistance of each sample to chloride ingress was determined by measuring its chloride diffusion coefficient. Instead of using a conventional method, the mini-migration test was conducted to evaluate the D_{eff}. The setup for the mini-migration test, shown in Figure 4.4, was similar to that described by Wilson et al. [37]. Samples were cut from cylindrical specimens after 28 days of curing with a thickness of 10 mm and a diameter of 33 mm, as

shown in Figure 4.3. The test was limited to a reservoir capacity of 230 mL. The curved surface of the samples was treated with two-component epoxy, left to dry for 24 hours, and covered with moist tissue to prevent drying. The samples were then immersed in 0.3 M NaOH solution (with slight vacuum) for 48 hours. The weight of samples before and after immersion was used to calculate the water-permeable porosity. The two reservoirs were attached to the sample, which was mounted in the middle with a rubber ring and held in place with four stainless screws. The upstream reservoir contained a 0.5 M NaCl and 0.3 M NaOH solution (to limit alkali leaching), while the downstream reservoir held only 0.3M NaOH. For each mix, two samples were measured and the average of them reported.
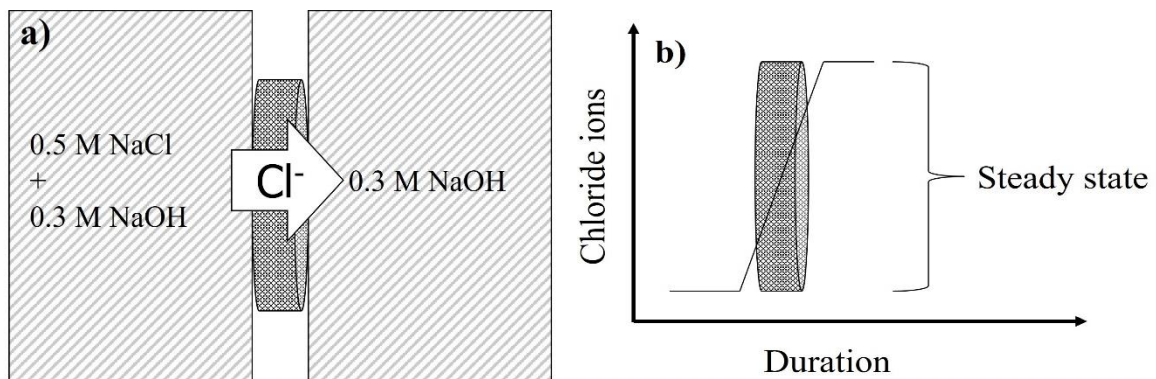

Figure 4.4 Mini-migration setup

The initial current for each sample was set by adjusting its voltage to fall between 5-25 mA. The applied voltage was then kept constant for 24 hours, with the voltage serving as the means to control the duration of the experiment. The actual voltage was measured in the solution across the sample at the start and end of the test and was adjusted downward by 1.5 V due to the electrode potential. The actual voltage of each specimen was used to determine its diffusion coefficient. Throughout the test, the current values were also monitored. The

minimum current indicated the time at which chloride started flowing from the upstream to the downstream reservoir. After that time, the movement of chloride became constant, and the rate of this movement was used to calculate the chloride diffusion coefficient.

The D_{eff} was calculated based on the evolution of chloride concentration in the downstream section. Every 2 days, 5 ml of solution from the downstream reservoir was collected to monitor chloride flow and a fresh 5 ml of 0.3 M NaOH solution was added to keep the solution level constant. The collected samples were titrated with a TitroLine 5000 using 0.1M $AgNO_3$ solution to determine the amount of chloride over time (as shown in Figure 4.5). The calibration was done using a standard solution of 0.1M NaCl. Only data from the constant migration phase was used. As shown in Figure 4.5, the slope of the data represented the chloride flow rate, which was used to calculate the D_{eff}.
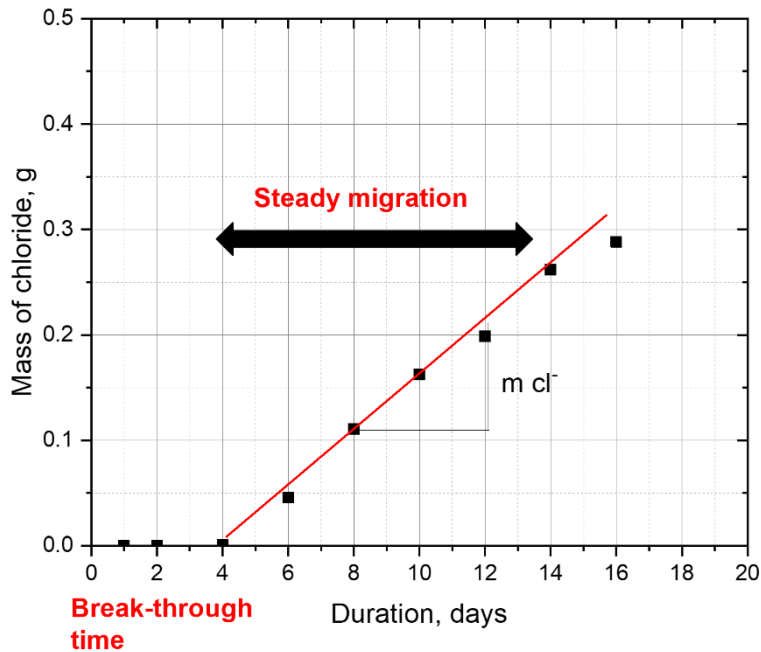

Figure 4.5 A typical plot of chloride gain in the downstream reservoir during mini-migration test.

The effective chloride diffusion coefficient (D_{eff}) was estimated with simplified Nernst-Plank equation (Eqn 4.1) for transport in solution:

$$D_{eff} = \frac{J_{down}\ RTl}{C_{up}\ F\varphi E} \qquad (4.1)$$

Where D_{eff} is the chloride effective diffusion coefficient, c_{up} is the chloride concentration in the upstream reservoir (mol/m^3), R is the gas constant, T is the temperature in Kelvin, F is the Faraday constant, l is the specimen thickness, φE is the actual voltage across the specimen, and J is the chloride flux through sample (mol/m^{2}s). J can be determined by the slope of chloride mass, m_{cl^-} (g/s) obtained from the chloride titration of the downstream reservoir solution as function of time and it is given in Eqn 4.2.

$$J_{down} = \frac{m_{cl}}{S\ M_{w\,cl}} \qquad (4.2)$$

Where S is the surface area of the sample (m^2), M_{wcl} is the molar mass of chloride (g/mol).

4.2.4 Chloride binding isotherms

After 28 days of curing in water, slices 5mm thick were cut from the central portion of cylindrical paste samples. The slices were then vacuum dried for approximately one month using a vacuum desiccator filled with silica gel. The dried slices were broken into smaller pieces and approximately 15 g samples were placed in 60 ml of NaCl solution at three different concentrations (0.1 M, 0.5 M, and 3 M). The samples were exposed for 16 weeks until the concentration of the solution reached a stable value. After the titration, binding isotherms were plotted with total bound chloride versus chloride concentration of solution.

4.2.5 Chloride species after equilibrium

a) Total chloride by difference in the exposure solution

The variation in chloride content of the exposure solution before and after reaching equilibrium was used to determine the total uptake of chloride by samples of known weight. The chloride content of the exposure solution was measured using 5ml subsamples and an automated process with the Titroline 5000 (SI Analytics) and a titration solution of 0.1M $AgNO_3$.

b) Acid and water-soluble chlorides

For each mixture and exposure condition, each mixture was ground enough for the chloride analysis. For acid soluble chloride, 1.5 g of sample was used to determine the acid-soluble according to EN 14629. For water soluble chloride, 1.5 g of sample was dispersed into 30 mL of distilled water and stirred and heated until boiling. After boiling, the samples were stored $20 \pm 1°C$ for 24 h and then filitered using filter paper with pore size of 2-3 μm in Buchner funnel and suction filtration flask. The filter paper, funnel, and flask were rinsed with distilled water for each measurement. The filtered solution was poured into 80 mL of distilled water and 2 mL of 5 M HNO_3. After, chloride content of the solution was determined as per EN 14629. The chlorides extracted using both methods were then titrated using an automated process with the Titroline 5000 (SI Analytics) and a 0.1M $AgNO_3$ titration solution. To ensure accurate measurement of the relatively low chloride content, 3 ml of a 0.1M NaCl standard solution was added to each solution before titration (and subtracted in the calculations) to improve precision.

4.2.6 Determination of hydration phases

The powder X-ray diffraction (XRD) analysis was carried out with a Bruker D8 DISCOVER diffractometer (Billerica, USA) with Cu-Kα radiation generated at 40 mA and 45 kV. Specimens were scanned from 5° to 60° 2θ at a step size of 0.2° 2θ. The powdered samples

used for both total and free chloride were prepared by mixing and grinding 1.80 g of sample and 0.20 g of high purity Al_2O_3 (Corundum). The acquired diffractograms were analyzed by the Rietveld procedure, using starting parameters for the individual phases from the Inorganic Crystal Structure Database. The addition of an internal standard allowed for a possible quantification of the observed phases (e.g Friedel's salt and portlandite), despite the presence of amorphous phases.

The presence of Friedel's salt (F_s) formation in the LC3 system has been confirmed after the exposure to salt solution by various sources. Studies have shown that Friedel's salt exists as a solid solution (F_{ss})[43][44], mostly with hemi-carboaluminates. Therefore, it is essential to isolate the Friedel's salt content from the solution and determine the amount. Additionally, the shift in the Fs peak at ~11.15 2θ was identified as slightly left when limestone was present in the system, due to the formation of solid solution [44]. Therefore, the measured Fs content from XRD pattern is not that of the pure phase, but rather the content of the solid solution. One way to determine the average stoichiometry of this solid solution is to look at the distance between the two pure phases from the peak. So, the stoichiometry is used to figure out how much chloride is in the solid solution (x ($Ca_4Al_2Cl_2(OH)_{12}$. $4H_2O$). (1-x) ($Ca_4Al_2(CO_3)_{0.5}(OH)_{13}$.5.5$H_2O$)). The value of 'x' determined by,

$$x = \frac{(d_{HC} - d_{SS})}{(d_{HC} - d_{Fs})} \qquad (4.3)$$

Where d_{HC} is the basal spacing of hemi-carboaluminate; d_{SS} is the basal spacing of solid solution; d_{Fs} is the basal spacing of Friedel's salt. The chloride content in the solid solution was considered as the chemically bound chloride in the system. The chemically bounded chloride and Friedel's salt content was determined only in the samples exposed to 0.5 M NaCl solution, which was used for mini-migration test.

4.2.7 Electrical bulk conductivity

Electrical Impedance Spectroscopy (EIS) was used to measure the bulk conductivity of the prismatic paste sample. The paste sample was made in a mould made of polystyrene foam that was 100 mm × 40 mm × 40 mm. Two stainless steel plates, one on each side of the mould, were used as electrodes for the EIS measurement. After 20 hours, all of the samples used to measure EIS were kept in a saturated state (>90% RH) and covered with a damp cloth to keep them from drying out. After 28 days of curing, the samples (with dampened cloth) were moved to an impedance analyser, and all measurements were done while the samples were still wet. With an AC voltage of 250 mV amplitude and a PalmSens 4 impedance analyser, the impedance was measured from 0.1 Hz to 1 MHz. Figure 4a-b shows a schematic of the sample that was used to measure the electrical conductivity and typical impedance spectra at 28 days with different systems. Using an equivalent electrical circuit method, the point where the arcs for the bulk and electrodes meet on the Nyquist plot was used to find the bulk resistance. The bulk resistance (R_B) of the system was used to determine the electrical conductivity [138]. Every set has a report of the average of three impedance measurements. The electrical conductivity of each specimen determined by Eqn. 4.4.
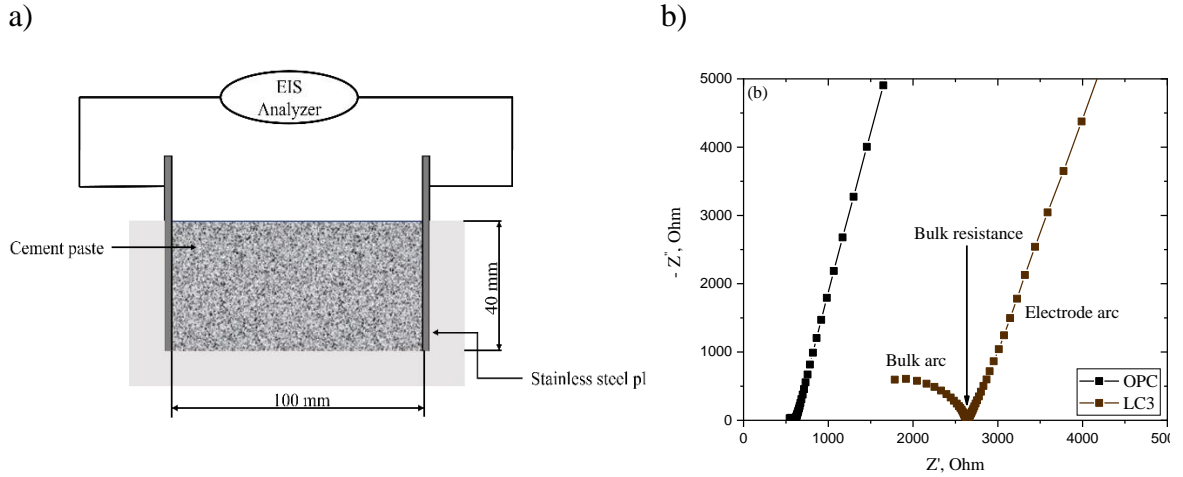
a)

b)

Figure 4.6 *Schematic diagrams of a) specimen for EIS analysis b) typical Nyquist plot*

$$Electrical\ conductivity\ (\rho), S/m = \frac{l}{R_B\ A} \qquad (4.4)$$

Where, '*l*' is the length of the specimen and '*A*' is the cross-section area.

4.2.8 Pore solution chemistry and pore solution conductivity

The elemental composition of the pore solution was determined using the high-pressure extraction die method (see Figure 4.7) on samples cured for 28 days under a 600 kN load. After extraction, the pH of the extracted pore solution was immediately measured with a pH meter (MPC 227, Mettlert Toledo, Greifensee, Switzerland). Prior to the chemical analysis, 10-15 mL of the solution was taken and sealed in a plastic test tube to prevent carbonation. The alkali (Na^+, K^+, and Ca^{2+}) content of the pore solution was measured using the Inductively Coupled Plasma Spectroscopy technique (ICP-MS). A portion of 1.0 mL of pore solution was diluted to a volume of 50 mL with deionized water, stabilized with nitric acid and hydrochloric acid, and the determination was performed in accordance with EN 17294-2016.

Figure 4.7 *High pressure machine to extract pore solution.*

As indicated by Snyder et al. [133]., the electrolyte conductivity of the pore solution was calculated by multiplying the concentration of ionic species by the equivalent conductivity given by the corresponding ionic species following the calculation of the alkali content. Using Equation 5.5, the equivalent conductivity was calculated.

$$\sigma_i = \frac{\sigma_i^o}{1+G_i.I_M^{0.5}}$$ (4.5)

The effective conductivity of pore solution ($\sigma_{pore\ solution}$, S/m) was calculated as the sum of the product of the valence of the ion (z_i), concentration (c_i), and the conductivity of an ionic species in infinite dilution (σ_i, S/m/mol), which is a function of the conductivity coefficient and ionic strength (I_M, mol/L), according to Eqn 4.6,

$$\sigma_{pore\ solution} = \sum_i \quad z_i.c_i.\sigma_i$$ (4.6)

4.2.9 Pore size distribution

After 28 days of curing, the pore structure distribution of each mixture was evaluated using Autopore 9500 Mercury Intrusion Porosimetry (MIP) (Micrometrics, Ottawa, Canada). After curing, samples from each combination were collected and hydration was stopped using the solvent exchange method [62]. In this approach, 3-4 mm thick slices were cut from the cylindrical sample and were exposed to isopropanol for seven days. During this time, the isopropanol was replenished after one and three days, followed by a minimum of 48h of vacuum drying.

The porosimeter contains two distinct devices, namely low pressure, and high pressure. The maximum applied pressure was 206 MPa, which encompassed a pore entry radius of up to 5 nm. Utilizing the Washburn equation, MIP data were transformed into pore volume against pore size [139]. Mercury's surface tension was calculated to be 0.4855 N/m, and its contact angle was 130°C. There were two replicates of each mixture tested and an average of them were reported. The total accessible porosity, threshold, and critical pore entry radius of each mixture were measured, showing the degree of pore refinement of each mixture. The total mercury penetration converted to the accessible porosity of each mixture. The critical pore size to the peak in the differential curve pore volume reveals the size corresponding to the highest volume intrusion. The classification of pores into macro, capillary, and gel porosity were done as per the pore entry size [71][114].

4.3 Results

4.3.1 Effective chloride diffusion coefficient (D_{eff})

Figure 4.8 depicts the effective chloride diffusion coefficients obtained from mini-migration test for all systems. The CEM I has the highest diffusion coefficient value. In relation to the

kaolinite content of LC3 samples, evident was the improvement in chloride ingress resistance with an increase in kaolinite content. LC3_A demonstrated the least chloride movement, while LC3_C demonstrated higher chloride penetration. The involvement of kaolinite in chloride transport has been discussed by previous researchers [100][31]. However, the kaolinite level of the majority of researchers was above 40% and therefore the system performed significantly better than control mixtures. In this instance, a kaolinite concentration of less than 20% outperformed the Portland system with relatively higher w/b ratio. The interpretation and understanding of these differences in the chloride penetration resistance with the kaolinite content, especially in low-grade clays, require detailed parametric analysis.
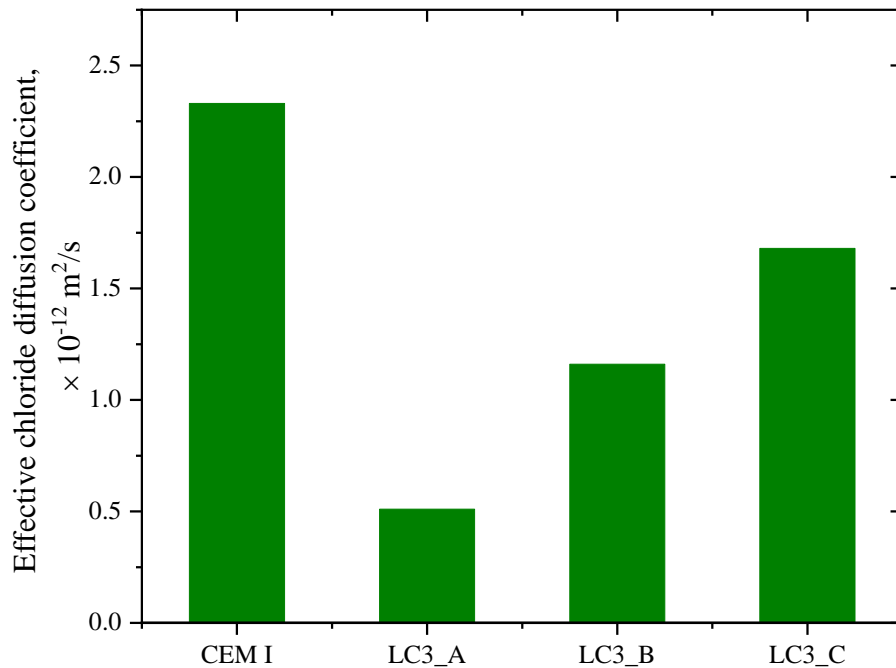

Figure 4.8 *Effective chloride diffusion coefficient, D_{eff}, measured from chloride flow rate from mini migration test.*

4.3.2 Chloride binding isotherms

a) Chloride contents after the equilibrium

Total chlorides in each mixture from each concentration of NaCl solution were estimated from the difference of concentration in the exposure solution before and after equilibrium with samples of known mass. After the total chloride, the acid soluble and water-soluble chlorides were determined using titration method. The difference between total chloride and water-soluble chloride was determined as strongly bound chloride.
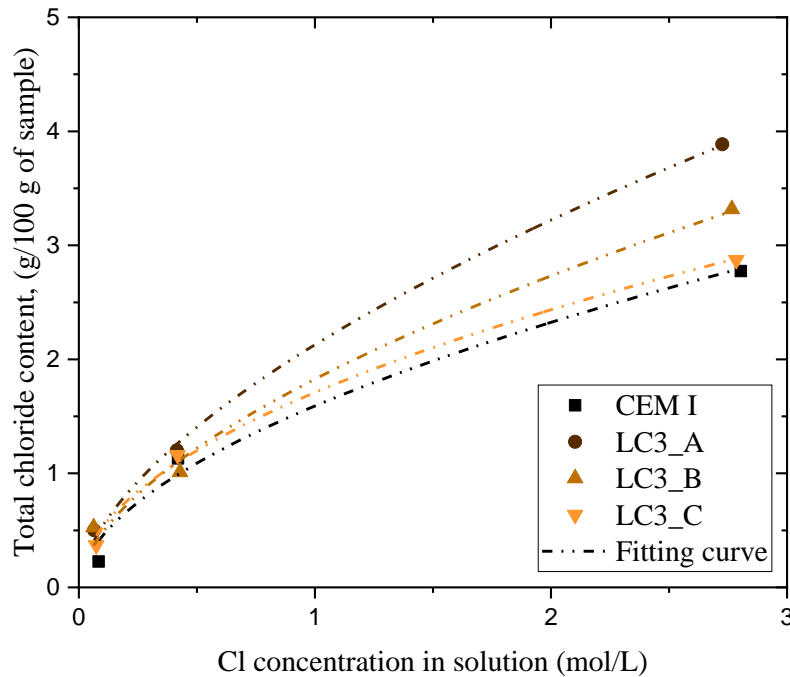

Figure 4.9 Binding isotherm of each system. Symbols are the original data point and dotted lines are Freundlich isotherm fitting.

The difference has been assumed as bound chloride and used to plot the binding isotherms. Free chloride was considered as the solution concentration after the equilibrium (which is assumed to be the same as the concentration of pore solution). The binding isotherms of each mixture were plotted in Figure 4.9. In this analysis, the best fitting was obtained with

Freundlich isotherm ($C_b = a \times C_f^b$). The values of a and b are given in Table 4.2. The binding capacities of CEM I was identified as the least and LC3_A attained the highest binding capacities.

Table 4.2 *Binding coefficients for Freundlich isotherm of each mixture.*

	Fitting parameters		
	a	b	R^2
CEM I	1.59	0.54	0.98
LC3_A	2.12	0.59	0.99
LC3_B	1.82	0.58	0.99
LC3_C	1.71	0.51	0.99

Several researchers reported binding capabilities by comparing the values of 'a', despite the fact that it is not directly related to the binding process [54]. Nevertheless, the value of 'a' for LC3_A was greater, and the value for CEM I was comparable to LC3_C. Even with two differing chloride penetration behaviors, the lower grade clay and Portland cement systems showed minimal difference in the binding capacity.

b) Phase assemblage of the system and strongly bounded chloride

The phase assemblage of the hydrates could give a better understanding of chloride binding in LC3 systems based on low-grade clay. The phases of each mixture were quantified by internal standard and depicted in Figure 4.10.
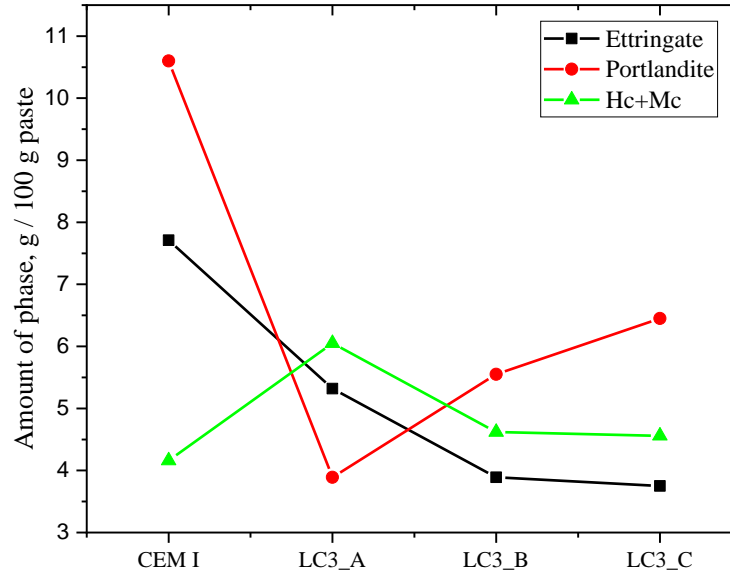
Figure 4.10 *Amount of phases after 28 days of curing*

The amount of portlandite was found to decrease with respect to the kaolinite content. LC3_A more mono and hemi-carboalunimates were identified. In addition, the LC3_B and LC3_C showed a similar range of hydration products even with two different kaolinite content. The XRD pattern of each sample is given in Figure 4a-b before and after the exposure to 0.5 M NaCl solution. Comparing the Figures, it can be observed that the amount of Friedel's salt formed was proportional to the total carboaluminates (hemi and mono carboaluminates) in the system before the exposure, i.e., system with higher amount of carboaluminates resulted in higher amount of Friedel's salt formation.

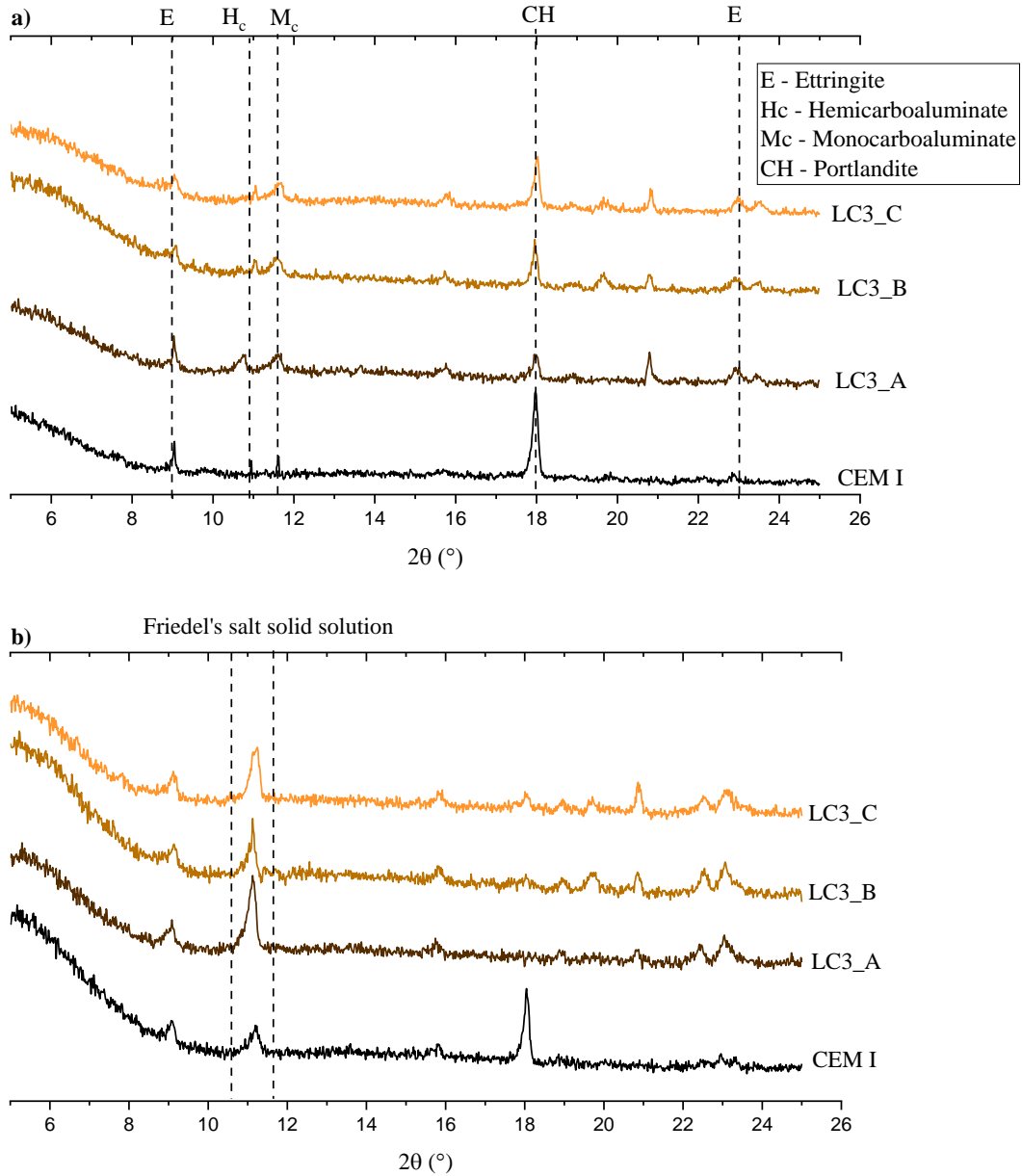***Figure 4.11*** *XRD patterns a) after 28 days of curing, b) after exposure 0.5M NaCl solution*

Therefore, the peak of Friedel's salt solution also increased with the kaolinite content. The total amount of Friedel's salt solid solution was quantified and determined the chloride content in the solid solution. The value of 'x' and amount of Friedel salt solid solution is given in Table 4.3.

Table 4.3 *Amount of Friedel's salt solid solution from XRD*

Mixture	Value of 'x'	Friedel's salt solid solution, g/ 100 g paste
CEM I	0.57	5.03
LC3_A	0.60	9.85
LC3_B	0.64	6.04
LC3_C	0.64	6.95

The chloride content in Friedel's salt solid solution was considered as chemically bound chloride. The amount of chloride physically bound on the hydration products (mainly on C-A-S-H) was assumed to be the difference between strongly bound chloride and chemically bound chloride. Figure 4.12 depicts different types of chlorides in each mixture after the exposure to 0.5 M NaCl solution.
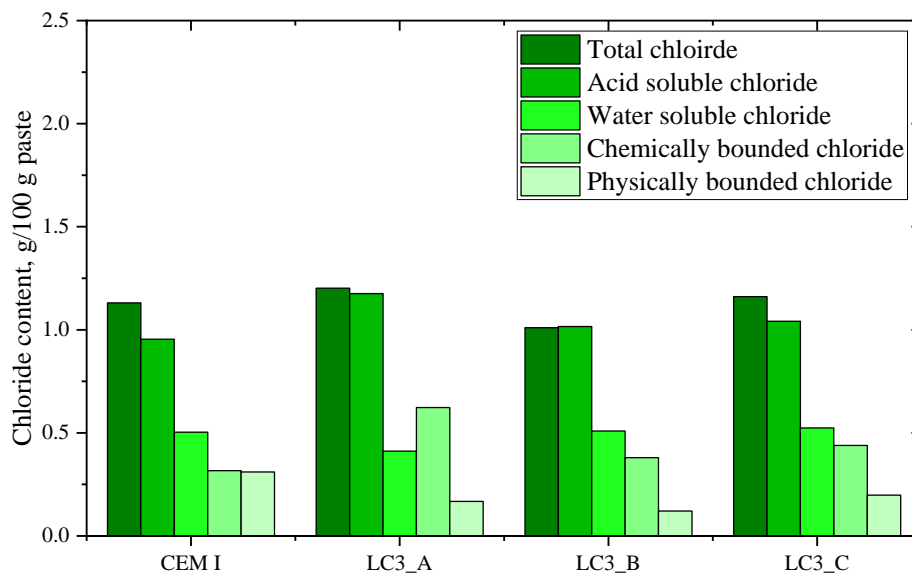

Figure 4.12 *Chloride species of each mixture after exposure to 0.5M NaCl solution*

4.3.3 Electrical bulk conductivity

The Nyquist plots of one sample from each system are shown in Figure 4.13. The value of bulk resistance increased substantially with kaolinite content. Unlike the chloride binding capacities, the difference between bulk resistance LC3_C and CEM I was evident. The significant improvement of the bulk resistance can be evidently correlated to the chloride penetration resistance of different mixes.
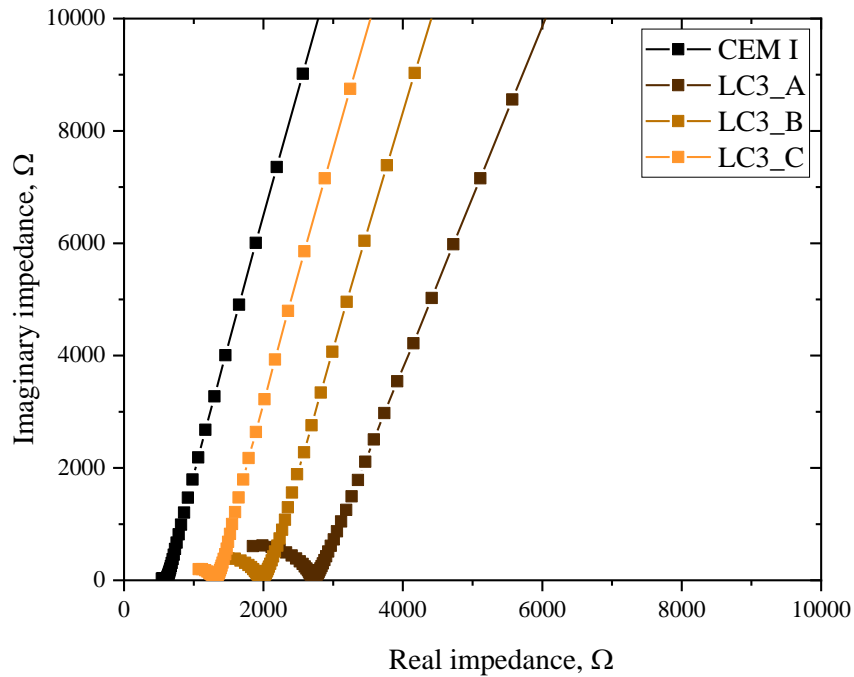

Figure 4.13 *Nyquist plot of each mixture after EIS measurement*

The bulk electrical conductivity, R_B, was calculated from EIS measurements and is given in Table 4.4. The conductivity of each mixture has a direct relation to the chloride penetration. The least conductive system, i.e., LC3_A, also performed well in the mini-migration test.

Table 4.4 *Electrical bulk resistance and conductivity of each mixture*

Mixture	Bulk resistance, R_B, ohm	Electrical bulk conductivity, S/m
CEM I	611 ± 41	0.0921 ± 0.010
LC3_A	2646 ± 67	0.0182 ± 0.009
LC3_B	1946 ± 96	0.0274 ± 0.001
LC3_C	1296 ± 65	0.0396 ± 0.001

4.3.4 Pore solution composition and conductivity

Table 4.5 summarizes the pore solution concentrations of samples cured for 28 days. Sodium and potassium are clearly the most abundant ions in the pore solution. The CEM I sample contains the highest concentration of alkali ions compared to the LC3 samples. The kaolinite concentration in LC3 samples reduces as the amount of alkali increases. In terms of pH, LC3_A has the lowest pH and the highest kaolinite content, whereas LC3_B has the highest alkali ion content. The conductivity of pore solution was determined as explained in the method section and is given in Table 4.5.

Table 4.5 *Pore solution alkali contents and pore solution conductivity*

Mixture	pH	Ca^{2+}, mmol/L	Na^+, mmol/L	K^+, mmol/L	Pore solution conductivity, S/m
CEM I	13.8	0.39	90.48	322.80	23.40
LC3_A	13.0	0.30	14.09	54.24	4.35
LC3_B	13.6	0.42	25.96	70.20	5.92
LC3_C	13.4	0.41	24.40	62.51	5.36

Similar to electrical conductivity, the pore solution conductivity of the LC3 mixtures was significantly lower compared to CEM I and was reduced with the kaolinite content of the clays. LC3_B and LC3_C had very similar conductivity of the pore solution, even with two

different kaolinite content. The sodium and potassium ions were found to be similar in both clays, which makes them almost equivalently conductive.

4.3.5 Pore size distribution

Figure 4.14 depicts the pore size distribution of all mixes produced using MIP analysis. For OPC and LC3_C, a similar critical pore entry size was identified. The observed porosity of LC3_A is much finer than that of CEM I (more skewed differential curve). Table 4.6 lists the total accessible porosity, water accessible porosity, capillary pores, and critical pore entry diameter. Overall, the kaolinite content resulted in more refined pore structure parameters. However, it was not demonstrated that these characteristics significantly influenced the chloride parameters. For example, in the case of LC3_B the number of capillary pores is higher than for LC3_C, however the chloride penetration resistance was lower.
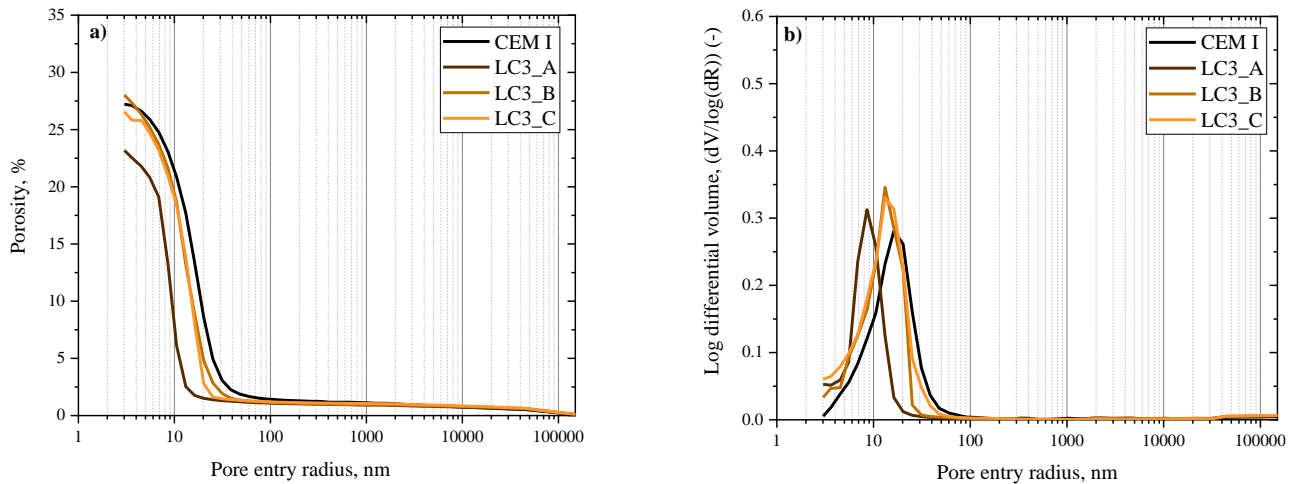

Figure 4.14 *Porosity distribution of PC and LC3 systems*

Table 4.6 *Pore structure parameters of each mixture.*

Mixture	Total accessible porosity, %	Water accessible porosity, %	Capillary pores, (5 nm to 5000 nm), %	Critical pore entry diameter, nm
CEM I	27.21	43.25	25.06	16.25
LC3_A	23.17	44.12	20.03	8.54
LC3_B	28.02	46.87	24.37	11.44
LC3_C	26.56	52.12	23.81	13.14

4.4 Discussion

In general, chloride transport in cementitious systems is influenced by their pore structure parameters, chloride binding capacities, and bulk and pore solution resistivities [34], [36], [117], [140][31], [141]–[143][35], [134], [144]. The pore structure mainly controls the physical parameters for chloride transport, while chemical parameters control chloride binding. The total resistivity of the system comes from both resistivity provided by the hydration products, pores, and pore solution. However, the main resistivity is provided by the liquid phases (both gel and capillary pores) [145], [146]. Moreover, the combined effect of all these factors drives the chloride through the cementitious system. Therefore, it is essential to understand the influence of each of these parameters on chloride transport in LC3 with lower kaolinite content.

4.4.1 Effect of pore structure

Pore refinement is a crucial factor affecting chloride transport in the LC3 system. The total porosity of all the mixes was within a similar range, and there was no discernible trend in the total porosity values with respect to the kaolinite content or the performance of the LC3 system. Typically, a decrease in clinker content results in a decrease in the volume of hydration products. However, due to the high pozzolanic reactivity caused by the high

kaolinite content, the difference in porosity between mixes with and without cement substitution was not significant [38], [115]. Nevertheless, the effects of clinker reduction and low clay reactivity were clearly evident in the LC3_B and LC3_C systems. Figure 4.15 shows the correlation between the effective diffusion, determined from the mini-migration tests, and the total porosity/capillary porosity, determined from the MIP. Interestingly, no trend was observed between these two parameters.

The critical pore entry diameter represents the overall permeability of the system and is critical for achieving higher durability. When clinker is replaced by SCM, the critical pore diameter usually decreases, indicating the refinement of the pore size, which is usually associated with the reactivity of pozzolanic materials. In LC3 systems of low-grade kaolin, a large capillary space is formed due to the dilution effect of limestone [147], which is not filled by additional hydration products due to the lower reactivity of the clay [38][148]. The effect of the dilution was clearly seen in water-accessible porosity - water-accessible porosities increased with decreasing kaolinite content. There were no significant differences in pore structure for clay containing 25 to 18% kaolinite. Nevertheless, the critical pore entry radius was finer for LC3_B and LC3_C than for CEM I, indicating that even with low kaolinite content and high-volume cement replacements, better pore refinement can be achieved, ultimately increasing the impermeability of these systems compared to OPC.

Although previous studies suggested that capillary porosity is the most important parameter affecting chloride transport in cementitious systems, our results show a flat correlation between total and capillary porosity and effective diffusion. Moreover, the correlation between capillary porosity and effective diffusion coefficient values was insufficient to explain chloride penetration, especially in LC3 systems. However, a trend was evident in the

critical pores, where higher critical pores resulted in greater chloride penetration. Nevertheless, this trend cannot fully explain the improvement in chloride resistance for LC3_A, which has about three times better effective chloride diffusion than LC3_C, despite the insignificant improvement in critical pore refinement. Therefore, it appears that the effects of pore structure alone are not sufficient to explain chloride penetration into the LC3 systems.
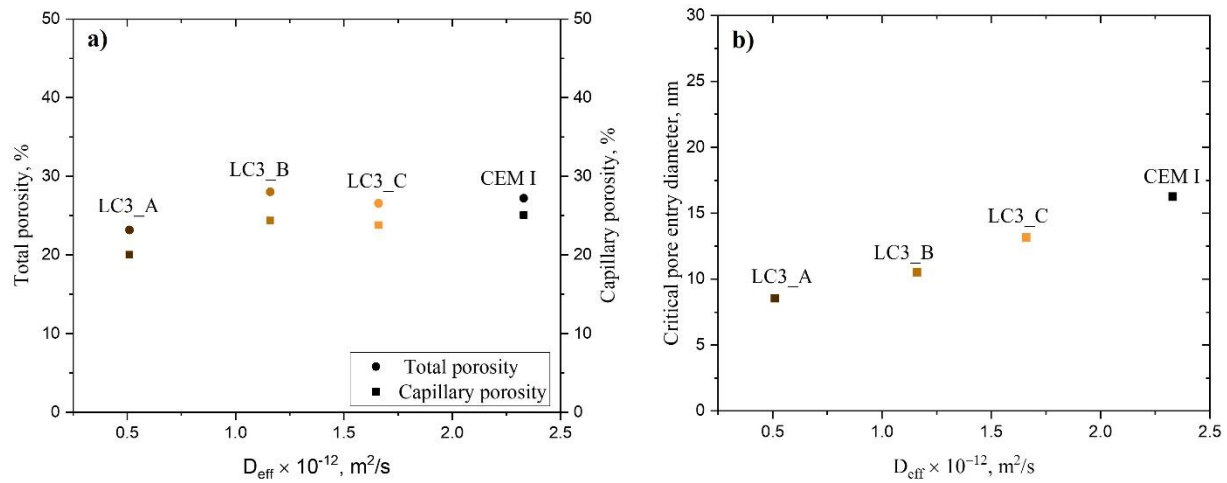

Figure 4.15 *Correlation of effective diffusion coefficient a) against total and capillary porosity, b) critical pore entry radius*

4.4.2 Effect of Bulk and pore solution conductivity

The bulk and pore solution conductivity values clearly demonstrate that there is a relationship between D_{eff} and bulk conductivity and pore solution conductivity. Figure 4.16a-b shows that the relationship between these parameters is quite strong and exponential, with an R^2 value of 0.98 for bulk conductivity and an R^2 value of 0.84 for pore solution. It was found that the alkali content in the pore solution is lower in the ternary system with limestone due to the dilution effect, and that the alkalis from the clinker phases also decrease proportionally due to the high-level replacement [149][74]. In addition, the lower Ca/Si ratio of the calcium

silicate hydrate in the blended system leads to alkali consumption, which decreases the alkalis in the pore solution. The lower Ca/Si ratio indicates that more siloxane bonds break in the silica chains, leading to the incorporation of alkali and the release of hydroxide ions into the pore solution [150], [151] [100], [152], [153] Avet et al. reported that LC3 samples with lower amounts of kaolinite had lower Ca/Si ratios, with a ratio of 1.61 for the LC3 sample with 17% kaolinite compared to 1.49 for the 50% kaolinite content [154]. Therefore, C-A-S-H in LC3_A causes more consumption of alkalis from pore solution than LC3_B and LC3_C. And hence, the total amount of alkalis was found to increase with decreasing kaolinite content. In addition, the amount of calcium ions in the pore solution was higher in LC3_B and LC3_C, which can be attributed to the lower consumption of portlandite by the pozzolanic reaction [24] of a clay system with low kaolinitic. The amount of alkalis is related to pH value; the lowest pH was determined for LC3_A.
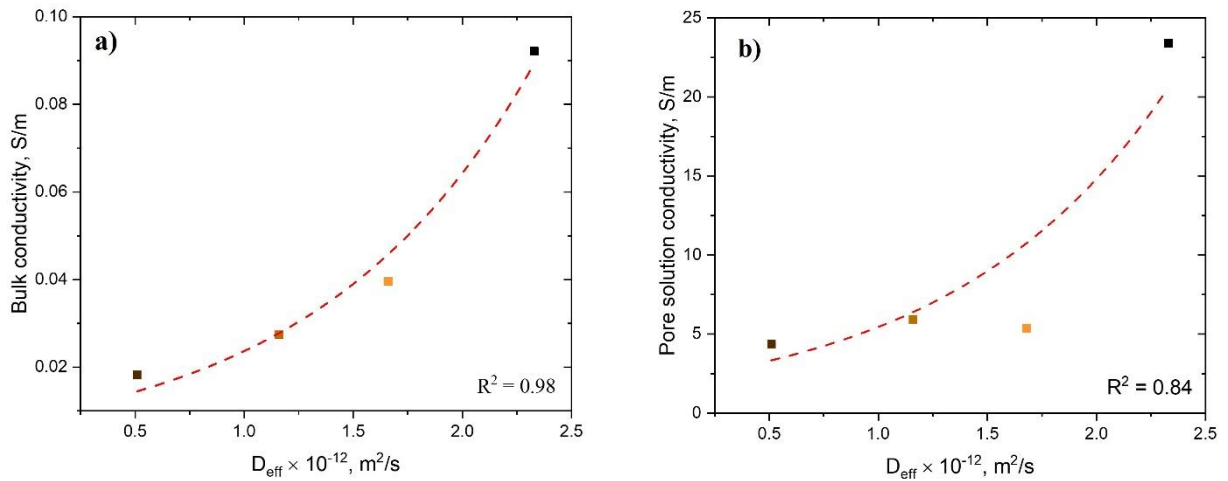

Figure 4.16 *Correlation of effective diffusion coefficient a) against bulk conductivity, b) against pore solution conductivity*

Regardless of the presence of kaolinite, the conductivity of the pore solution of the LC3 system was found to be in a similar range. However, the overall bulk conductivity decreased with increasing kaolin content. Therefore, it is crucial to consider the contribution of the pore solution resistivity to the bulk resistivity and consequently to the chloride penetration. To separate the first order effect of pore solution resistivity from the bulk resistivity, the concept of formation resistivity factor (F) might be a better option [155]–[158]. The basic idea of the formation factor goes back to Archie's law, which establishes a relationship between the specific resistivity of the water-saturated rock R_0 and the specific electrical resistivity of the brine R_w, which is the specific electrical resistivity of a clean, porous rock [155]. The basic equation is (Eqn. 4.7)

$$R_O = F \times R_w \qquad (4.7)$$

In a cementitious system, R_w represents the conductivity of the pore solution and R_O the bulk resistivity. The idea of formation factor indicates the relative increase in resistivity of the conductive solution due to the solid formation. The porosity and complexity of pore structure of solid formation was affected on the formation factor. While the lower formation factor generally indicates a higher porosity and low bulk resistivity. On the other side, when the formation factor has a higher value, the solid fraction contributes more to the total resistivity of the system than the resistivity of the conductive solution. The formation factor of all mixtures was calculated based on the above equation and is given in Table 4.7.

Table 4.7 *Formation factor of each mixture*

Mixtures	Formation factor, $F = \frac{R_O}{R_w}$
CEM I	254.48
LC3_A	242.08
LC3_B	219.60
LC3_C	137.62

The formation factor of LC3 was found to decrease as the kaolinite content decreased, indicating that the contribution of the solid portion towards the overall resistivity of the system was decreasing. However, the conductivity of the pore solution remained similar or decreased slightly with the addition of kaolinite. Therefore, the pore solution conductivity of the LC3 system, particularly with low-kaolinite clay, was limiting the overall conductivity of the system, which in turn controlled the penetration of chloride. LC3_C had the lowest formation factor, indicating the least contribution of resistivity from the solid portion to the total resistivity of the system among all mixtures. According to the theory of formation factor, a lower value leads to higher chloride penetration, but this was not observed for LC3_C and CEM I in this study. Hence, a general conclusion about the relationship between formation factor and chloride diffusion cannot be drawn for these mixes but it helped to draw the importance of pore solution conductivity to overall conductivity of the system. Overall, the improved resistance of chloride ingress in the LC3 system is mainly due to the pore solution or ions of the pore solution. However, the importance of the pore solution resistivity in LC3 with low kaolinite clay is clear.

4.4.3 Effect of chloride binding

William et al. reported that the chloride binding capacities of the individual mixtures do not affect the effective diffusion measured using mini-migration [100]. Nevertheless, they can be used to study the relative difference in binding capacities and the corresponding difference in effective diffusion coefficient between the systems. Table 4.8 shows the relative binding capacity as a percentage of total chloride, with the total chloride capacity of each system determined as the percentage of strong bound chloride in total chloride, and the chemical and physical binding capacities determined as the percentage of chloride content in each category in strong bound chloride.

Table 4.8 *Binding capacities of each mixture in terms of total bounded chloride.*

Mixture	Total binding capacity, %	Binding capacities physically or chemically	
		Chemical binding capacity, %	Physical binding capacity, %
CEM I	55.47	50.52	49.47
LC3_A	65.73	76.97	23.02
LC3_B	49.58	75.83	24.16
LC3_C	54.90	68.90	31.08

The LC3_A system had the highest total binding capacity, while LC3_B had the lowest. The total binding capacity varied among the different LC3 systems, depending on the kaolinite content and competing ions seeking to be incorporated into the alumina hydrates. Interestingly, contrary to the observed trend, LC3_B showed a lower binding capacity compared to LC3_C, even though it had a higher kaolinite content. The reason for the lower binding capacity of LC3_B compared to LC3_C, independent of the higher kaolinite content,

remains unclear. Similar to the values of the conductivity of pore solution, clay B and clay C displayed varying trends. Since the differences in values are not significant, it is possible to attribute them to statistical error. Moreover, Table 4.1 indicates that the total alkalis (Na_2O + K_2O) in Clay B were higher than those in Clay C. This difference in alkali content is evident in the pH of the pore solution of these mixtures. In fact, Avet al. found that a higher pH in the LC3 system resulted in a decrease in the bound chloride or a reduction in the formation of Friedel's salt [153]. However, it is worth noting that the formation of Friedel's salt solution was higher in the LC3 system, and this phenomenon is directly related to the total aluminum content present in the system [141][40], [44], [159].

4.4.4 Combined influence from all parameters

Chloride transport through cementitious systems is influenced to varying degrees by a variety of parameters. However, the combination of these parameters results in the lowest chloride penetration in the LC3 system. In systems with high kaolinite clay content, the capillary pores in the region were found to be very narrow according to MIP diagrams, which can lead to their walls being ionized and negatively charged due to interaction with the pore solution [160]–[164]. This leads to the formation of electrical double layers (EDL) along the pore walls, which can extend to the Debye length and depend mainly on the pore solution [160], [163], [165]–[167]. The LC3 system has a higher proportion of fine capillary pores, which leads to a stronger formation of the EDL region. The overlap of EDL can significantly increase the chloride entrapment, as shown in Figure 4.17. Finer pores between 5 nm and 10 nm have a stronger influence on chloride movement, especially where the influence of surface charge plays a crucial role in the adsorption of chloride ions.
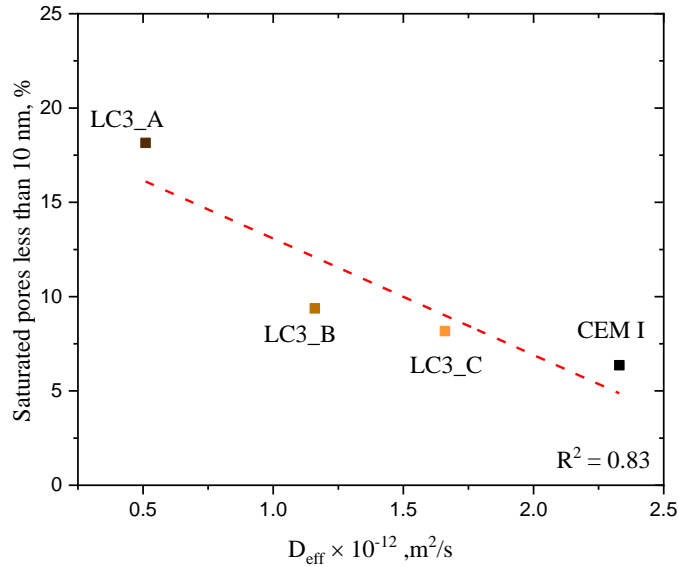
Figure 4.17 *Correlation of saturated fine pores against effective diffusion coefficient*

In the low-grade clay system, the chemistry of the pore solution shows that the amount of calcium ions is higher and has a greater affinity to adsorb on the pore walls than other alkalis due to its high valence electron [168]. In addition, the better physical adsorption of the low-grade clay system could be related to the pH, the amount of potassium/sodium ions in the pore solution, and the Ca/(Al+Si) ratio [153][40][44]. As a result, a higher amount of physically adsorbed chloride can be expected in low-grade clay mixes, which compensates for the low chemical binding capacities compared to high-grade clays. However, the EDL effect is expected to be more pronounced in high-kaolinitic clays due to their finer pore structure. In low-grade clays, the pore structure is much coarser, which weakens the effect of the electrical double layer. In addition, the amount of individual ions in the pore solution also affects the movement of chloride ions. The amount of individual ions (i.e., the total alkali content) increases with a decrease in the kaolinite content in the LC3 system. The higher amount of these individual ions leads to a high global diffusion resistance near negatively charged pore walls, making them less mobile and affecting the movement of

chloride ions in the pore solution[169], [170] [168]. In summary, the chemistry of the pore solution, together with the better pore structure and chloride binding capacity, plays a crucial role in making low-grade clay perform better than OPC.

4.5 Conclusions

Based on the findings of the systematic study conducted on chloride ingress in limestone calcined clay system with varying kaolinite content, the following conclusions were drawn:

1. The resistance of limestone low-grade calcined clay cementitious systems against chloride diffusion is better than OPC, but varies depending on the clay quality, especially the kaolinite content.

2. The bulk conductivity and pore solution conductivity are the most important factors controlling chloride penetration, and they show a strong correlation with the effective diffusion coefficient. In general, LC3 has a lower amount of alkali in the pore solution due to the low clinker content and high alkali binding capacity of C-A-S-H. It was found that the alkali content increases with the decrease of kaolinite content. However, the reduced clinker content resulted in lower conductivity of the systems based on low-grade clay, which ultimately led to lower chloride diffusion compared to the Portland system.

3. It was found that the effect of pore solution resistivity on bulk resistivity is higher for LC3, regardless of their kaolinite content. Higher pore solution resistivity and bulk resistivity cause the clays with low kaolinite to have better chloride resistance than the Portland cement system.

4. Chloride transport in the LC3 system is only slightly affected by total porosity and capillary porosity but is correlated to critical pore entry diameters. Moreover, the effective diffusion coefficients are inversely correlated with the presence of finely saturated pores in the range of 5 nm to 10 nm pore radius, i.e., the more finely saturated pores were measured in the system, the lower was the diffusion coefficient of the system.

5. The amount of Friedel's salt in the LC3 system is higher than in the Portland system, and the XRD patterns show that the amount of Friedel's salt correlates linearly with the kaolinite content. Despite the higher Friedel's salt content, the total binding capacities increased by a maximum of 20% between the system with the lowest and the one with the highest chloride penetration. At the same time, the effective diffusion coefficient was found to be five times lower in the case of LC3_A compared to OPC. Also, the differences between the different chloride contents are minimal, especially for the total chloride contents, indicating that the binding of chloride has less influence on the chloride transport. Although chloride binding affects chloride transport, it is not as critical as the pore solution chemistry of the system.

Chapter 5 Impact of lowering cement content and clinker replacement

The aim of this study is to evaluate how much the changes in the concrete mix design, which enable carbon footprint reduction, are impacting mechanical properties and predicted service life of concrete structure. The starting point of this study was concrete mix used in a recent reinforced concrete Pelješac Bridge in the Adriatic. In the first round of experiments the amount of cement in this initial mix was significantly lowered, without jeopardising workability of the mix. In the second round, the main part of the cement was substituted with the combination of fly ash and limestone or calcined clay and limestone. All supplementary cementitious materials used were sourced in the region of the structure. The calcined clays used in this study were collected locally and found to have a low kaolin content. On all mixes fresh and mechanical properties were tested to ensure that the requested equal or better workability and mechanical stability were reached. Furthermore, on each mix chloride migration was tested to evaluate the resistance of mix to chloride penetration. All mixtures were evaluated based on the overall performance considering mechanical, durability, and carbon footprints. The results indicate that the total cement content had a significant effect on durability and thus service life. The bridge mix design was determined to be 'over

designed,' as all alternative mixes achieved a similar or higher sustainability index with lower amount of cement.

Keywords: Low clinker cement, Chloride penetration, Service life, Environmental impact assessment, Sustainability

5.1 Introduction

Concrete is known to be the most sought-after building material in the world. Among all other industries, the cement industry has a significant carbon footprint of about 8% [20]. Consequently, concrete has a significant impact on the environment due to the cement industry. Current projections indicate that by 2050, approximately 18 billion tonnes of concrete will be required for worldwide construction, leading to an increase in carbon dioxide emissions from cement production. In recent decades, several attempts have been made to manufacture ecologically friendly concrete while also enhancing the efficiency of clinker [171][172][173][174][175][176].

Performance-based concrete design is one of the most straightforward and effective methods for enhancing clinker efficiency. In accordance with the 2016 United Nations Environment Program standards (UNEP-SBCI) [1], clinker efficiency must be enhanced by optimizing mix design with industry participation. The primary objective of mix design optimization is to prevent overdesigning of concrete, which can lower the amount of cement in concrete and its carbon impact. Standards prescribing a minimum cement content and a maximum water content for concrete to achieve the required characteristics are the most significant barrier to reducing the cement content of concrete [177][178]. Therefore, such a rigid, prescriptive design contributes to the reluctance of engineers to use alternative approaches based on concrete performance.

Other obstacles include concerns about long-term durability due to lower binder content, loss

of workability due to insufficient cement paste volume, and problems with the bond between

the steel and cement matrix [5]. Because of these technical concerns, engineers are unwilling

to take the risk of incorporating the reduced binder content into their mix design, even though

most of these concerns have been addressed. For example, workability of concrete is

maintained by using a high-range water reducer without increasing the w/b ratio [179][180]

[72] or without adding any water or cement to the system. There are some studies that have

looked at the durability of concrete with a lower binder content. In these studies, it was

reported that the cement content can be lowered without sacrificing durability, especially

maintaining equal penetrability of the concrete [10], [180]–[182]. Due to the higher

proportion of aggregate compared to cement paste, the permeability of the concrete can be

significantly reduced. In addition, the cement in the concrete may not be fully hydrated [183],

especially in a concrete with a very low water-cement ratio (w/c). The extent of cement

hydration is limited due to the lack of water in these systems, and the unhydrated cement

particles end up acting as fillers [184] – which can be trail by inexpensive filler such as

limestone without significant environmental or economic impact [185], [186].

The second most applied strategy of increasing clinker efficiency is introducing

supplementary cementitious materials (SCMs), such as fly ash (FA) and blast furnace slag

(BFS), for low CO_2 cements. Low-CO_2 cements containing SCM have shown improved

mechanical strength, durability, and sustainability, resulting in blended cements being the

most produced cements worldwide [187][188][189]. However, given the changes in the

energy sector and the greening of other industries, these usual SCMs will not be available on

a scale to meet the global demand for concrete and cement. Therefore, other materials need

to be considered as potential cement substitutes. Recent research studies have confirmed that kaolin clays can be used as a pozzolanic material, ensuring good performance of concrete and offering economic and environmental advantages [21][99][190]. However, most of these studies focused on high-purity kaolin clays, metakaolin, and clays with a kaolin content of at least 40%, which are difficult to find worldwide. Therefore, it is important to consider the possibility of using lower-grade clays (with less than 40 percent kaolinite), especially where high-purity clays are in short supply.

The objective of this work was to determine if reducing cement content and substituting it with locally available SCMs would affect the overall performance of the concrete structure in a marine environment. The effect of changes at the material level on the overall performance of structures is of paramount importance for wider acceptance and application of these solutions in practice. Numerous published studies attempt to comprehend the material properties resulting from variations in concrete formulation, which is undeniably essential and frequently leads to significant advances in cement research. The intent of this manuscript, on the other hand, is to demonstrate the impact of these changes in material properties on the overall performance of structures. The manuscript is based on a case study that takes the actual mix design for a built bridge, attempts to produce alternative mixes using locally available materials, and evaluates their overall performance in the structure. Therefore, the idea of this study is to analyse the limit to which it is possible to reduce the environmental impact of materials without compromising the performance of the structure.

The performance criteria were taken from a real concrete structure of Peljesac Bridge, a recently completed monumental structure designed for a 100-year service life in an aggressive Adriatic marine environment. Beginning with the actual concrete mix for the

bridge, fifteen mixtures were examined, ranging from a reduction in cement content to a
high-volume cement substitute. The high-volume replacement was achieved using a
combination of limestone – fly ash and limestone - calcined clay, with all materials readily
available in the cement plant region. The performance of the materials and their individual
contribution to the overall performance are beyond the scope of this study. Rather, the
purpose is to demonstrate whether the mechanical stability and service life of concrete
structures are affected by the selection of mixes with lower environmental impacts.
Therefore, the overall performance of all mixes in this study included a combination of the
following parameters: i) mechanical properties based on compressive strength, ii) service life
calculated based on chloride diffusion coefficient and Fick's second law, iii) economic
impact based on material price, iv) environmental impact based on global warming potential
(GWP), and v) environmental impact based on embodied energy.

5.2 Materials and methods

5.2.1 Binder composition

The bridge mix was designed using blended cement with slag addition, CEM II B-S in
accordance with EN 196-1. The primary material in all alternative binder systems was
Portland cement (CEM I 42,5R) according to EN 196-1. The physical and chemical
composition, as well as the mean particle size of all cementitious materials were determined
using X-Ray Fluorescence method and Laser diffraction technique (please see Table 5.A.1
and Figure 5.A.1 in appendix). All materials were obtained locally in the region of the cement
plant. The chemical admixture employed in the mixture is based on polycarboxylate ether,
and the solid content was determined as 35%, using the ASTM C484 method.

Two clays from distinct sources were employed in the investigation, and both had a lower amount of kaolinite. The kaolinite content was determined using the thermogravimetric analysis method [62]. Clay labelled as CC1 contains 14% kaolin and clay labelled as CC2 contains 18% kaolin. Fly ash was obtained from the Tuzla Thermal Power Plant in Bosnia and Herzegovina. The fly ash and raw clay were dried for 24 hours at $60 \pm {}^{0}C$ to remove all moisture. Following the drying process, they were ground for 30 seconds in a laboratory ball mill (each batch of 300 g material). Finally, the clays were calcined for an hour at 800 °C in a high-temperature laboratory furnace according to the procedure described in [191]. To ensure homogeneity, the ternary binder systems were pre-mixed prior to mixing.

5.2.2 Mixture details

The performance indicators were adopted from the bridge design. The targeted strength and slump fixed 50 MPa and 80-120 mm respectively. Throughout the service life the bridge will be exposed to harsh marine environment, already proven by other major reinforced concrete bridges in Croatia [192]. It is therefore that the bridge mix was designed with splash zone durability in mind, which means that diffusion coefficients should be kept to a minimum.

Two bridge mixes were prepared denoted BD435 and BD340. In BD435, the whole mix design was derived from the real mix (binder content, water/binder ratio, and aggregate amount), whereas in BD340, the binder content was reduced while maintaining the same water/binder ratio. All other mixes in the study followed equivalent mix design method. Initially, the cement type in the bridge mix was replaced with CEM I, to optimize the binder content and achieve the desired strength and workability. At this stage, mixtures with varying binder contents ranging from 350 to 200 kg/m^3 were prepared using CEM I cement with a w/b ratio of 0.40. Thereafter, the binder content and w/b ratio were adjusted based on the

fresh properties and compressive strength to avoid the out-flow performance of strength. Next, binder content was fixed to the chosen optimum of 340 kg/m^3 and w/b to 0.4 on which cement was substituted by fly ash and limestone or calcined clay and limestone. The cement replacement level of blended mixture varied from 30% to 45%. The combination of calcined clay/fly ash and limestone powder was in the ratio of 2:1 by total replacement volume of clinker. To achieve the maximum packing of aggregate, all aggregates were arranged based on the modified Andersson curve [193]. With the optimum packing of aggregate the paste volume can be reduced, at the same time increasing the workability [194]. In the next round, the amount of cement was further decreased, increasing at the same time water content. In this round, mixtures with varying binder contents ranging from 300 to 250 kg/m^3 were prepared using CEM I cement with a w/b ratio of 0.45. Here chosen binder content was 300 kg/m^3 and w/b to 0.45 for high volume cement substitution with fly ash/calcined clay and limestone. The details of all mixtures were given in appendix (see Table 5.A.2).

5.2.3 Preparation of concrete, fresh properties, and compressive strength

All the mixes were prepared and tested in fresh state according to EN 12350. Specimens were demoulded 24 hours after casting and then cubes were transferred to the humidity chamber (relative humidity maintained more than 95% and temperature of 20 ± 1 ^{o} C) until testing day. In designing the experimental plan, an engineering approach was used, employing standardized methods, methods normally used in practice. Since the basic idea of the work was to show the effects of cement reduction on a real case in a real environment, the methods and concrete age at which the tests were performed were the same for all mixes and conformed to standards. Although further environmental savings would be possible if the performance of the materials were considered at a later age (for example 56 or 90 days),

this rigorous and conservative approach was nevertheless used to clearly demonstrate potential savings from changes in concrete formulations.

Three concrete specimen of 15 cm $\times$ 15 cm $\times$ 15 cm were prepared to measure the compressive strength after 7 and 28 days of curing as per EN 12390-3 standard. Cylindrical specimen of 20 cm height and 10 cm diameter were prepared to test the chloride penetration resistance of the mixtures. After the 28 days of curing, the cylindrical specimens were split diametrically into three slices with thickness of 5 cm for the experiment.

5.2.4 Chloride penetration

The chloride ingress resistance was expressed in terms of chloride migration coefficient, which was determined by Nord Test Build 492 [64]. After the specified test duration, the specimen was splatted diametrically, and were sprayed with silver nitrate solution. The chloride penetration depth, x_d, was visible as whitish colour. Then the non-steady state migration coefficients (D_{nssm}) were determined based on the Nernst-Plank equation.

$$D_{nssm} = RT/zFE.(x_d - \alpha\sqrt{x_d})/t \tag{5.1}$$

5.2.5 Service life estimation

In this study, the calculation of service life of the reinforced structure included the corrosion initiation and propagation time. The initiation time was calculated based on the Fick's 2nd law of diffusion [195][196] as a time needed for the critical chloride content (Cl_{th}) to penetrate through a cover depth (d) and initiate the corrosion of reinforcement [197]. Therefore, the time to initiate the corrosion depends on the surface chloride concentration (Cl_s), chloride diffusion coefficients (D_{cl}) and the ageing coefficients (m). Therefore, the service life of structure is written as a function of each above-mentioned parameter.

$$Service\ life\ of\ a\ structure = f_n\ (d, Cl_{th}, m, D_{cl}, Cl_s) \qquad (3.2)$$

In this study, a reinforcement square column of 250 mm width and 50 mm cover depth was taken as the structural member for the determination of service life. The location of the bridge was taken as the location of Peljesac Bridge, Croatia. The chloride threshold value was taken as 0.05% (by weight of concrete) and the maximum surface chloride content was 0.8% by weight of binder. The cumulative probability of structural failure was taken as 0.5 for all mixtures. The ageing coefficient was assumed as 0.6 regardless of the mix. Pillai et al. [30] reported that ageing coefficients for fly ash and limestone-calcined clay cement are in the range of 0.5 to 0.7, and for Portland cement less than 0.20. At the same time, chloride thresholds were found to be lower in the blended system compared to the Portland cement system. The use of a higher aging coefficient for the blended system and a lower one for the Portland cement mix would result in a more significant decrease in the chloride diffusion coefficient with aging for the blended system compared to the Portland cement mix. However, the use of lower chloride thresholds for the blended system would result in a more rapid onset of corrosion compared to the Portland cement mix. Since the aging factor and chloride threshold were not measured for these particular alternative binders used in the present study, the maximum values for these two parameters were taken for all mixes [198]. However, for a more accurate calculation, the actual values of the aging factor and chloride thresholds should be measured.

Previous investigations on these and related systems found that chloride migration produces higher values than bulk diffusion. Since chloride migration was measured for all systems, a correlation factor was used to compare the two approaches.

$$D_{nssm} = k \times D_{cl} \qquad (3.3)$$

The value of 'k' determined experimentally from several previous studies by the authors was

taken as 1.69 [199].

5.2.6 Evaluation of environmental impact and material cost

The environmental impact and materials costs (A_{total}) were calculated for one cubic meter of

concrete, which were total sum of each individual values of materials multiplied (x_i) by

corresponding quantity (q_i) in one cubic meter of concrete.

$$A\_total = \sum\nolimits \llbracket (q_i \ \times x_i) \rrbracket \tag{5.4}$$

a) Environmental impact

The environmental impact assessment considered the environmental impact of producing

concrete constituents from raw materials, transporting the raw materials, and finally the

production of one cubic meter of concrete. The construction phase, service phase and

demolition phase were not considered in the analysis since they were presumed to be equal

for all systems. The present work environmental impact was expressed in terms of embodied

carbon and energy as per the guidelines in ISO 14040. Embodied carbon is expressed as

Global Warming Potential (GWP). GWP is a measure of the total emission of greenhouse

gases (equivalent to CO_2) to the atmosphere. Each material was analyzed up to the point of

manufacturing, excluding the sources of raw materials. The conversion parameters for each

material used to calculate the total embodied carbon/energy are given in appendix (see Table

5.A.3), along with their corresponding references. For mixes with calcined clay and

limestone (LC2 blend) mixtures, it was assumed that they were pre-mixed and used as a

single binder material [200]. The emission data for the transportation and production were

taken from Simapro data base [201], as well as from the literature and product data sheets

[12, 42-46] (for exact numbers used, please see Table 5.A.3). The production of concrete was assumed to occur at the bridge site, and the average distance between the production plant of each constituent and concrete plant was assumed to be 100 kilometers. The embodied carbon for the transportation was taken as 0.131 kg eq. CO_2/ kg [201].

b) Material cost

The total cost of a cubic meter of concrete was calculated as a sum of individual material costs multiplied by their quantity per cubic meter of concrete. Each material's cost was expressed in price (Euro) per kilogram, and data were gathered from local suppliers. Fly ash and calcined clay are still not commercially available, and as a result, a similar price was assumed for fly ash-limestone and LC2 blends. The prices of each material used in the study are given in additional documents (see Table 5.A.4 in Appendix).

5.2.7 Overall performance in terms of sustainability

Reducing the binder content or using alternative binders in concrete without considering the impact on durability would be a failure in terms of sustainability. Moreover, in today's world, economic advantages will be to the detriment of a more environmentally friendly concrete. Therefore, the sustainability of any concrete mix is a function of these parameters. To allow comparison of the mixes, the values of all parameters were converted into a single value indicating the sustainability of each mix. The overall performance of each mix was expressed using two different approaches: 1) sustainability factor (β) proposed by Muller et al. [202], and 2) five-performance index (I_{5P}) based on the study by Yu et al. [203].

a) Sustainability factor (β)

Muller et al. proposed a sustainability factor to evaluate the concrete mixture in terms of durability and environmental impact. The factor is determined by following relationship [202]:

$$Sustainability\ factor,\ \beta = (f_{ck} \times t_{SL})/(Embodied\ carbon\ (GWP))$$

(5.5)

where f_{ck} is 28-day compressive strength of the mixture, t_{SL} is the service life of the structure and embodied carbon is expressed as Global Warming Potential.

b) Five performance indices

This approach considers five distinct factors and weighs them differently. For example, the global sustainability of concrete is determined more by its life span, embodied energy, and cost than by its strength. The concept is derived from a study [203], and is then modified by incorporating the service life factor. While the first approach (see 3.2.7a) is relatively simple, incorporating additional factors and influences in the second approach may provide additional insight into an overall sustainability of proposed concrete mix. Additionally, this factor would indicate whether the mixture is compromising any means of sustainability when the cement content is significantly reduced. The overall performance indicator was calculated based on five different performance indices given in Table 5.1.

Table 5.1 *Five performance indices for estimation of overall performance indicator*

Index (I)	Weighting (w)	Equation
Embodied carbon index (I_{EC})	3	$I_{EC} = (GWP\ of\ reference\ mixture)$ $/(GWP\ of\ selected\ mixture)$
Service life index (I_{SL})	3	I_{SL} $= (Service\ life\ (in\ years)\ of\ reference\ mixture)$ $/(Service\ life\ (in\ years)\ of\ selected\ mixture)$
Cost index (I_C)	3	I_C $= (Cost\ of\ m\textasciicircum3\ concrete\ using\ reference\ mixture)$ $/(Cost\ of\ m\textasciicircum3\ concrete\ using\ selected\ mixture)$
Embodied energy index (I_E)	1	I_E $= (Embodied\ energy\ of\ reference\ mixture)$ $/(Embodied\ energy\ of\ selected\ mixture)$
Strength Index (I_S)	1	$I_S = (f\_ck\ of\ reference\ mixture)$ $/(f\_ck\ of\ selected\ mixture)$

After determining each index, the overall performance indicator called the five-performance

index (I_{5P}) is calculated based on the following relationship:

$$I_{5P} = (\sum_{i=5} \llbracket (I_i \times w_i)of\ selected\ mixture \rrbracket)/(\sum_{i=5} \llbracket (I_i \times$$

$$w_i)\ of\ reference\ mixture) \tag{5.6}$$

Where I_i are the five different indices and w_i is the weight of each index presented in Table

5.1.

5.3 Results and discussion

5.3.1 Evolution of strength

The fresh properties of all mixes are given in the Table 5.2. The reduction in the total binder

content significantly affected the workability of the mixture. For instance, C200 mixture was

totally unacceptable even with high amount of superplasticizer due to the very low amount

of paste in the system [204]. Also, the workability retention considerably reduced for C200

and C250. However, all the mixes surpassed the target strength of 50 MPa.

Table 5.2 *Fresh properties of bridge mixtures and alternative mixtures*

Mixture	Paste volume, l/m^3	Slump, mm	Temperature, ^{o}C	Wet density, kg/m^3	Air content, %
BD435	310.6	105	24.2	2482.2	2.4
BD340	242.4	105	24.1	2539.9	3.1
C350	252.9	90	26.9	2461.3	2.9
C340	246.03	90	24.3	2512.1	3.5
C300	231.80	90	27.8	2502.2	3.2
C250	180.60	80	27.8	2513.3	3.2
C200	144.50	78	28.9	2541	1.5
FA40	246.42	100	24.3	2512.1	2.1
LC2-45	243.65	90	24.9	2505.1	2.8
C300	232.40	100	22.3	2490.8	2.9
C250	215.42	95	24.2	2501.1	3.2
FA40	246.42	95	23.8	2498.9	3.4
FA30	242.08	95	25.3	2361.2	3.1
LC1-45	243.65	95	22.3	2395.3	2.8
LC1-45	243.5	95	23.3	2341.3	2.7

The effect of paste reduction on compressive strength is depicted in Figure 5.1. The strength

increased from mix C350 to C300 and then to C250. The tendency of compressive strength

to increase as paste content decreases is related to the decrease in the interfacial transition

zone (ITZ), which surrounds aggregates. An ITZ has a more fragile structure than bulk

hydrated cement and is more susceptible to mechanical loads. In addition, Jones et al.

reported that a reduction in the cement paste (which is highly porous) and an increase in

aggregate make the mixture less porous, thereby enhancing the physical contact between

aggregates. Even with reduced binder content, densified interfacial transition zones (ITZ)

could help to balance the strength [205], [206][207].
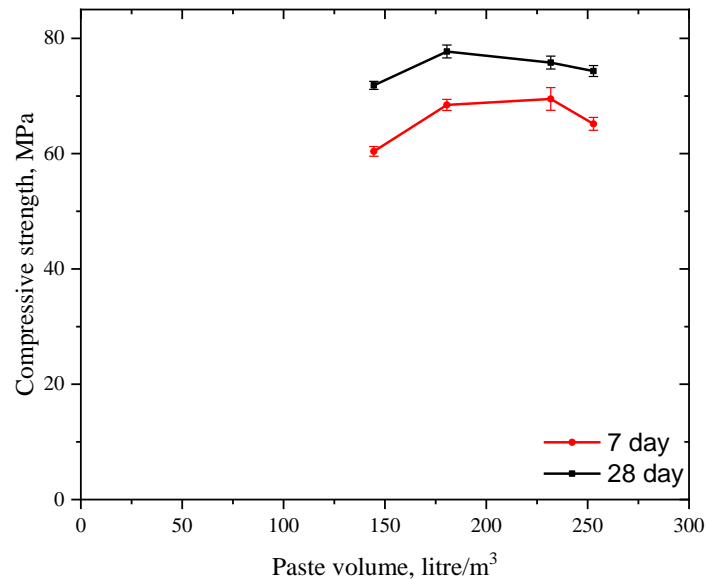
Figure 5.1 *Variation in compressive strength with respect to paste volume.*

Although all mixes satisfied criteria for compressive strength, due to the workability

retention the binder content of 300 kg/m^3 was chosen as a base reference for the alternative

cementitious systems. Additional to this, the binder content of 340 kg/m^3 was also used as a

base reference to compare the overall performance of mixes with high volume cement

substitution.

The compressive strength of the mixes that satisfied the targeted compressive strength after

7 and 28 days is depicted in Figure 5.2. In Figure 6, the C300 and C340 were taken as the

reference mixes for corresponding alternative binder system. Compressive strengths of

BD435 and BD340 were comparable, and a 22% decrease in cement content had no

discernible effect on compressive strength. In general, decreasing the cement content of

concrete at same w/b results in increased aggregate content, which has a detrimental effect

on the workability of the mixture and enhances compressive strength performance [208]. In

this case study, the issue of workability was resolved through the use of appropriate chemical

admixtures and optimized aggregate packing [182].
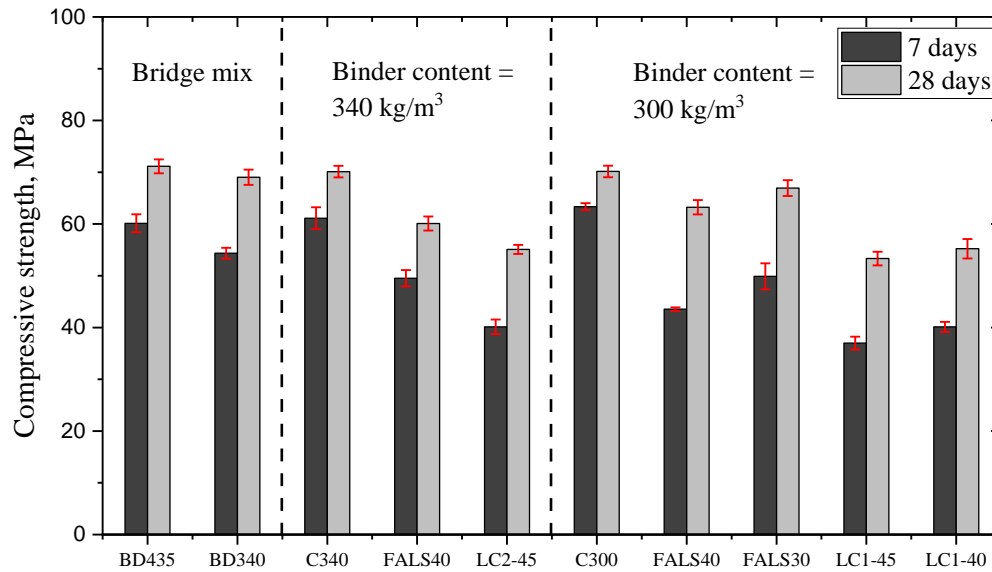
Figure 5.2 Compressive strength of all the mixture

It is visible that the FALS40 is a promising mixture, capable of achieving at least 80%

strength when compared to BD435. The addition of limestone in the system with fly ash and

cement resulted in increased compressive strength even at 40% of cement replacement and

even at early ages, contrary to the fly ash-Portland cement mixture [209]. Although the

performance of the calcined clay mixture was slightly lower than that of fly ash, compressive

strength still exceeded 50 MPa at 28 days with a high level of cement replacement. The

pozzolanic reaction kinetics and strength development of limestone-calcined clay are highly

dependent on kaolinite [24], which may explain why the compressive strength is lower than

that of the FALS mix. Despite the lower kaolinite content, the compressive strength of

concrete incorporating both clays were found to be satisfactory and met current performance criteria.

5.3.2 Chloride penetration

The durability performance of each mixture was evaluated by measuring non-stead state chloride migration coefficient (D_{nssm}). This coefficient was then transferred into the chloride diffusion coefficient shown in Figure 5.3 by using the Equation 5.2. Values of chloride diffusion coefficient were used to calculate the service life of each mixture in the following section.
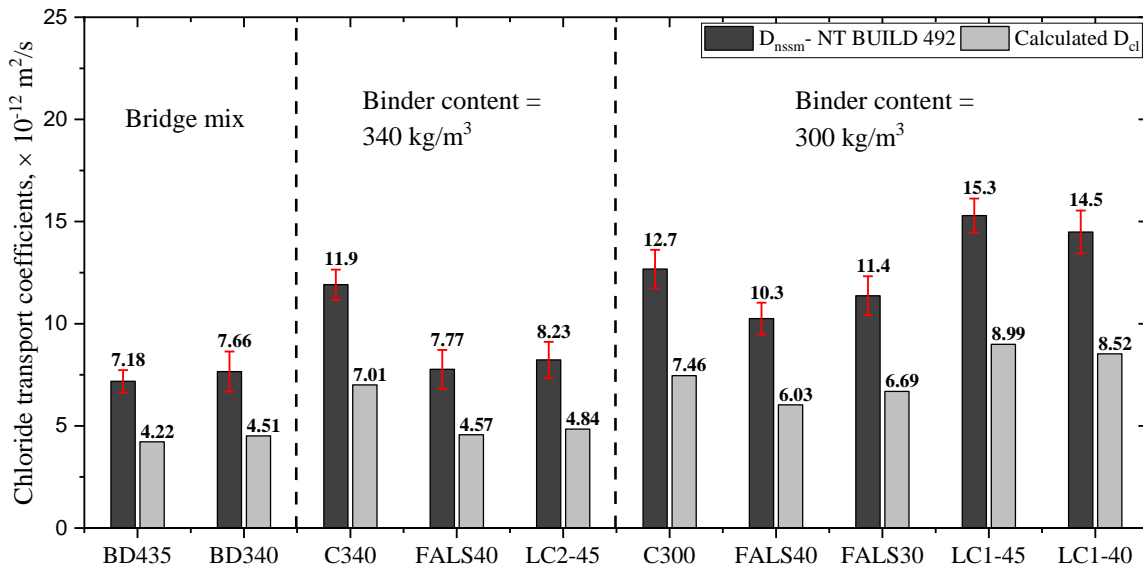
Figure 5.3 *Chloride migration coefficients (Dnssm)of all mixture and chloride diffusion values (Dcl) calculated using the relation Dnssm = 1.69 × Dcl*

In contrast to the compressive strength, the chloride penetration resistance of alternative binders was found to be dependent on the binder content and type of binder. Among all the mixtures, BD435 demonstrated the highest resistance to chlorides. Clearly, the bridge mix exhibits the least penetration due to the presence of blast furnace slag in cement itself. As the secondary hydrates formed, they densified the microstructure and inhibited the penetration

of the chloride ion, lowering the migration coefficients [209]. However, in BD340, the 95 kg/m^3 reduction in the total binder content did not result in a significant decrease in chloride penetration resistance, and the same compressive strength was achieved. Furthermore, when in the system with 340 kg/m^3 of cement part of the cement was substituted with fly ash and limestone or calcined clay and limestone, a significant improvement in chloride resistance was achieved. Finally, when the binder content was further decreased from 340 to 300 kg/m^3, the performance against chloride ingress significantly declined. In the systems with 300 kg/m^3 of cement even the substitution of cement with fly ash and calcined clay did not result in a significant improvement in requested resistance and the resistance remained lower than that of the bridge mix design. Nevertheless, chloride migration coefficient of system with 300 kg/m^3 and fly ash and limestone were still lower than that of 340 kg/m^3 of cement, which is important to highlight.

Comparing bridge mix BD425 and BD340, where the only difference is 20% reduction in cement content, it can be observed that the mix with 340 kg/m^3 achieved similar value of chloride transport. Furthermore, similar values of chloride transport were obtained when additional 40 to 45% of cement is substituted with fly ash and limestone and calcined clay and limestone, demonstrating that the reduction in cement content and substitution of clinker up to 45 percent has little effect on chloride penetration. In other words, overdesign in cement content is not required to improve the durability of concrete. However, the binder content of 300 kg/m^3 demonstrated poorer performance than BD435, indicating that there is a reduction limit beyond which concrete structures would be negatively affected.

5.3.3 Service year determination

The service year of each mixture was calculated by the method explained in Section 2 and

the cumulative probabilistic curve illustrated in the Figure 5.4a and 5.4b give the values of

service life at cumulative failure probability = 0.5.
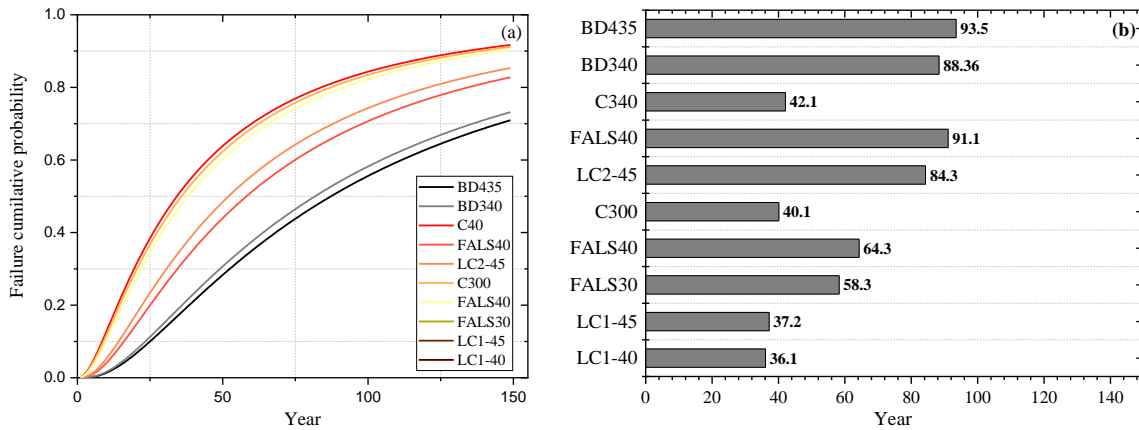
Figure 5.4 *a) Cumulative probability curves b) Service life in year of all the mixtures*

The service life is calculated as the sum of the corrosion initiation and propagation times,

with the propagation time for all the mixes assumed to be six years. In comparison to BD435,

the FALS40 mixture had a similar expected service life. The addition of 21% binder content

to BD435 had no effect on service life when compared to BD340 – due to the similar chloride

penetration resistance. Therefore, the reduction of cement content in the bridge design had

no effect on its service life. Despite the shorter service life of C300 and C340, the addition

of alternative binders with the same binder content increased their service life, with the fly

ash-limestone mixture exhibiting the greatest improvement. In the case of calcined clay, the

proportion of kaolinite and binder affects the service life; LC2-45 exhibited a significantly

longer service life than LC1-45. The difference in life span of each mixture demonstrates

that the binder type has a crucial role in durability performance of concrete, rather than the

amount of cement.

5.3.4 Environmental impact assessment and materials cost

a) Embodied carbon and embodied energy:

Environmental impact indicators (Global Warming Potential and embodied energy) are illustrated in Figure 5.5a and 5.5b, respectively. Additionally, the percentage of reduction compared to BD435 is clearly indicated in figures.
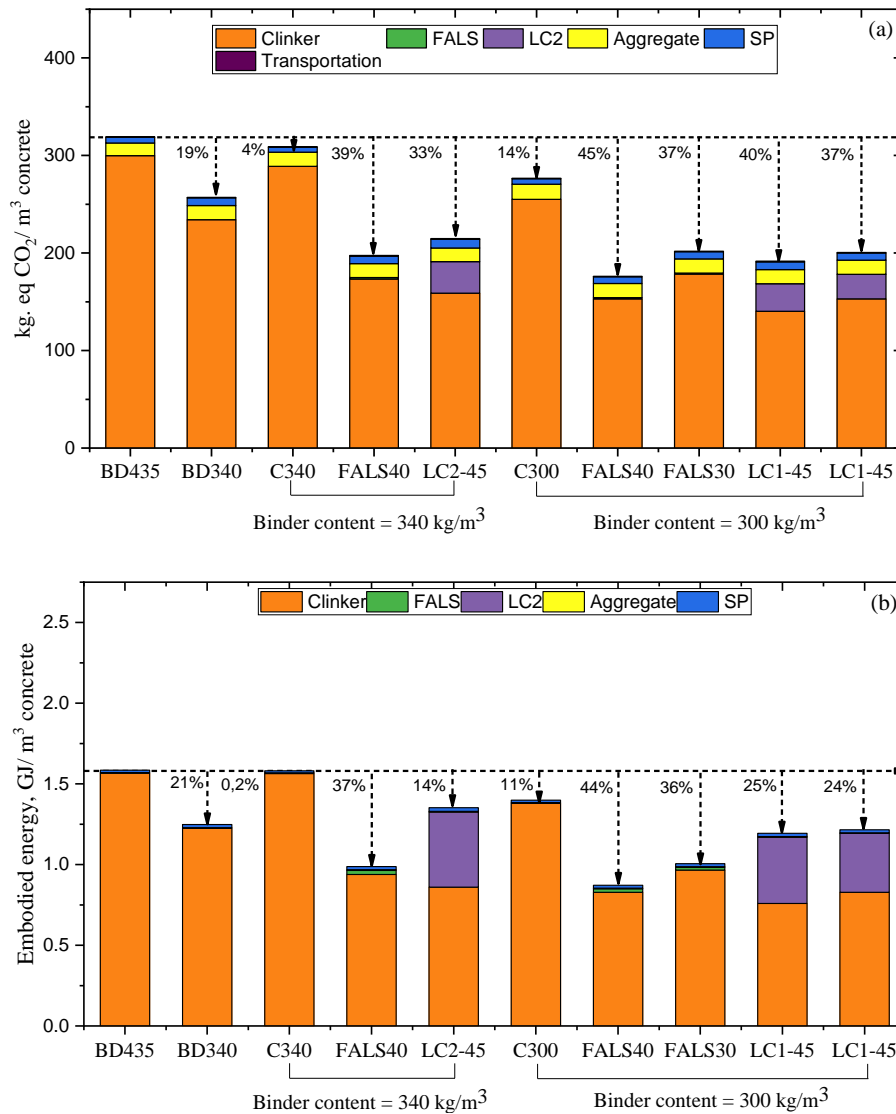
Figure 5.5 *a) Global Warming Potential, and b) Embodied energy of all mixtures compared to BD435.*

The figure demonstrated that the clinker component accounted for more than 70% of the

carbon and energy embodied in $1m^3$ concrete. As a result, reducing the binder content and

substituting with alternative binders can create a significant reduction of the overall

environmental impact of concrete. Additionally, the FALS mixture demonstrated the greatest

reduction in carbon footprint in this case. In the case of calcined clay, the GWP was found

to be reduced by between 30% and 40%, but the embodied energy was just 15%-25%.

Although the embodied energy of calcined clay is primarily due to the calcination process,

some studies indicate that it could be further reduced. The primary issue is a lack of sufficient

or accurate data for calcined clay. However, all alternative mixtures demonstrated a reduction

in environmental impact compared to mix BD435.

b) Material cost

The material cost for the unit-volume of concrete calculated and given in Table 5.3.

Table 5.3 *Total material cost of each mixture*

Mixture	Clinker	Fly ash/calcined clay + Limestone	Aggregate	Water	Superplasticizer	Total cost in Euro per m³
BD435	40.40	--	18.70	0.14	4.26	63.49
BD340	31.62	--	20.60	0.11	5.71	58.03
C340	33.66	--	20.38	0.11	3.81	57.96
FALS40	20.19	6.12	20.08	0.11	5.71	52.15
LC2-45	18.51	6.88	20.04	0.11	6.67	52.21
C300	29.70	--	21.96	0.11	4.20	55.97
FALS40	17.82	5.40	20.49	0.11	5.04	48.85
FALS30	20.79	4.05	20.57	0.11	5.46	50.98
LC1-45	16.33	6.06	20.53	0.11	5.88	48.91
LC1-40	17.82	5.40	20.53	0.11	5.46	49.32

The contribution from the clinker phase to the overall cost was found to be significant and hence it is clear that blended mixtures were more economical than 100% Portland cement mixtures.

5.3.5 Overall performance

Several parameters were discussed in the preceding sections, along with their individual contributions to each mixture. However, the overall performance of each mixture in terms of mechanical properties, environmental impact, and material cost must be discussed collectively. Therefore, each mixture should be ranked according to its sustainability. As mentioned in Section 5.2.7, two distinct approaches to analysing sustainable performance were considered.

The sustainability factor for each mixture is depicted in Figure 5.6 using Eq 5.5. Increased values denote a more sustainable mixture. The highest value was obtained for FALS40 with a binder content of 340 kg/m^3, while the lowest values were obtained for C300 and C340. Considering overall performance, the higher binder content with alternative binders were better than BD435.
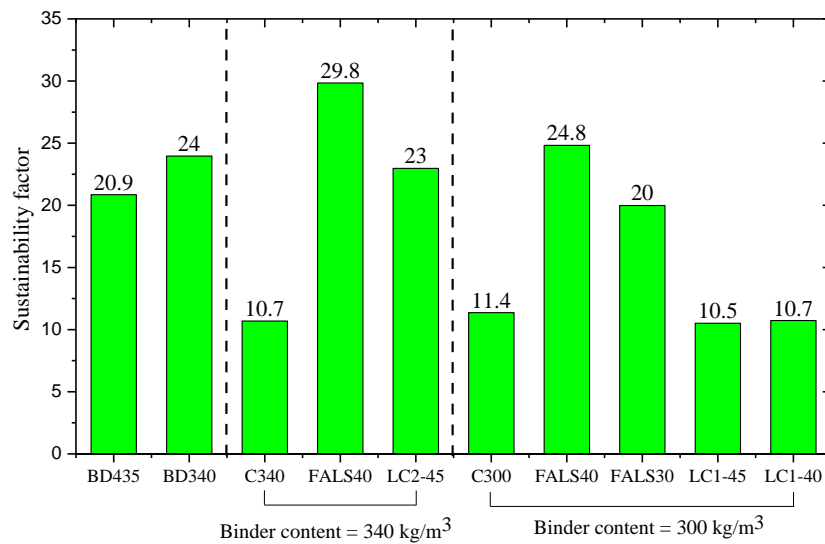
Figure 5.6 *Sustainability factor of each mixture considering compressive strength, service life, and GWP.*

In this technique, all sustainability parameters were weighted equally. In a concrete construction, for instance, service life is more significant than strength, particularly if the same desired compressive strength is achieved. On the other hand, stronger concrete does not always imply more durable concrete across all environments. Simultaneously, not all concrete with superior durability must be high strength. Strength should be specified in terms of the structure's ability to withstand applied loads, not as a performance metric for durability. As a result, the sustainability approach should be weighed differently and include additional parameters such as material cost. As a result, the second approach would provide a more

precise picture of sustainability. Section 5.2.7 explained about the five-performance indicator

and the distribution of each index illustrates each parameter's performance. The I_{5P} values

determined with BD435 as reference mixture are shown in Figure 5.7 and overall

performance indicator illustrated in Figure 5.8. Here also, a higher value of index is attributed

to the better performing mix for the specific property of this index.

(b)

(c)
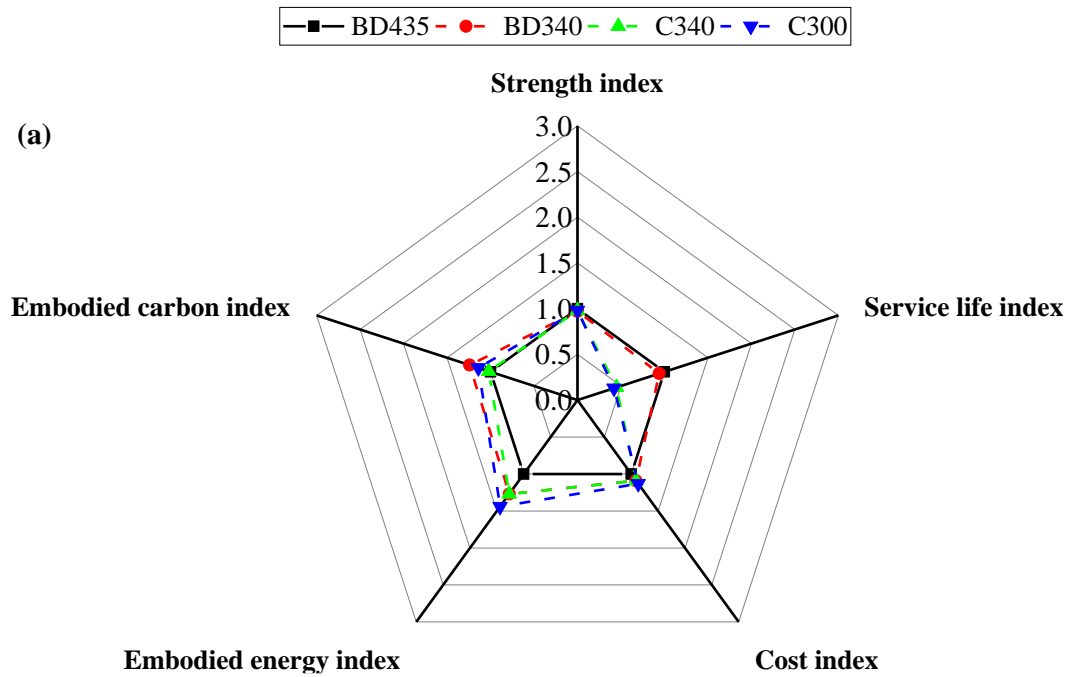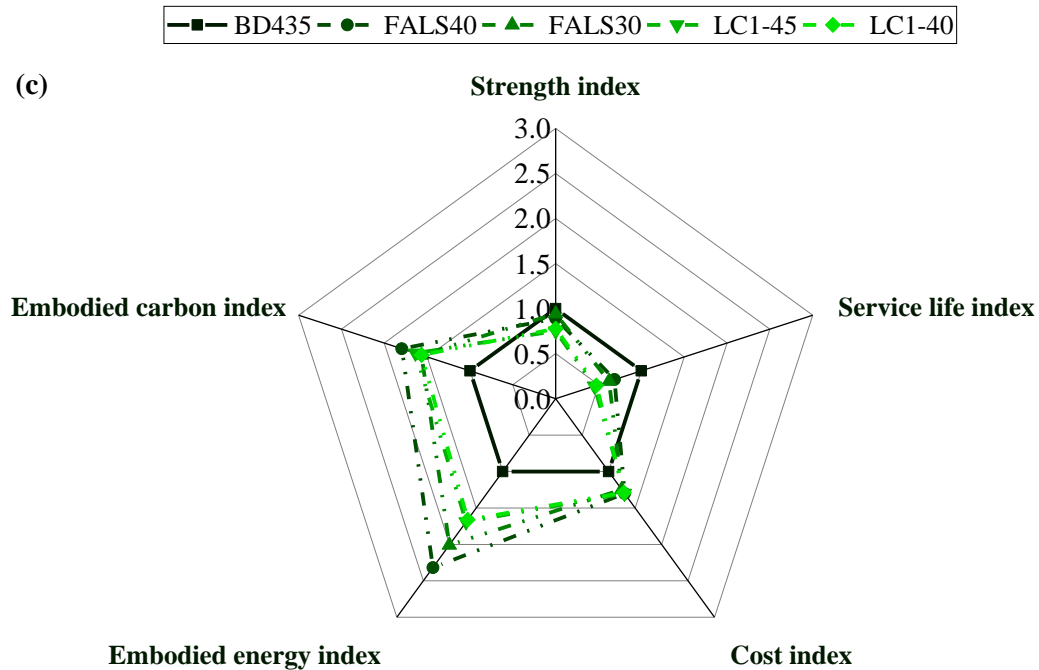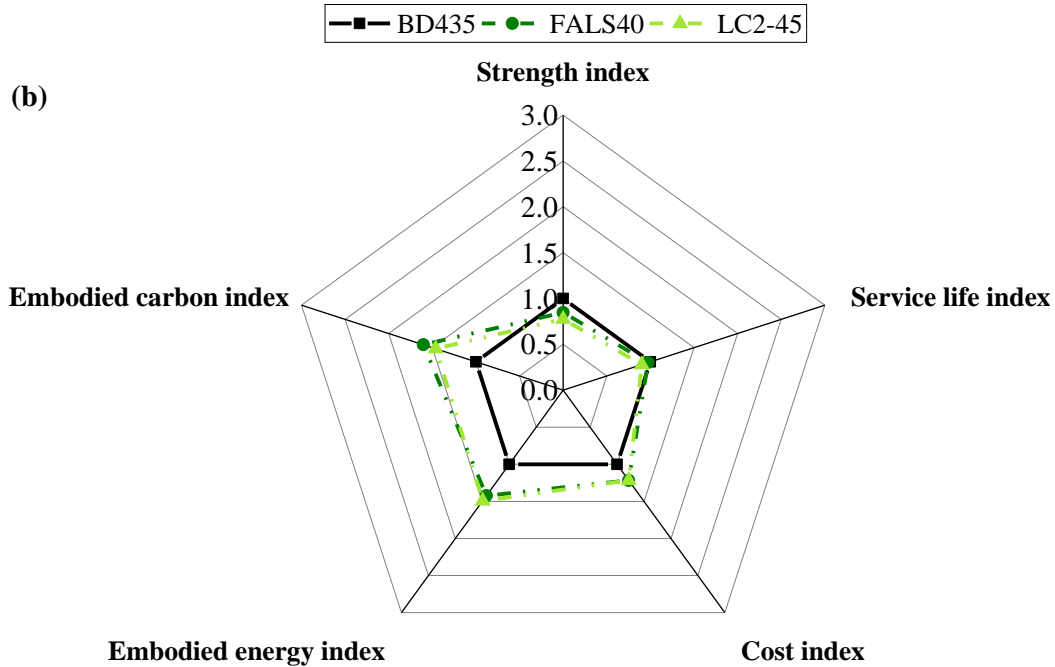
Figure 5.7 *Comparison of individual indices of all mixes a) BD435 vs control mixes with*
lowering cement content b) BD435 vs alternative binder content = 340 kg/m3, and b)
BD435 vs alternative binder content = 300 kg/m3

In the Figure 5.7a, the individual indices of BD435 (the original bridge mix design), BD340,

C340, and C300 are shown. From this first image it is visible that by just lowering cement

content, higher indices connected to environmental impact can be achieved. However, there is a tipping point, at which the mix is increasing the indices connected to environmental impact, but at the same time with the sacrifice of service life, therefore having lower overall performance indicator (shown in Figure 5.8). In the case of alternative binders with a total binder content of 340 kg/m^3 (Figure 5.7b), the significant reduction in the cement content and at the same time better durability (service life) was possible, leading to similar mechanical and service life indices and higher environmental indices. Overall performance indicator was therefore higher for mixes with alternative binder in total amount of 340 kg/m^3, compared to that of original bridge mix design. Finally, when considering mixes with a total binder content of 300 kg/m^3, compared to the original bridge mix design, it is evident that a limit in performance was reached. While alternative mixes do reach significantly higher environmental impact indices, the performance (mechanical and durability) are impaired. However, since all indices were considered with the same significance, all mixture performed significantly better than BD435, with the exception of the control mixtures in Figure 5.8.
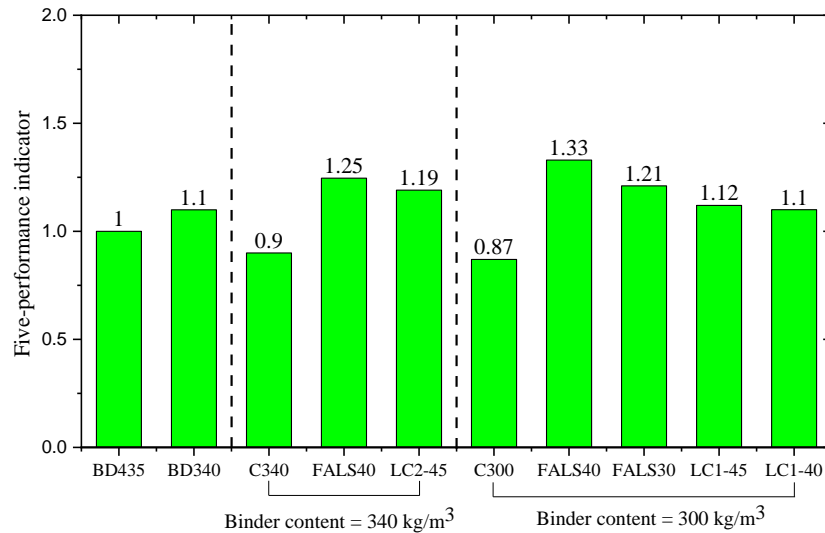
Figure 5.8 *Five-performance indicator of all the mixture compared BD435 as reference mixture.*

In comparison to the first method, the calcined clay mixture with both binder content levels showed good performance when compared to the bridge mixture. Even though the LC mixture demonstrated poor performance in terms of service life, they were still successful in achieving good sustainability in terms of environmental impact and materials cost. In the case of fly ash mixture, both mixes were significantly better than BD435.

Comparison of overall performance indicators shows how decreasing the amount of cement used alone cannot result in an overall better performance, as was demonstrated by mixes C340 and C300. But reducing the amount of cement in the mixture and supplementing it with other cementitious materials that are locally available could produce mixtures with competitive sustainability performance indicators. Therefore, all alternative systems with reduced total binder have exhibited very good potential in practical application. Additional to this, this study proved that good quality concrete can be produced with very low kaolin clay, producing concrete with comparable performance in terms of strength and durability

compared to cement with slag or fly ash. Therefore, the performance-based design by optimisation of binder content and usage of alternative binder would be a good strategy for a more sustainable approach in concrete industry.

5.4 Conclusion

In this experimental study, a real-structure concrete mix design was compared to different approaches of lowering carbon footprint of concrete. The concrete was prepared with reduced binder contents of $340 \, kg/m^3$ and $300 \, kg/m^3$. Next, the Portland cement was replaced by 30% and 45% with fly ash/calcined clay and limestone. The compressive strength and non-steady state chloride migration coefficients were evaluated for all the mixtures. From these results, the service life, environmental impact, and materials cost were evaluated. The overall sustainability of each mixture was evaluated and discussed using two different approaches.

Results presented in the study demonstrated on a real case scenario that the total binder content of concrete could be significantly reduced without compromising the mechanical and durability performance of concrete used in this specific structure exposed to harsh marine environment. Additionally, the usage of alternative binders along with reduction in the total binder content, provides an extra pull towards sustainability. The fly ash used, which was collected as waste stream, showed good results compared to the bridge mixture even with low binder content. The calcined clays used in this study was technically low-grade clay, and still it provided satisfying results in the overall sustainability performance. Unlike the fly ash and limestone mixture, in the case of calcined clay and limestone mixture, the kaolinite content and total binder significantly influenced the individual parameters. However, the

five-performance sustainability approach demonstrated that low grade clay could also be a

viable alternative to the original bridge design.

The study demonstrates unequivocally that optimizing total binder content and utilizing

alternative binders (particularly those that are locally available) are critical factors in

ensuring the overall sustainability of concrete. The study also experimentally proves that a

significant savings in carbon footprint can be achieved without compromising mechanical

stability or service life of concrete in structures even when exposed to aggressive marine

environment.

Appendix 5.A

Table 5.A.1 *Chemical composition (oxides) of each binder material and particle mean size*

Component	CEM I	CEM II	Fly ash (FA)	Calcined clay 1 (CC1)	Calcined clay 2 (CC2)	Limestone (LS)
CaO	63.19	46.94	11.52	2.57	2.17	71.59
SiO_2	19.51	33.65	53.28	63.70	62.41	20.21
Al_2O_3	4.21	7.55	19.11	19.53	21.35	4.32
Fe_2O_3	2.85	2.38	9.05	6.80	7.26	1.43
MgO	0.85	3.39	2.78	2.34	1.78	1.69
Na_2O	0.20	0.78	0.26	1.26	1.05	0
K_2O	0.48	0.74	1.51	2.52	2.50	0.15
TiO_2	0.12	0.22	0.52	0.76	0.94	0.52
P_2O_5	0.45	0.01	0.36	0.35	0.36	0.42
SO_3	2.3	4.02	1.48	0.12	0.07	1.48
D_{10}, µm	0.32	0.45	1.55	3.13	4.03	3.43
D_{50}, µm	9.95	12.71	15.24	12.16	10.72	18
D_{90}, µm	50	58.85	72.68	42.43	24.79	63.82
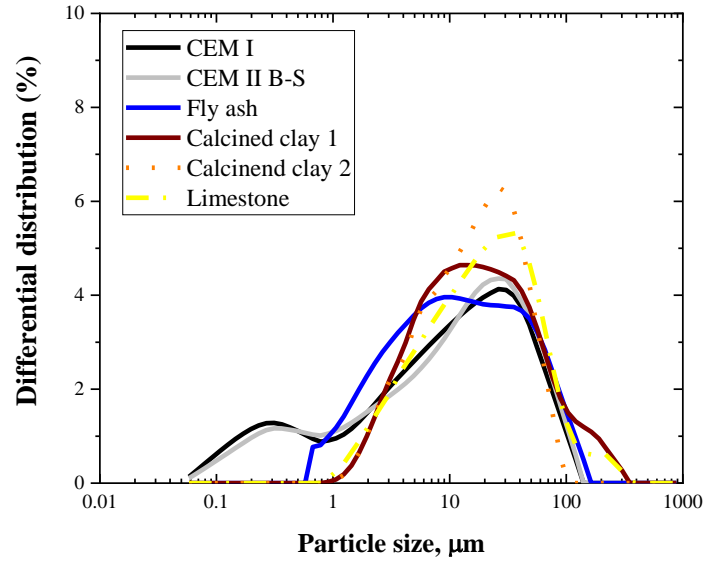
Figure 5.A.1 *Particle size distribution of each binder materials*

Table 5.A.2 Mix design.

Mixture	Binder kg/m^3	w/b	Water, kg/m^3	Cement, kg/m^3	FA kg/m^3	CC kg/m^3	L kg/m^3	SP* %	Aggregate, kg/m^3		
									16 – 8	8 – 4	4 – 0
BD435	435		169	435	-	-	-	0.7	470	472	934
		0.39									
BD340	340		132	340	-	-	-	1.2	518	520	1029
C350	350		140	350	-	-	-	0.7	510	512	1014
C340	340		136	340	-	-	-	0.8	513	514	1018
C300	300		120	300	-	-	-	1.1	536	538	1064
C250	250	0.40	100	250	-	-	-	2.1	561	563	1115
C200	200		80	200	-	-	-	2.8	586	588	1165
FA40	340		136	204	91.12	-	46.92	1.2	505	507	1003
LC2-45	340		136	187	-	102	51	1.4	504	505	1001
C300	300		135	300	-	-	-	1.0	525	527	1043
C250	250		135	250	-	-	-	1.9	538	539	1066
FA40	300		135	180	80.4	-	39.6	1.2	515	517	1023
		0.45									
FA30	300		135	210	60.3	-	29.7	1.3	517	519	1028
LC1-45	300		135	165	-	90	45	1.4	516	518	1025
LC1-40	300		135	180	-	80.4	39.6	1.3	516	518	1025

Table 5.A.3 *Embodied carbon and energy of ingredients in the mixture*

Material	Embodied carbon, (kg eq. CO_2/ kg)	Embodied energy, MJ/kg	Reference
CEM I 42.5R	0.803	5.05	[210]
CEM II B-S	0.646	4.5	[211]
LC2 blend	0.210	3.04	[179]
Fly ash	0.008	0.1	[212]
Limestone powder	0.0172	0.35	[202]
Crushed aggregate	0.00702	0.113	[202]
Superplasticizer	1.88	4.8	[213]

Table 5.A.4 *Material cost of each ingredient*

Material	Price in Euro/kg of material	Reference
CEM I 42.5R	0.099	Local supplier
CEM II B-S	0.093	
LC2 blend	0.008	[214]
Fly ash-limestone blend	0.045	
Crushed aggregate	0.00997	Local supplier
Superplasticizer	1.4	

Chapter 6 Conclusions

The current research was mainly put forward to highlight the importance of performance-based concrete using locally available materials with minimum ecological footprint. Throughout this thesis, the focus was on the potential of using low-grade kaolinitic clays in high-performance cementitious materials, particularly in limestone calcined clay cement (LC3). Following are the concluding remarks based on entire work of this thesis:

1. The results showed that LC3 with lower grade clay demonstrated performance equivalent to the Portland system in terms of compressive strength, durability, cost, service life, and sustainability.

2. The durability of LC3 with lower-grade clay was found to be better than the Portland system in terms of chloride diffusion, chloride migration, and sorptivity, particularly with clay containing 40% kaolinite content. However, the purity or kaolinite content of the clays strongly influenced the variation of LC3 properties.

3. The chloride transport in LC3 with lower kaolinite content was mainly driven by the conductivity of the pore solution, whereas in LC3 with higher kaolinite content, it was enabled by the combination of pore structure, chloride binding of AFm phases, and overall conductivity. LC3 demonstrated a higher amount of finer capillary pores and gel pores compared to Portland cement, which may enhance physical absorption of chloride ions on the pore walls due to the effect of electrical double layer. At the same time, the total porosity and binding capacities were found to be similar in both systems, indicating lower impact of these parameters on chloride transport in LC3 systems based on low grade kaolin clay.

4. Green concrete with the targeted properties was achieved, with concrete from Pelješac Bridge used as a benchmark. The study confirmed that by at the same time enhancing the total efficiency of the binder and the efficiency of clinker, concrete with lower ecological footprint and equal performance can be designed.

5. A simple sustainability framework was proposed to evaluate concrete mixtures based on their compressive strength, service life, cost, and ecological carbon footprint.

Future recommendation

1. Long-term studies on durability and service life: While the study has shown promising results for the performance of LC3 concrete with lower grade kaolinitic clays in terms of compressive strength and durability, it's important to conduct long-term studies to evaluate its performance under different environmental conditions. This could include exposure to freeze-thaw cycles, acid attack, and alkali-silica reaction, which are common durability issues for concrete structures. By evaluating the performance of LC3 concrete under these conditions, we can better understand its long-term sustainability and service life, which is critical for large-scale construction projects.

2. In-depth study on chloride adsorption: The study has shown that LC3 concrete with lower kaolinite content has a higher amount of finer capillary pores and gel pores, which may enhance the physical absorption of chloride ions on the pore walls. An in-depth study on chloride adsorption and its influence on chloride transport, especially with lower kaolinite clay-based concrete, would be valuable. This could include investigating the relationship between pore structure, chloride binding of AFm

phases, and overall conductivity, as well as understanding the impact of electrical double layer on chloride transport.

3. Workability and retention time: While LC3 concrete with lower-grade kaolinitic clays has shown to have comparable performance to Portland cement-based concrete, there may be challenges in terms of workability and retention time. An in-depth study on the influence of different minerals from clays on the workability and retention time of LC3 concrete could provide valuable insights into how to optimize the mix design and processing conditions to achieve desired performance. This could include investigating the use of chemical admixtures, curing conditions, and processing techniques to enhance the workability and retention time of LC3 concrete.

References

[1] SCRIVENER, K. L. et all, Eco-efficient cements: Potential, economically viable solutions for a low-CO2 cement based industry, p. 64, 2016.

[2] de Brito, J. and Kurda, R., The past and future of sustainable concrete: A critical review and new strategies on cement-based materials, *J. Clean. Prod.*, vol. 281, p. 123558, 2021, doi: 10.1016/j.jclepro.2020.123558.

[3] Damineli, B. L., Kemeid, F. M., Aguiar, P. S., and John, V. M., Measuring the eco-efficiency of cement use, *Cem. Concr. Compos.*, vol. 32, no. 8, pp. 555–562, 2010, doi: 10.1016/j.cemconcomp.2010.07.009.

[4] Habert, G. and Roussel, N., Study of two concrete mix-design strategies to reach carbon mitigation objectives, *Cem. Concr. Compos.*, vol. 31, no. 6, pp. 397–402, 2009, doi: 10.1016/j.cemconcomp.2009.04.001.

[5] Wassermann, R., Katz, A., and Bentur, A., Minimum cement content requirements: A must or a myth?, *Mater. Struct. Constr.*, vol. 42, no. 7, pp. 973–982, 2009, doi: 10.1617/s11527-008-9436-0.

[6] Barbudo, A., De Brito, J., Evangelista, L., Bravo, M., and Agrela, F., Influence of water-reducing admixtures on the mechanical performance of recycled concrete, *J. Clean. Prod.*, vol. 59, pp. 93–98, 2013, doi: 10.1016/j.jclepro.2013.06.022.

[7] Papayianni, I., Tsohos, G., Oikonomou, N., and Mavria, P., Influence of superplasticizer type and mix design parameters on the performance of them in concrete mixtures, *Cem. Concr. Compos.*, vol. 27, no. 2, pp. 217–222, 2005, doi: 10.1016/j.cemconcomp.2004.02.010.

[8] Breilly, D., Fadlallah, S., Froidevaux, V., Colas, A., and Allais, F., Origin and industrial applications of lignosulfonates with a focus on their use as superplasticizers in concrete, *Constr. Build. Mater.*, vol. 301, p. 124065, 2021, doi: 10.1016/j.conbuildmat.2021.124065.

[9] Wasserman, R. and Bentur, A., Effect of concrete composition on durability in natural

acidic environment, *Adv. Cem. Res.*, vol. 18, no. 4, pp. 135–143, 2006.

[10]   Buenfeld, N. R. and Okundi, E., Effect of cement content on transport in concrete, *Mag. Concr. Res.*, vol. 50, no. 4, pp. 339–351, 1998, doi: 10.1680/macr.1998.50.4.339.

[11]   Yousuf, S., Structural low cement content (LCC) concrete: An eco-friendly alternative for construction industry. Université d'Ottawa/University of Ottawa, 2018.

[12]   Concrete, T. M., Sika Concrete Handbook.

[13]   Fennis, S. A. A. M. and Walraven, J. C., Using particle packing technology for sustainable concrete mixture design, *Heron, 57 2*, no. January 2012, 2016.

[14]   Furnas, C. C., Grading aggregates-I.-Mathematical relations for beds of broken solids of maximum density, *Ind. Eng. Chem.*, vol. 23, no. 9, pp. 1052–1058, 1931.

[15]   Feret, R., Sur la compacité des mortiers hydrauliques, *Ann. Pntas Chaussees, Mem Doc*, vol. 4, pp. 5–164, 1892.

[16]   Andreasen, A. H. M. and Andersen, J., Relation between grain size and interstitial space in products of unconsolidated granules, *Kolloid-Zeitschrift*, vol. 50, no. 3, pp. 217–228, 1930.

[17]   Talbot, A. N., Brown, H. A., and Richart, F. E., *The strength of concrete: its relation to the cement aggregates and water*, no. 137–138. University of Illinois, 1923.

[18]   Fuller, W. B. and Thompson, S. E., The laws of proportioning concrete, 1907.

[19]   Toufar, W., BEITRAG ZUR OPTIMIERUNG DER PACKUNGSDICHTE POLYDISPERSER KOERNIGER SYSTEME., 1976.

[20]   Scrivener, K. L., John, V. M., and Gartner, E. M., Eco-efficient cements: Potential economically viable solutions for a low-CO2 cement-based materials industry, *Cem. Concr. Res.*, vol. 114, no. March, pp. 2–26, 2018, doi: 10.1016/j.cemconres.2018.03.015.

[21]   Scrivener, K., Martirena, F., Bishnoi, S., and Maity, S., Calcined clay limestone

cements (LC3), *Cem. Concr. Res.*, vol. 114, no. March 2017, pp. 49–56, 2018, doi: 10.1016/j.cemconres.2017.08.017.

[22]   Antoni, M., Rossen, J., Martirena, F., and Scrivener, K., Cement substitution by a combination of metakaolin and limestone, *Cem. Concr. Res.*, vol. 42, no. 12, pp. 1579–1589, 2012, doi: 10.1016/j.cemconres.2012.09.006.

[23]   Vizcaíno, L., Antoni, M., Alujas, A., Martirena, F., and Scrivener, K., Industrial manufacture of a low-clinker blended cement using low-grade calcined clays and limestone as SCM: the Cuban experience, in *Calcined Clays for Sustainable Concrete*, vol. 10, Springer, 2015, pp. 347–358.

[24]   Avet, F. and Scrivener, K., Investigation of the calcined kaolinite content on the hydration of Limestone Calcined Clay Cement (LC3), *Cem. Concr. Res.*, vol. 107, no. February, pp. 124–135, 2018, doi: 10.1016/j.cemconres.2018.02.016.

[25]   Hollanders, S., Mineralogical study of the pozzolanic properties of calcined clays, no. April, p. 236, 2017, [Online]. Available: https://limo.libis.be/primo-explore/fulldisplay?docid=LIRIAS1727587&context=L&vid=Lirias&search_scope=Lirias&tab=default_tab&lang=en_US&fromSitemap=1.

[26]   Mohammed, S., Processing, effect and reactivity assessment of artificial pozzolans obtained from clays and clay wastes: A review, *Constr. Build. Mater.*, vol. 140, pp. 10–19, 2017, doi: 10.1016/j.conbuildmat.2017.02.078.

[27]   Scrivener, K. *et al.*, Impacting factors and properties of limestone calcined clay cements (LC3), *Green Mater.*, vol. 7, no. 1, pp. 3–14, Nov. 2018, doi: 10.1680/jgrma.18.00029.

[28]   Alujas, A., Fernández, R., Quintana, R., Scrivener, K. L., and Martirena, F., Pozzolanic reactivity of low grade kaolinitic clays: Influence of calcination temperature and impact of calcination products on OPC hydration, *Appl. Clay Sci.*, vol. 108, pp. 94–101, 2015, doi: 10.1016/j.clay.2015.01.028.

[29]   Dhandapani, Y., Sakthivel, T., Santhanam, M., Gettu, R., and Pillai, R. G., Mechanical properties and durability performance of concretes with Limestone Calcined Clay

Cement (LC3), *Cem. Concr. Res.*, vol. 107, no. March, pp. 136–151, 2018, doi: 10.1016/j.cemconres.2018.02.005.

[30] Pillai, R. G. *et al.*, Service life and life cycle assessment of reinforced concrete systems with limestone calcined clay cement (LC3), *Cem. Concr. Res.*, vol. 118, no. July, pp. 111–119, 2019, doi: 10.1016/j.cemconres.2018.11.019.

[31] Maraghechi, H., Avet, F., Wong, H., Kamyab, H., and Scrivener, K., Performance of Limestone Calcined Clay Cement (LC3) with various kaolinite contents with respect to chloride transport, *Mater. Struct. Constr.*, vol. 51, no. 5, pp. 1–17, 2018, doi: 10.1617/s11527-018-1255-3.

[32] Koch, G., Varney, J., Thompson, N., Moghissi, O., Gould, M., and Payer, J., International measures of prevention, application, and economics of corrosion technologies study, *NACE Int.*, vol. 216, pp. 2–3, 2016.

[33] Basdeki, M. and Apostolopoulos, C., Mechanical Behavior Evaluation of Tempcore and Hybrid Reinforcing Steel Bars via a Proposed Fatigue Damage Index in Long Terms, *Met. - Open Access Metall. J.*, vol. 11, p. 25, 2021, doi: 10.3390/met11050834.

[34] Sui, S., Georget, F., Maraghechi, H., Sun, W., and Scrivener, K., Cement and Concrete Research Towards a generic approach to durability : Factors a ff ecting chloride transport in binary and ternary cementitious materials, *Cem. Concr. Res.*, vol. 124, no. July 2018, p. 105783, 2019, doi: 10.1016/j.cemconres.2019.105783.

[35] Dhandapani, Y. and Santhanam, M., Investigation on the microstructure-related characteristics to elucidate performance of composite cement with limestone-calcined clay combination, *Cem. Concr. Res.*, vol. 129, no. October 2019, p. 105959, 2020, doi: 10.1016/j.cemconres.2019.105959.

[36] Dhandapani, Y. and Santhanam, M., Assessment of pore structure evolution in the limestone calcined clay cementitious system and its implications for performance, *Cem. Concr. Compos.*, vol. 84, pp. 36–47, 2017, doi: 10.1016/j.cemconcomp.2017.08.012.

[37] Wilson, W., Georget, F., and Scrivener, K., Cement and Concrete Research

Unravelling chloride transport / microstructure relationships for blended- cement pastes with the mini-migration method, *Cem. Concr. Res.*, vol. 140, no. October 2020, p. 106264, 2021, doi: 10.1016/j.cemconres.2020.106264.

[38]   Zunino, F. and Scrivener, K., Microstructural developments of limestone calcined clay cement (LC3) pastes after long-term (3 years) hydration, *Cem. Concr. Res.*, vol. 153, p. 106693, 2022, doi: 10.1016/j.cemconres.2021.106693.

[39]   Briki, Y., Avet, F., Zajac, M., Bowen, P., Ben, M., and Scrivener, K., Cement and Concrete Research Understanding of the factors slowing down metakaolin reaction in limestone calcined clay cement (LC 3) at late ages, *Cem. Concr. Res.*, vol. 146, no. April, p. 106477, 2021, doi: 10.1016/j.cemconres.2021.106477.

[40]   Lc, C., Avet, F., and Scrivener, K., Cement and Concrete Research In fl uence of pH on the chloride binding capacity of Limestone Calcined Clay, *Cem. Concr. Res.*, vol. 131, no. March, p. 106031, 2020, doi: 10.1016/j.cemconres.2020.106031.

[41]   Zolfagharnasab, A., Ramezanianpour, A. A., and Bahman-zadeh, F., Investigating the potential of low-grade calcined clays to produce durable LC 3 binders against chloride ions attack, *Constr. Build. Mater.*, vol. 303, no. May, p. 124541, 2021, doi: 10.1016/j.conbuildmat.2021.124541.

[42]   Georget, F., Calixe, B., Wilson, W., and Scrivener, K. L., Cement and Concrete Research Chloride sorption by C-S-H quantified by SEM-EDX image analysis, vol. 152, no. November 2021, pp. 1–11, 2022, doi: 10.1016/j.cemconres.2021.106656.

[43]   Sui, S. *et al.*, Cement and Concrete Research Quantification methods for chloride binding in Portland cement and limestone systems, *Cem. Concr. Res.*, vol. 125, no. August, p. 105864, 2019, doi: 10.1016/j.cemconres.2019.105864.

[44]   Wilson, W., Nicolas, J., Georget, F., and Scrivener, K. L., Cement and Concrete Research Insights on chemical and physical chloride binding in blended cement pastes, *Cem. Concr. Res.*, vol. 156, p. 106747, 2022, doi: 10.1016/j.cemconres.2022.106747.

[45]   Krishnan, S., Gopala Rao, D., and Bishnoi, S., Why Low-Grade Calcined Clays Are

the Ideal for the Production of Limestone Calcined Clay Cement (LC3) BT - Calcined Clays for Sustainable Concrete, 2020, pp. 125–130.

[46]   Du, H. and Pang, S. D., High-performance concrete incorporating calcined kaolin clay and limestone as cement substitute, *Constr. Build. Mater.*, vol. 264, Dec. 2020, doi: 10.1016/j.conbuildmat.2020.120152.

[47]   Fernandez, R., Martirena, F., and Scrivener, K. L., Cement and Concrete Research The origin of the pozzolanic activity of calcined clay minerals : A comparison between kaolinite , illite and montmorillonite, *Cem. Concr. Res.*, vol. 41, no. 1, pp. 113–122, 2011, doi: 10.1016/j.cemconres.2010.09.013.

[48]   Frías, M. and Cabrera, J., Pore size distribution and degree of hydration of metakaolin-cement pastes, *Cem. Concr. Res.*, vol. 30, no. 4, pp. 561–569, 2000, doi: 10.1016/S0008-8846(00)00203-9.

[49]   Halamickova', P., Detwiler, R. J., Bentz3, D. P., and Garbocz, E. J., Permeability and Chloride Diiffusion, *Cem. Concr. Res.*, vol. 25, no. 4, pp. 790–802, 1995.

[50]   Diamond, S., Mercury porosimetry: an inappropriate method for the measurement of pore size distributions in cement-based materials, *Cem. Concr. Res.*, vol. 30, no. 10, pp. 1517–1525, 2000, doi: 10.1016/S0008-8846(00)00370-7.

[51]   Willis, K. L., Abell, A. B., and Lange, D. A., Image-based characterization of cement pore structure using Wood's metal intrusion, *Cem. Concr. Res.*, vol. 28, no. 12, pp. 1695–1705, 1998, doi: 10.1016/S0008-8846(98)00159-8.

[52]   Das, B. B. and Kondraivendhan, B., Implication of pore size distribution parameters on compressive strength, permeability and hydraulic diffusivity of concrete, *Constr. Build. Mater.*, vol. 28, no. 1, pp. 382–386, 2012, doi: 10.1016/j.conbuildmat.2011.08.055.

[53]   Bhattacharjee, B. and Krishnamoorthy, S., Permeable Porosity and Thermal Conductivity of Construction Materials, *J. Mater. Civ. Eng.*, vol. 16, no. 4, pp. 322–330, 2004, doi: 10.1061/(asce)0899-1561(2004)16:4(322).

[54] Sui, S., Georget, F., Maraghechi, H., Sun, W., and Scrivener, K., Towards a generic approach to durability: Factors affecting chloride transport in binary and ternary cementitious materials, *Cem. Concr. Res.*, vol. 124, no. June, p. 105783, 2019, doi: 10.1016/j.cemconres.2019.105783.

[55] Monfore, G. E., The electrical resistivity of concrete, 1968.

[56] Hope, B. B., Ip, A. K., and Manning, D. G., Corrosion and electrical impedance in concrete, *Cem. Concr. Res.*, vol. 15, no. 3, pp. 525–534, 1985.

[57] Whittington, H. W., McCarter, J., and Forde, M. C., The conduction of electricity through concrete, *Mag. Concr. Res.*, vol. 33, no. 114, pp. 48–60, 1981.

[58] Layssi H., Ghods, P., Alizadeh, Aali, R., and Salehi, M., Electrical Resistivity of Concrete, *Concr. Int.*, no. MAY 2015, pp. 41–46, 2016.

[59] Feliu, S., Andrade, C., González, J. A., and Alonso, C., A new method forin-situ measurement of electrical resistivity of reinforced concrete, *Mater. Struct.*, vol. 29, no. 6, pp. 362–365, 1996.

[60] Shi, C., Yuan, Q., He, F., and Hu, X., *Transport and Interactions of Chlorides in Cement-based Materials*. CRC Press, 2019.

[61] Flegar, M., Serdar, M., Londono-Zuluaga, D., and Scrivener, K., Regional waste streams as potential raw materials for immediate implementation in cement production, *Materials (Basel).*, vol. 13, no. 23, pp. 1–15, 2020, doi: 10.3390/ma13235456.

[62] Scrivener, K., Snellings, R., and Lothenbach, B., *A practical guide to microstructural analysis of cementitious materials*, vol. 540. Crc Press, 2016.

[63] 196-10:2016, B. E., BSI Standards Publication Methods of testing cement, no. Vi, 2016.

[64] NT Build 492, Concrete, mortar and cement-based repair materials: Chloride migration coefficient from non-steady-state migration experiments, *Measurement*, pp. 1–8, 1999.

[65]   Lebedev, A. V., The synthesis of multi-channel adaptive control system for the autonomous underwater robot, *RPC 2010 - 1st Russ. Pacific Conf. Comput. Technol. Appl.*, pp. 324–328, 2010.

[66]   BSI, BS EN 14629:2007 Products and systems for the protection and repair of concrete structures - Test methods - Determination of chloride content in hardened concrete, vol. 3, 2007.

[67]   Test, C. C., Cabinets, M., Rooms, M., Test, C. C., Drilled, T., and Ag-, C., Standard Test Method for Bulk Electrical Conductivity of Hardened Concrete 1, pp. 4–7, 2013, doi: 10.1520/C1760-12.2.

[68]   FDOT, F. M., FM 5-578: Florida method of test for concrete resistivity as an electrical indicator of its permeability, *Florida Dep. Transp.*, 2004.

[69]   Alexander, M., Ballim, Y., and Mackechnie, J. M., Durability Index Testing Procedure Manual, *Res. Monogr. No.4,* vol. 2018, no. February, p. 29, 2018.

[70]   Kumar, R. and Bhattacharjee, B., Porosity, pore size distribution and in situ strength of concrete, *Cem. Concr. Res.*, vol. 33, no. 1, pp. 155–164, 2003, doi: 10.1016/S0008-8846(02)00942-0.

[71]   Moro, F. and Böhni, H., Ink-bottle effect in mercury intrusion porosimetry of cement-based materials, *J. Colloid Interface Sci.*, vol. 246, no. 1, pp. 135–149, 2002, doi: 10.1006/jcis.2001.7962.

[72]   Nair, N., Mohammed Haneefa, K., Santhanam, M., and Gettu, R., A study on fresh properties of limestone calcined clay blended cementitious systems, *Constr. Build. Mater.*, vol. 254, p. 119326, 2020, doi: 10.1016/j.conbuildmat.2020.119326.

[73]   Chen, H.-J., Shih, N.-H., Wu, C.-H., and Lin, S.-K., Effects of the loss on ignition of fly ash on the properties of high-volume fly ash concrete, *Sustainability*, vol. 11, no. 9, p. 2704, 2019.

[74]   De Weerdt, K., Haha, M. Ben, Le Saout, G., Kjellsen, K. O., Justnes, H., and Lothenbach, B., Hydration mechanisms of ternary Portland cements containing

limestone powder and fly ash, *Cem. Concr. Res.*, vol. 41, no. 3, pp. 279–291, 2011, doi: 10.1016/j.cemconres.2010.11.014.

[75] Antiohos, S. and Tsimas, S., Investigating the role of reactive silica in the hydration mechanisms of high-calcium fly ash/cement systems, *Cem. Concr. Compos.*, vol. 27, no. 2, pp. 171–181, 2005, doi: 10.1016/j.cemconcomp.2004.02.004.

[76] Ramezanianpour, A. A., Pilvar, A., Mahdikhani, M., and Moodi, F., Practical evaluation of relationship between concrete resistivity, water penetration, rapid chloride penetration and compressive strength, *Constr. Build. Mater.*, vol. 25, no. 5, pp. 2472–2479, 2011, doi: 10.1016/j.conbuildmat.2010.11.069.

[77] Wang, J. and Liu, E., The relationship between steady-state chloride diffusion and migration coefficients in cementitious materials, *Mag. Concr. Res.*, vol. 72, no. 19, pp. 1016–1026, 2020.

[78] Alexander, M. G., Mackechnie, J. R., and Ballim, Y., Guide to the use of durability indexes for achieving durability in concrete structures, *Res. Monogr.*, vol. 2, p. 102, 1999.

[79] Castellote, M. *et al.*, Round-Robin test on methods for determining chloride transport parameters in concrete, *Mater. Struct. Constr.*, vol. 39, no. 294, pp. 955–990, 2006, doi: 10.1617/s11527-006-9193-x.

[80] Yuan, Q., Fundamental Studies on Test Methods for the Transport ofChloride Ions in Cementitious Materials. Ghent University, 2009.

[81] Li, K., Li, Q., Zhou, X., and Fan, Z., Durability Design of the Hong Kong–Zhuhai–Macau Sea-Link Project: Principle and Procedure, *J. Bridg. Eng.*, vol. 20, no. 11, p. 04015001, 2015, doi: 10.1061/(asce)be.1943-5592.0000741.

[82] Gao, P., Wei, J., Zhang, T., Hu, J., and Yu, Q., Modification of chloride diffusion coefficient of concrete based on the electrical conductivity of pore solution, *Constr. Build. Mater.*, vol. 145, pp. 361–366, 2017, doi: 10.1016/j.conbuildmat.2017.03.220.

[83] Shi, C., Effect of mixing proportions of concrete on its electrical conductivity and the

rapid chloride permeability test (ASTM C1202 or ASSHTO T277) results, *Cem. Concr. Res.*, vol. 34, no. 3, pp. 537–545, 2004, doi: 10.1016/j.cemconres.2003.09.007.

[84] Thomas, M., The effect of supplementary cementing materials on alkali-silica reaction: A review, *Cem. Concr. Res.*, vol. 41, no. 12, pp. 1224–1231, 2011, doi: 10.1016/j.cemconres.2010.11.003.

[85] Conciatori, D., Sadouki, H., and Brühwiler, E., Capillary suction and diffusion model for chloride ingress into concrete, *Cem. Concr. Res.*, vol. 38, no. 12, pp. 1401–1408, 2008, doi: 10.1016/j.cemconres.2008.06.006.

[86] Popovics, S., New formulas for the prediction of the effect of porosity on concrete strength, in *Journal Proceedings*, 1985, vol. 82, no. 2, pp. 136–146.

[87] Shi, C., Strength, pore structure and permeability of alkali-activated slag mortars, *Cem. Concr. Res.*, vol. 26, no. 12, pp. 1789–1799, 1996.

[88] O'Farrell, M., Wild, S., and Sabir, B. B., Pore size distribution and compressive strength of waste clay brick mortar, *Cem. Concr. Compos.*, vol. 23, no. 1, pp. 81–91, 2001.

[89] Wen, C. E., Yamada, Y., Shimojima, K., Chino, Y., Hosokawa, H., and Mabuchi, M., Compressibility of porous magnesium foam: dependency on porosity and pore size, *Mater. Lett.*, vol. 58, no. 3–4, pp. 357–360, 2004.

[90] Atzeni, C., Effect of pore distribution on strength of hardened cement pastes, in *Pore Structure and Materials Properties, Proceedings of the First International RILEM Congress*, 1987, vol. 1, pp. 195–202.

[91] Yang, C.-C. C., On the relationship between pore structure and chloride diffusivity from accelerated chloride migration test in cement-based materials, *Cem. Concr. Res.*, vol. 36, no. 7, pp. 1304–1311, 2006, doi: 10.1016/j.cemconres.2006.03.007.

[92] Yang, C.-C. C., Cho, S. W., and Wang, L. C., The relationship between pore structure and chloride diffusivity from ponding test in cement-based materials, *Mater. Chem. Phys.*, vol. 100, no. 2–3, pp. 203–210, 2006, doi:

10.1016/j.matchemphys.2005.12.032.

[93]   Garboczi, E. J. and Bentz, D. P., Computer simulation of the diffusivity of cement-based materials, *J. Mater. Sci.*, vol. 27, no. 8, pp. 2083–2092, 1992.

[94]   Li, C., Jiang, L., Xu, N., and Jiang, S., Pore structure and permeability of concrete with high volume of limestone powder addition, *Powder Technol.*, vol. 338, pp. 416–424, 2018, doi: 10.1016/j.powtec.2018.07.054.

[95]   Glass, G. K. and Buenfeld, N. R., Chloride-induced corrosion of steel, *Prog. Struct. Eng. Mater.*, vol. 2, no. 4, pp. 448–458, 2000.

[96]   Filho, J. H., Medeiros, M. H. F., Pereira, E., Helene, P., and Isaia, G. C., High-Volume Fly Ash Concrete with and without Hydrated Lime: Chloride Diffusion Coefficient from Accelerated Test, *J. Mater. Civ. Eng.*, vol. 25, no. 3, pp. 411–418, 2013, doi: 10.1061/(asce)mt.1943-5533.0000596.

[97]   Wu, K., Shi, H., Xu, L., Ye, G., and De Schutter, G., Microstructural characterization of ITZ in blended cement concretes and its relation to transport properties, *Cem. Concr. Res.*, vol. 79, pp. 243–256, 2016, doi: 10.1016/j.cemconres.2015.09.018.

[98]   Yuan, Q., Shi, C., De Schutter, G., Audenaert, K., and Deng, D., Chloride binding of cement-based materials subjected to external chloride environment–a review, *Constr. Build. Mater.*, vol. 23, no. 1, pp. 1–13, 2009, doi: 10.1016/j.conbuildmat.2008.02.004.

[99]   Sharma, M., Bishnoi, S., Martirena, F., and Scrivener, K., Limestone calcined clay cement and concrete: A state-of-the-art review, *Cem. Concr. Res.*, vol. 149, no. March, p. 106564, 2021, doi: 10.1016/j.cemconres.2021.106564.

[100]   Wilson, W., Georget, F., and Scrivener, K., Unravelling chloride transport/microstructure relationships for blended-cement pastes with the mini-migration method, *Cem. Concr. Res.*, vol. 140, no. October 2020, p. 106264, 2021, doi: 10.1016/j.cemconres.2020.106264.

[101]   Tang, S. W. *et al.*, The review of pore structure evaluation in cementitious materials by electrical methods, *Constr. Build. Mater.*, vol. 117, pp. 273–284, 2016, doi:

10.1016/j.conbuildmat.2016.05.037.

[102] Hearn, N., Hooton, R. D., and Nokken, M. R., Pore structure, permeability, and penetration resistance characteristics of concrete, in *Significance of tests and properties of concrete and concrete-making materials*, ASTM International, 2006.

[103] Zhang, Y., Yang, Z., and Ye, G., Dependence of unsaturated chloride diffusion on the pore structure in cementitious materials, *Cem. Concr. Res.*, vol. 127, no. August 2019, p. 105919, 2020, doi: 10.1016/j.cemconres.2019.105919.

[104] Poon, C.-S., Kou, S. C., and Lam, L., Compressive strength, chloride diffusivity and pore structure of high performance metakaolin and silica fume concrete, *Constr. Build. Mater.*, vol. 20, no. 10, pp. 858–865, 2006.

[105] Liu, J., Tang, K., Qiu, Q., Pan, D., Lei, Z., and Xing, F., Experimental investigation on pore structure characterization of concrete exposed to water and chlorides, *Materials (Basel).*, vol. 7, no. 9, pp. 6646–6659, 2014.

[106] Ngala, V. T. and Page, C. L., Effects of carbonation on pore structure and diffusional properties of hydrated cement pastes, *Cem. Concr. Res.*, vol. 27, no. 7, pp. 995–1007, 1997.

[107] Hu, X., Shi, C., Shi, Z., and Zhang, L., Compressive strength, pore structure and chloride transport properties of alkali-activated slag/fly ash mortars, *Cem. Concr. Compos.*, vol. 104, no. August, p. 103392, 2019, doi: 10.1016/j.cemconcomp.2019.103392.

[108] Olsson, N. *et al.*, Moisture and ion transport properties in blended pastes and their relation to the refined pore structure, *Cem. Concr. Res.*, vol. 161, no. August, p. 106949, 2022, doi: 10.1016/j.cemconres.2022.106949.

[109] Panesar, D. K. and Francis, J., Influence of limestone and slag on the pore structure of cement paste based on mercury intrusion porosimetry and water vapour sorption measurements, *Constr. Build. Mater.*, vol. 52, pp. 52–58, 2014.

[110] Kim, G. M., Nam, I. W., Yang, B., Yoon, H. N., Lee, H.-K., and Park, S., Carbon

nanotube (CNT) incorporated cementitious composites for functional construction materials: The state of the art, *Compos. Struct.*, vol. 227, p. 111244, 2019.

[111] Zhang, J., Bian, F., Zhang, Y., Fang, Z., Fu, C., and Guo, J., Effect of pore structures on gas permeability and chloride diffusivity of concrete, *Constr. Build. Mater.*, vol. 163, pp. 402–413, 2018.

[112] Chen, S. *et al.*, Pore structure of geopolymer materials and its correlations to engineering properties: A review, *Constr. Build. Mater.*, vol. 328, p. 127064, 2022.

[113] He, R., Ye, H., Ma, H., Fu, C., Jin, X., and Li, Z., Correlating the chloride diffusion coefficient and pore structure of cement-based materials using modified noncontact electrical resistivity measurement, *J. Mater. Civ. Eng.*, vol. 31, no. 3, p. 4019006, 2019.

[114] Zhang, Y., Wu, K., Yang, Z., and Ye, G., A reappraisal of the ink-bottle effect and pore structure of cementitious materials using intrusion-extrusion cyclic mercury porosimetry, *Cem. Concr. Res.*, vol. 161, p. 106942, 2022.

[115] Arora, A., Sant, G., and Neithalath, N., Ternary blends containing slag and interground/blended limestone: Hydration, strength, and pore structure, *Constr. Build. Mater.*, vol. 102, pp. 113–124, 2016, doi: 10.1016/j.conbuildmat.2015.10.179.

[116] Villagr, Y., Alderete, N., and Heede, P. Van Den, applied sciences Pore Size Distribution and Surface Multifractal Dimension by Multicycle Mercury Intrusion Porosimetry of GGBFS and Limestone Powder Blended Concrete, 2021.

[117] Zhang, Y., Ye, G., and Yang, Z., Pore size dependent connectivity and ionic transport in saturated cementitious materials, *Constr. Build. Mater.*, vol. 238, p. 117680, 2020, doi: 10.1016/j.conbuildmat.2019.117680.

[118] Martın-Pérez, B., Zibara, H., Hooton, R. D., and Thomas, M. D. A., A study of the effect of chloride binding on service life predictions, *Cem. Concr. Res.*, vol. 30, no. 8, pp. 1215–1223, 2000.

[119] Li, S., Jin, Z., and Yu, Y., Chloride binding by calcined layered double hydroxides

and alumina-rich cementitious materials in mortar mixed with seawater and sea sand, *Constr. Build. Mater.*, vol. 293, p. 123493, 2021.

[120] McPolin, D., Basheer, P. A. M., Long, A. E., Grattan, K. T. V, and Sun, T., Obtaining progressive chloride profiles in cementitious materials, *Constr. Build. Mater.*, vol. 19, no. 9, pp. 666–673, 2005.

[121] Samson, E. and Marchand, J., Multiionic approaches to model chloride binding in cementitious materials, in *Gagné M. Jolin F. Paradis J. Marchand, B. Bissonnette, éditeur: Proc. 2nd Int. RILEM symp. on Advances in concrete through science and engineering*, 2006, pp. 101–122.

[122] Nielsen, E. P. and Geiker, M. R., Chloride diffusion in partially saturated cementitious material, *Cem. Concr. Res.*, vol. 33, no. 1, pp. 133–138, 2003.

[123] Thomas, M. D. A. A., Hooton, R. D., Scott, A., and Zibara, H., The effect of supplementary cementitious materials on chloride binding in hardened cement paste, *Cem. Concr. Res.*, vol. 42, no. 1, pp. 1–7, 2012, doi: 10.1016/j.cemconres.2011.01.001.

[124] Zhang, Y., Ye, G., and Yang, Z., New insights into long-term chloride transport in unsaturated cementitious materials: Role of degree of water saturation, *Constr. Build. Mater.*, vol. 238, p. 117677, 2020.

[125] Ma, Z., Hu, R., Shen, J., Wang, C., and Wu, H., Chloride diffusion and binding capacity of sustainable cementitious materials with construction waste powder as cement replacement, *Constr. Build. Mater.*, vol. 368, p. 130352, 2023.

[126] Sahmaran, M., Li, M., and Li, V. C., Transport properties of engineered cementitious composites under chloride exposure, *ACI Mater. J.*, vol. 104, no. 6, pp. 604–611, 2007.

[127] Jafari Azad, V., Erbektas, A. R., Qiao, C., Isgor, O. B., and Weiss, W. J., Relating the formation factor and chloride binding parameters to the apparent chloride diffusion coefficient of concrete, *J. Mater. Civ. Eng.*, vol. 31, no. 2, p. 4018392, 2019, doi: 10.1061/(asce)mt.1943-5533.0002615.

[128] Basheer, P. A. M., Gilleece, P. R. V, Long, A. E., and Mc Carter, W. J., Monitoring electrical resistance of concretes containing alternative cementitious materials to assess their resistance to chloride penetration, *Cem. Concr. Compos.*, vol. 24, no. 5, pp. 437–449, 2002.

[129] Song, H. W., Lee, C. H., Jung, M. S., and Ann, K. Y., Development of chloride binding capacity in cement pastes and influence of the pH of hydration products, *Can. J. Civ. Eng.*, vol. 35, no. 12, pp. 1427–1434, 2008.

[130] Li, C. and Jiang, L., The role of chloride binding mechanism in the interpretation of chloride profiles in concrete containing limestone powder, *J. Sustain. Cem. Mater.*, vol. 12, no. 1, pp. 24–35, 2023.

[131] Huang, X. *et al.*, The effect of supplementary cementitious materials on the permeability of chloride in steam cured high-ferrite Portland cement concrete, *Constr. Build. Mater.*, vol. 197, pp. 99–106, 2019.

[132] Cascudo, O., Pires, P., Carasek, H., Castro, A. De, and Lopes, A., Evaluation of the pore solution of concretes with mineral additions subjected to 14 years of natural carbonation, *Cem. Concr. Compos.*, vol. 115, no. April 2020, p. 103858, 2021, doi: 10.1016/j.cemconcomp.2020.103858.

[133] Snyder, K. A., Feng, X., Keen, B. D., and Mason, T. O., Estimating the electrical conductivity of cement paste pore solutions from OH-, K+ and Na+ concentrations, *Cem. Concr. Res.*, vol. 33, no. 6, pp. 793–798, 2003, doi: 10.1016/S0008-8846(02)01068-2.

[134] Plusquellec, G., Geiker, M. R., Lindgård, J., Duchesne, J., Fournier, B., and Weerdt, K. De, Cement and Concrete Research Determination of the pH and the free alkali metal content in the pore solution of concrete : Review and experimental comparison, *Cem. Concr. Res.*, vol. 96, pp. 13–26, 2017, doi: 10.1016/j.cemconres.2017.03.002.

[135] Manchiryal, R. K. and Neithalath, N., Analysis of the influence of material parameters on electrical conductivity of cement pastes and concretes, vol. 9831, no. 4, pp. 257–270, 2009, doi: 10.1680/macr.2008.00064.

[136] Ram, K., Serdar, M., Londono-Zuluaga, D., and Scrivener, K., Does carbon footprint reduction impair mechanical properties and service life of concrete?, *Mater. Struct. Constr.*, vol. 56, no. 1, 2023, doi: 10.1617/s11527-022-02090-9.

[137] Ram, K., Flegar, M., Serdar, M., and Scrivener, K., Influence of Low- to Medium-Kaolinite Clay on the Durability of Limestone Calcined Clay Cement (LC3) Concrete, *Materials (Basel).*, vol. 16, no. 1, pp. 1–18, 2023, doi: 10.3390/ma16010374.

[138] Sanish, K. B., Neithalath, N., and Santhanam, M., Monitoring the evolution of material structure in cement pastes and concretes using electrical property measurements, *Constr. Build. Mater.*, vol. 49, pp. 288–297, 2013, doi: 10.1016/j.conbuildmat.2013.08.038.

[139] E.W. Washburn, Note on a Method of Determining the Distribution of Pore Sizes in a Porous Material, *Proc. Natl. Acad. Sci.*, vol. 7, no. 4, pp. 115–116, 1921, [Online]. Available: https://doi.org/10.1073/pnas.7.4.115.

[140] Olsson, N., Yang, Z., and Li, Y., Cement and Concrete Research Moisture and ion transport properties in blended pastes and their relation to the refined pore structure, vol. 161, no. August, 2022, doi: 10.1016/j.cemconres.2022.106949.

[141] Weerdt, K. De, Chloride binding in concrete : recent investigations and recognised knowledge gaps : RILEM Robert L ' Hermite Medal Paper 2021, *Mater. Struct.*, vol. 54, no. 6, pp. 1–16, 2021, doi: 10.1617/s11527-021-01793-9.

[142] Marangu, J. M., Thiong'O, J. K., and Wachira, J. M., Chloride Ingress in Chemically Activated Calcined Clay-Based Cement, *J. Chem.*, vol. 2018, 2018, doi: 10.1155/2018/1595230.

[143] Dieu Nguyen, Q., Khan, M. S. H., and Castel, A., Chloride diffusion in limestone flash calcined clay cement concrete, *ACI Mater. J.*, vol. 117, no. 6, pp. 165–175, 2020, doi: 10.14359/51725986.

[144] Thesis, A., Rengaraju, S., Philosophy, D. O. F., and Technology, B., ELECTROCHEMICAL RESPONSE AND CHLORIDE THRESHOLD OF STEEL IN HIGHLY RESISTIVE CONCRETE SYSTEMS, no. July, 2019.

[145] Rajabipour, F., Insitu electrical sensing and material health monitoring in concrete structures. Purdue University, 2006.

[146] Rajabipour, F. and Weiss, Æ. J., Electrical conductivity of drying cement paste, pp. 1143–1160, 2007, doi: 10.1617/s11527-006-9211-z.

[147] Dhandapani, Y., Santhanam, M., Kaladharan, G., and Ramanathan, S., Towards ternary binders involving limestone additions — A review, *Cem. Concr. Res.*, vol. 143, no. April 2020, p. 106396, 2021, doi: 10.1016/j.cemconres.2021.106396.

[148] Berodier, E. and Scrivener, K., Evolution of pore structure in blended systems, *Cem. Concr. Res.*, vol. 73, pp. 25–35, 2015, doi: 10.1016/j.cemconres.2015.02.025.

[149] Vollpracht, A., Lothenbach, B., Snellings, R., and Haufe, J., The pore solution of blended cements: a review, *Mater. Struct. Constr.*, vol. 49, no. 8, pp. 3341–3367, 2016, doi: 10.1617/s11527-015-0724-1.

[150] Stade, H., On the reaction of CSH (di, poly) with alkali hydroxides, *Cem. Concr. Res.*, vol. 19, no. 5, pp. 802–810, 1989.

[151] Hong, S.-Y. Y. and Glasser, F. P., Alkali binding in cement pastes: Part I. The CSH phase, *Cem. Concr. Res.*, vol. 29, no. 12, pp. 1893–1903, 1999, doi: 10.1016/S0008-8846(99)00187-8.

[152] Bu, Y. and Weiss, J., The influence of alkali content on the electrical resistivity and transport properties of cementitious materials, *Cem. Concr. Compos.*, vol. 51, pp. 49–58, 2014, doi: 10.1016/j.cemconcomp.2014.02.008.

[153] Avet, F. and Scrivener, K., Influence of pH on the chloride binding capacity of Limestone Calcined Clay Cements (LC3), *Cem. Concr. Res.*, vol. 131, no. July 2019, p. 106031, 2020, doi: 10.1016/j.cemconres.2020.106031.

[154] Avet, F., Boehm-Courjault, E., and Scrivener, K., Investigation of C-A-S-H composition, morphology and density in Limestone Calcined Clay Cement (LC3), *Cem. Concr. Res.*, vol. 115, no. July 2018, pp. 70–79, 2019, doi: 10.1016/j.cemconres.2018.10.011.

[155] Archie, G., The Electrical Resistivity Log as an Aid in Determining Some Reservoir Characteristics. Petroleum Technology 1942. October.

[156] Garboczi, E. J., Permeability, diffusivity, and microstructural parameters: a critical review, *Cem. Concr. Res.*, vol. 20, no. 4, pp. 591–601, 1990, doi: 10.1016/0008-8846(90)90101-3.

[157] Weiss, W. J., Spragg, R. P., Isgor, O. B., Ley, M. T., and Van Dam, T., Toward performance specifications for concrete: linking resistivity, RCPT and diffusion predictions using the formation factor for use in specifications, in *High Tech Concrete: Where Technology and Engineering Meet: Proceedings of the 2017 fib Symposium, held in Maastricht, The Netherlands, June 12-14, 2017*, 2018, pp. 2057–2065.

[158] Snyder, K. A., The relationship between the formation factor and the diffusion coefficient of porous materials saturated with concentrated electrolytes : theoretical and experimental considerations, vol. 3, no. 12, pp. 216–224, 2001.

[159] Hemstad, P., Babaahmadi, A., Machner, A., and Kunther, W., Cement and Concrete Research Chloride binding in Portland composite cements containing metakaolin and silica fume, vol. 161, no. August, 2022, doi: 10.1016/j.cemconres.2022.106924.

[160] Chatterji, S. and Kawamura, M., Electrical double layer, ion transport and reactions in hardened cement paste, *Cem. Concr. Res.*, vol. 22, no. 5, pp. 774–782, 1992, doi: 10.1016/0008-8846(92)90101-Z.

[161] Yang, Y. and Wang, M., Pore-scale modeling of chloride ion diffusion in cement microstructures, *Cem. Concr. Compos.*, vol. 85, pp. 92–104, 2018, doi: 10.1016/j.cemconcomp.2017.09.014.

[162] Elakneswaran, Y., Iwasa, A., Nawa, T., Sato, T., and Kurumisawa, K., Ion-cement hydrate interactions govern multi-ionic transport model for cementitious materials, *Cem. Concr. Res.*, vol. 40, no. 12, pp. 1756–1765, 2010, doi: 10.1016/j.cemconres.2010.08.019.

[163] Friedmann, H., Amiri, O., and Aït-Mokhtar, A., Physical modeling of the electrical

double layer effects on multispecies ions transport in cement-based materials, *Cem. Concr. Res.*, vol. 38, no. 12, pp. 1394–1400, 2008, doi: 10.1016/j.cemconres.2008.06.003.

[164] Feng, G. L., Li, L. Y., Kim, B., and Liu, Q. F., Multiphase modelling of ionic transport in cementitious materials with surface charges, *Comput. Mater. Sci.*, vol. 111, pp. 339–349, 2016, doi: 10.1016/j.commatsci.2015.09.060.

[165] Hu, X., Shi, C., Yuan, Q., and de Schutter, G., AC impedance spectroscopy characteristics of chloride-exposed cement pastes, *Constr. Build. Mater.*, vol. 233, 2020, doi: 10.1016/j.conbuildmat.2019.117267.

[166] Nguyen, P. T. and Amiri, O., Study of electrical double layer effect on chloride transport in unsaturated concrete, *Constr. Build. Mater.*, vol. 50, pp. 492–498, 2014, doi: 10.1016/j.conbuildmat.2013.09.013.

[167] Friedmann, H., Ait-Mokhtar, A., and Amiri, O., Modelling of EDL effect on chloride migration in cement-based materials, *Mag. Concr. Res.*, vol. 64, no. 10, pp. 909–917, 2012, doi: 10.1680/macr.11.00122.

[168] Johannesson, B., Yamada, K., Nilsson, L. O., and Hosokawa, Y., Multi-species ionic diffusion in concrete with account to interaction between ions in the pore solution and the cement hydrates, *Mater. Struct. Constr.*, vol. 40, no. 7, pp. 651–665, 2007, doi: 10.1617/s11527-006-9176-y.

[169] Goto, S., Shigeru, K., Takagi, T., and Daimon, M., Pore-size distribution and diffusion of ions in hardened cement paste, *Cem. Sci Concr. Technol*, vol. 36, pp. 49–52, 1982.

[170] Goto, S. and Roy, D. M., Diffusion of ions through hardened cement pastes, *Cem. Concr. Res.*, vol. 11, no. 5–6, pp. 751–757, 1981.

[171] Collivignarelli, M. C., Abbà, A., Carnevale Miino, M., Cillari, G., and Ricciardi, P., A review on alternative binders, admixtures and water for the production of sustainable concrete, *J. Clean. Prod.*, vol. 295, 2021, doi: 10.1016/j.jclepro.2021.126408.

[172] Serdar, M., Bjegovic, D., Stirmer, N., and Banjad Pecur, I., Alternative binders for concrete: opportunities and challenges, no. October 2019, pp. 199–218, 2019, doi: 10.5592/co/ftce.2019.09.

[173] Coppola, L. *et al.*, Binders alternative to Portland cement and waste management for sustainable construction—Part 1, *J. Appl. Biomater. Funct. Mater.*, vol. 16, no. 3, pp. 186–202, 2018, doi: 10.1177/2280800018782845.

[174] Ahmad, M. R., Chen, B., and Ali Shah, S. F., Mechanical and microstructural characterization of bio-concrete prepared with optimized alternative green binders, *Constr. Build. Mater.*, vol. 281, p. 122533, 2021, doi: 10.1016/j.conbuildmat.2021.122533.

[175] Gartner, E. and Hirao, H., A review of alternative approaches to the reduction of CO2 emissions associated with the manufacture of the binder phase in concrete, *Cem. Concr. Res.*, vol. 78, pp. 126–142, 2015, doi: 10.1016/j.cemconres.2015.04.012.

[176] Bun, P., Cyr, M., Laniesse, P., Bun, K. N., and Idir, R., Concrete made of 100% recycled materials - Feasibility study, *Resour. Conserv. Recycl.*, vol. 180, no. January, p. 106199, 2022, doi: 10.1016/j.resconrec.2022.106199.

[177] Damineli, B. L. and John, V. M., Developing Low CO 2 Concretes : Is Clinker Replacement Sufficient ? The Need of Cement Use Efficiency Improvement, vol. 517, pp. 342–351, 2012, doi: 10.4028/www.scientific.net/KEM.517.342.

[178] European, T. H. E., The role of CEMENT in the 2050 LOW CARBON ECONOMY.

[179] Gettu, R. *et al.*, Influence of supplementary cementitious materials on the sustainability parameters of cements and concretes in the Indian context, *Mater. Struct. Constr.*, vol. 52, no. 1, pp. 1–11, 2019, doi: 10.1617/s11527-019-1321-5.

[180] Yaphary, Y. L., Lam, R. H. W., and Lau, D., Reduction in cement content of normal strength concrete with used engine oil (UEO) as chemical admixture, *Constr. Build. Mater.*, vol. 261, p. 119967, 2020, doi: 10.1016/j.conbuildmat.2020.119967.

[181] Loo, Y. H., Chin, M. S., Tam, C. T., and Ong, K. C. G., A carbonation prediction

model for accelerated carbonation testing of concrete, *Mag. Concr. Res.*, vol. 46, no. 168, pp. 191–200, 1994, doi: 10.1680/macr.1994.46.168.191.

[182] Dhir, R. K., McCarthy, M. J., Zhou, S., and Tittle, P. A. J., Role of cement content in specifications for concrete durability: cement type influences, *Struct. <html_ent glyph="@amp;" ascii="&"/> Build.*, vol. 157, no. 2, pp. 113–127, Apr. 2004, doi: 10.1680/stbu.157.2.113.36479.

[183] Powers, T. C., A discussion of cement hydration in relation to the curing of concrete, in *Highway Research Board Proceedings*, 1948, vol. 27.

[184] Ding, M. *et al.*, Possibility and advantages of producing an ultra-high performance concrete (UHPC) with ultra-low cement content, *Constr. Build. Mater.*, vol. 273, p. 122023, 2021, doi: 10.1016/j.conbuildmat.2020.122023.

[185] Wang, D., Shi, C., Farzadnia, N., Shi, Z., and Jia, H., A review on effects of limestone powder on the properties of concrete, *Constr. Build. Mater.*, vol. 192, pp. 153–166, 2018, doi: 10.1016/j.conbuildmat.2018.10.119.

[186] Bonavetti, V., Donza, H., Menéndez, G., Cabrera, O., and Irassar, E. F., Limestone filler cement in low w/c concrete: A rational use of energy, *Cem. Concr. Res.*, vol. 33, no. 6, pp. 865–871, 2003, doi: 10.1016/S0008-8846(02)01087-6.

[187] Moodi, F., Ramezanianpour, A. A., and Safavizadeh, A. S., Evaluation of the optimal process of thermal activation of kaolins, *Sci. Iran.*, vol. 18, no. 4 A, pp. 906–912, 2011, doi: 10.1016/j.scient.2011.07.011.

[188] Hemalatha, T. and Ramaswamy, A., A review on fly ash characteristics – Towards promoting high volume utilization in developing sustainable concrete, *J. Clean. Prod.*, vol. 147, pp. 546–559, 2017, doi: 10.1016/j.jclepro.2017.01.114.

[189] Liew, K. M., Sojobi, A. O., and Zhang, L. W., Green concrete : Prospects and challenges, *Constr. Build. Mater.*, vol. 156, pp. 1063–1095, 2017, doi: 10.1016/j.conbuildmat.2017.09.008.

[190] Beuntner, N. and Thienel, K. C., Properties of Calcined Lias Delta Clay---

Technological Effects, Physical Characteristics and Reactivity in Cement, in *Calcined Clays for Sustainable Concrete*, 2015, pp. 43–50.

[191] Scrivener, K., Impacting factors and properties of limestone calcined clay cements (LC 3), vol. 7, pp. 3–14, 2019.

[192] Stipanovic Oslakovic, I., Bjegovic, D., and Mikulic, D., Evaluation of service life design models on concrete structures exposed to marine environment, *Mater. Struct. Constr.*, vol. 43, no. 10, pp. 1397–1412, 2010, doi: 10.1617/s11527-010-9590-z.

[193] Yu, R., Spiesz, P., and Brouwers, H. J. H., Mix design and properties assessment of Ultra-High Performance Fibre Reinforced Concrete (UHPFRC), *Cem. Concr. Res.*, vol. 56, pp. 29–39, 2014, doi: 10.1016/j.cemconres.2013.11.002.

[194] Wong, H. H. C. H. and Kwan, A. K. H. H., Packing density : a key concept for mix design of high performance concrete, *Mater. Sci. Technol. Eng. Conf. Hong Kong*, pp. 1–15, 2005.

[195] Schiessl, P., Helland, S., Gehlen, C., Nilsson, L. O., and Rostam, S., *Model code for service life design (MC-SLD)*, vol. 1. 2005.

[196] Life-365™ Consortium III, Life-365 Service Life Prediction Model Version 2.2.3 User's Manual, 2020, [Online]. Available: http://www.life-365.org/download/Life-365_v2.2.3_Users_Manual.pdf.

[197] Angst, U., Elsener, B., and Larsen, C. K., Vennesland (2009) Critical chloride content in reinforced concrete: a review, *Cem. Concr. Res.*, vol. 139, no. 12, p. 1122.

[198] Gettu, R., Pillai, R. G., Santhanam, M., Basavaraj, A. S., Rathnarajan, S., and Dhanya, B. S., Sustainability-based decision support framework for choosing concrete mixture proportions, *Mater. Struct. Constr.*, vol. 51, no. 6, pp. 1–16, 2018, doi: 10.1617/s11527-018-1291-z.

[199] Ram, K., Serdar, M., Londono-Zuluaga, D., and Scrivener, K., THE EFFECT OF PORE MICROSTRUCTURE ON STRENGTH AND CHLORIDE INGRESS IN BLENDED CEMENT BASED ON LOW KAOLIN CLAY, *Case Stud. Constr.*

Mater., p. e01242, 2022.

[200] Bhattacherjee, S. *et al.*, Sustainable materials for 3D concrete printing, *Cem. Concr. Compos.*, vol. 122, no. December 2020, p. 104156, 2021, doi: 10.1016/j.cemconcomp.2021.104156.

[201] SimaPro - Sustainability, (n.d.). https://pre-sustainability.com/solutions/tools/simapro/.

[202] Müller, H. S., Haist, M., and Vogel, M., Assessment of the sustainability potential of concrete and concrete structures considering their environmental impact, performance and lifetime, *Constr. Build. Mater.*, vol. 67, no. PART C, pp. 321–337, 2014, doi: 10.1016/j.conbuildmat.2014.01.039.

[203] Yu, J., Mishra, D. K., Hu, C., Leung, C. K. Y., and Shah, S. P., Mechanical, environmental and economic performance of sustainable Grade 45 concrete with ultrahigh-volume Limestone-Calcined Clay (LCC), *Resour. Conserv. Recycl.*, vol. 175, no. February, p. 105846, 2021, doi: 10.1016/j.resconrec.2021.105846.

[204] Chen, Y. Y., Tuan, B. L. A., and Hwang, C. L., Effect of paste amount on the properties of self-consolidating concrete containing fly ash and slag, *Constr. Build. Mater.*, vol. 47, pp. 340–346, 2013, doi: 10.1016/j.conbuildmat.2013.05.050.

[205] Elsharief, A., Cohen, M. D., and Olek, J., Influence of lightweight aggregate on the microstructure and durability of mortar, *Cem. Concr. Res.*, vol. 35, no. 7, pp. 1368–1376, 2005, doi: 10.1016/j.cemconres.2004.07.011.

[206] Elsharief, A., Cohen, M. D., and Olek, J., Influence of aggregate size, water cement ratio and age on the microstructure of the interfacial transition zone, *Cem. Concr. Res.*, vol. 33, no. 11, pp. 1837–1849, 2003, doi: 10.1016/S0008-8846(03)00205-9.

[207] Jones, R. and Kaplan, M. F., The effect of coarse aggregate on the mode of failure of concrete in compression and flexure, *Mag. Concr. Res.*, vol. 10, no. 28, pp. 39–42, 1958, doi: 10.1680/macr.1958.10.28.39.

[208] Seddik, M., Zitouni, S., and Belâabes, S., Effect of content and particle size

distribution of coarse aggregate on the compressive strength of concrete, *Constr. Build. Mater.*, vol. 24, no. 4, pp. 505–512, 2010, doi: 10.1016/j.conbuildmat.2009.10.009.

[209] Thongsanitgarn, P., Wongkeo, W., Chaipanich, A., and Poon, C. S., Heat of hydration of Portland high-calcium fly ash cement incorporating limestone powder: Effect of limestone particle size, *Constr. Build. Mater.*, vol. 66, pp. 410–417, 2014, doi: 10.1016/j.conbuildmat.2014.05.060.

[210] The European Cement Association, Environmental Product Declaration: Portland Cement (CEM I) produced in Europe, no. Cem I, 2020, [Online]. Available: https://cembureau.eu/media/3lplreko/epd-for-cement-cem-i.pdf.

[211] Holcim, 2. EPD Holcim CEMENTY.pdf. 2013.

[212] Ice, E., Prof, B., Hammond, G., Jones, C., Lowrie, E. F., and Tse, P., A BSRIA guide Embodied Carbon The Inventory of Carbon and.

[213] Federation, T. E. *et al.*, Declaration of conformity for products with Model EPDs.

[214] Yu, J. *et al.*, Compressive strength and environmental impact of sustainable blended cement with high-dosage Limestone and Calcined Clay (LC2), *J. Clean. Prod.*, vol. 278, p. 123616, 2021, doi: 10.1016/j.jclepro.2020.123616.

List of figures

List of tables

Biography

Kiran Ram Porikam Poil was born on April 19, 1991, in Kozhikode, India. He completed his undergraduate studies in Civil Engineering in 2014 at Government Engineering College, Thrissur, India. In July 2017, he received a master's degree in construction technology and management from the National Institute of Technology Karnataka, India. During his master's program, he conducted research on the effect of different types of cement on the corrosion of reinforced concrete. In 2017, he joined the Indian Institute of Technology Madras, India, as a research assistant. Since September 27, 2019, he has been a Ph.D. student at the Department of Materials, Faculty of Civil Engineering at the University of Zagreb in Croatia. His research topic is the development of high-performance concrete with a lower ecological footprint as part of the ACT (Advanced Low Cementitious Materials) project.

List of published papers

Papers in journals

1. Ram, Kiran, Marijana Serdar, Diana Londono-Zuluaga, and Karen Scrivener. "The effect of pore microstructure on strength and chloride ingress in blended cement based on low kaolin clay." Case Studies in Construction Materials 17 (2022): e01242.

2. Ram, Kiran, Marijana Serdar, Diana Londono-Zuluaga, and Karen Scrivener. "Does carbon footprint reduction impair mechanical properties and service life of concrete?" Materials and Structures 56, no. 1 (2023): 6.

3. Ram, Kiran, Matea Flegar, Marijana Serdar, and Karen Scrivener. "Influence of Low-to-Medium-Kaolinite Clay on the Durability of Limestone Calcined Clay Cement (LC3) Concrete." Materials 16, no. 1 (2023): 374.

Papers, posters, and presentations in conferences

1. Ram, Kiran; Serdar, Marijana; Londono-Zuluaga, Diana; Scrivener, Karen. "Developing high-performance concrete using locally available materials", 6th Symposium on Doctoral

Studies in Civil Engineering, Faculty of Civil Engineering, University of Zagreb, Zagreb, Croatia: University of Zagreb Faculty of Civil Engineering, 2020. p. 139-151

2. Ram, Kiran; Londono-Zuluaga, Diana; Serdar, Marijana; Scrivener, Karen, "The Effect of Cement Reduction and Substitution on the Mechanical and Durability Properties of Concrete", MATEC Web Conferences Volume 364, 2022 Cape town, South Africa, 2022. p. 1-5 doi:10.1051/matecconf/202236402008

3. Ram, Kiran; Londono-Zuluaga Diana; Serdar, Marijana; Scrivener, Karen, "Correlating chloride migration, diffusion and resistivity of limestone calcined clay mortar based on low grade clay", 76th Rilem Annual Week 2022 Kyoto, Japan, 2022. str. 1-4.

4. Ram, Kiran; Londono-Zuluaga; Serdar, Marijana; Scrivener, Karen, "Reactivity enhancement of low kaolin clay using particle separation technique -a feasibility study on Croatian clays", International Conference on Calcined Clays for Sustainable Concrete 2022, Switzerland, 2022. p. 19-20.

5. Ram, Kiran; Londono-Zuluaga, Diana; Serdar, Marijana; Scrivener, Karen, "Chloride transport in concrete based on clays with different kaolin content", International Conference on Calcined Clays for Sustainable Concrete 2022 Lausanne, 2022. str. 1-2.

6. Ram, Kiran; Londono-Zuluaga, Diana; Serdar, Marijana; Scrivener, Karen, "Chloride penetration resistance of high-performance concrete based on limestone-calcined clay", The Corvallis Workshops Concrete Fit for Purpose and Planet Oregon, USA, 2022.